米
日

U.S. - JAPAN COORDINATED PROGRAM

FOR

MASONRY BUILDING RESEARCH

REPORT NO. 2.3-6

PB93-214492

COMPARISON OF THE DYNAMIC RESPONSE OF A DAMPED MDOF NONLINEAR BEAM MODEL WITH AN EQUIVALENT SDOF HYSTERETIC MODEL

by

OMAR M. WAQFI
JOHN C. KARIOTIS

APRIL 1992

Kariotis &Associates

COMPARISON OF THE DYNAMIC RESPONSE
OF A DAMPED MDOF NONLINEAR BEAM MODEL
WITH AN EQUIVALENT SDOF HYSTERETIC MODEL

by

Omar M. Waqfi
John C. Kariotis

April 27, 1992

Report No. 2.3-6

KARIOTIS & ASSOCIATES
711 Mission Street, Suite D
South Pasadena, California 91030
(213) 682-2871

1b

.

PREFACE

This report presents the results of Category 2.0, Task 2.3 of the U.S. Coordinated Program for Masonry Building Research. The program constitutes the United States part of the United States-Japan coordinated masonry research program conducted under the auspices of The Panel on Wind and Seismic Effects of the U.S.-Japan Natural Resources Development Program (UJNR).

Any opinions, findings, and conclusions or recommendations expressed in this publication are those of the authors and do not necessarily reflect the views of the National Science Foundation and/or the United States Government.

CONTENTS

SECTION 1

INTRODUCTION

These studies of the comparative behavior of nonlinear single-degree-of-freedom (SDOF) and nonlinear multiple-degree-of-freedom (MDOF) models were made to better understand the dynamic behavior of a dynamic model with hysteretic damping, the SDOF, and of a model with specified damping, the MDOF. Each of these models can be used for dynamic modeling of structures. The limitations of each of the nonlinear models provided the impetus for the development of these two nonlinear lumped parameter models.

The SDOF model can have three degrees of freedom, rotational, vertical and horizontal for replication of a shear wall rotating and uplifting on the supporting soils. It can represent a multistory structure if the dynamic displacement at each story level can be represented by only a translation degree of freedom at that level. The SDOF model can model multistory shear walls by converting the multi-story shear wall structure into an equivalent SDOF model (Biggs, 1964 and Saiidi, 1981). This SDOF model uses hysteretic damping by replicating the loading, unloading and reloading stiffnesses of the reinforced masonry shear wall. The rules for describing the stiffness parameters are obtained from cyclic testing of experimental specimens. However, the SDOF model is limited to predicting only the dynamic displacements of the fundamental mode of the structure. The shear calculated by the SDOF model is limited to the shear forces caused by primary mode response.

The MDOF model replicates a cantilever shear wall, either fixed at its base, or with a rotational spring at its base. The rotational spring at the base cannot fully simulate uplifting at the foundation-soil interface but can represent foundation flexibility. The MDOF model has the capacity to simulate stiffness degradation in the story-height beam elements that is due to tensile cracking, reinforcement yielding and crushing of the compression zone at the

edges of the shear wall. However, a preplanned amount of damping must be added to the beam elements of the MDOF model. The quantity of damping should replicate the hysteretic damping of the SDOF model as closely as possible.

This study is of how to specify the quantity of damping of the MDOF model. Two SDOF models, one with a very low quantity of hysteretic damping and one with a more typical quantity of hysteretic damping were comparing to MDOF models with specified damping. The goal of these studies was to have equal dynamic response of the two nonlinear models.

SECTION 2
MDOF NONLINEAR BEAM

2.1 INTRODUCTION

A nonlinear model of reinforced masonry shear walls has been developed to study the response of multi-story reinforced masonry structures subjected to earthquake ground motions (Kariotis, 1992). The structure used in this study is represented by a massless shear wall that provides the stiffness and has lumped masses at floor levels. A nonlinear finite element analysis program was used to establish the stiffness/rotation relationship for each of the story height panels.

2.2 MODEL DESCRIPTION

The model consists of a 60 feet tall shear wall as shown in Figure 2-1. It has a width of 20 feet and it is 7 5/8 inches thick. Properties of the masonry wall between floor levels is given in Table 2-1. The properties of the strip of the wall at each floor level is given in Table 2-2. The wall is assumed to be rigidly fixed with the base, thus, allowing no rotation. Five lumped masses equivalent to a weight of 30 kips each represent the floor masses that are located at each floor level and are spaced equally along the height of the shear wall. Additional horizontal reinforcement was included in a thin strip at each floor level. This reinforcement represents the diaphragm reinforcement that is mobilized with the wall reinforcement.

2.3 STIFFNESS/ROTATION RELATIONSHIP

The stiffness of a single panel of a story height was evaluated from the moment/rotation relationship. A finite element mesh of two stories was constructed as shown in Figure 2-2. The top of the model is statically displaced by subjecting the top nodes to a controlled displacement. The reaction at the top nodes was

calculated for each displacement increment and an equal force is applied at the top of the lower story. The additional reinforcement in the diaphragm contributes towards reducing the local deformations due to load application.

The top panel is used to apply the loading uniformly to the lower panel which is the segment of the wall represented by the beam element. The stiffness degradation of this beam element is evaluated.

The stiffness was evaluated using simple beam theory with pure bending. The moment/deflection relationship is described by the following equation:

$$M(x) = EI \times \frac{d^2v}{dx^2} \qquad\qquad 2\text{-}1$$

where

    M(x):   Moment at location x

    v   :   Lateral deflection of the beam

    EI   :   Effective stiffness factor of the beam

so

$$EI = M/\frac{d\theta}{dx} \qquad\qquad 2\text{-}2$$

where

    θ :   Angle of rotation, dv/dx

The rotation angle θ of the axis of the beam, as shown in Figure 2-3, is equivalent to the relative rotation between the two end surfaces of the beam. The net rotation was calculated by monitoring the relative translational displacement at the edges of the top surface of the panel as shown in Figure 2-3; such that:

$$\tan \theta = [\Delta y_2 - \Delta y_1]/[L + \Delta x_2 - \Delta x_1] \qquad\qquad 2\text{-}3$$

where

Δy	:	Difference in vertical deflection
Δx	:	Difference in horizontal deflection
L	:	Wall depth

The moment in the beam section is defined as:

$$M(x) = -(P1-P2)x + (2P1-P2)L \qquad \text{2-4}$$

Combining Equations 2-2 and 2-4:

$$\frac{dv}{dx} = -\frac{1}{EI}\left[(2P1 - P2)Lx - (P1 - P2)\frac{x^2}{2}\right] \qquad \text{2-5}$$

and for x = L:

$$\frac{dv}{dx} = -\frac{L^2}{EI}\left[\frac{3}{2}P1 - \frac{1}{2}P2\right] \qquad \text{2-6}$$

and:

$$EI = -\frac{L^2}{\theta}\left[\frac{3}{2}P1 - \frac{1}{2}P2\right] \qquad \text{2-7}$$

In the case of P1 = P2:

$$EI = -\frac{P1L}{\theta}xL = -\frac{ML}{\theta} \qquad \text{2-8}$$

A moment versus rotation plot is presented in Figure 2-4. The relationship between EI and θ as illustrated by Equation 2-7 is shown in Figure 2-5. This figure shows the rate of degradation of stiffness caused by the internal rotation due to the presence of moment only and the absence of shear. The relationship between effective EI and θ is dependent on the loading system. In the presence of substantial shear in the section, a different relationship between EI and θ exists. Double curvature of the beam element would produce significant degradation in stiffness with

2-3

little change in the rotation. Thus, the EI/θ relationship is valid for primary mode deflection of multi-story walls, where cantilever curvature is predominate.

2.4 DYNAMIC MODEL

A MDOF system of beam elements with degrading stiffness can be modeled. A computer program, LPM/II, was developed (Kariotis, 1992) for the dynamic analysis of nonlinear lumped parameter models. The solution techniques are similar to LPM/I (Kariotis, 1992). The nonlinearity of the beam elements is defined by the relationship between effective EI and θ. This relationship is defined as a stair-step type function. At each time step of the dynamic solution, a net relative rotation θ is calculated for each beam element and the effective EI is determined from the EI/θ relationship for that rotation of each beam. The new stiffness is compared to the previous value for each beam and if there is any reduction in the local stiffness of any beam element, the local stiffness is adjusted and the global stiffness matrix is updated and the solution is continued.

The degradation is related to the direction of the deformation, where it is assumed that net positive internal deformation influences the stiffness for the positive rotation and a similar relationship holds for negative deformation, so there are two local stiffness matrices for each element; one for the positive deformation and one for the negative deformation. The appropriate stiffness values are adopted based on the direction of internal deformation of each individual element. This is based on the assumption that the degradation of stiffness is a result of cracking in the concrete or yielding of the steel. The location of the cracked concrete and the yielding steel depends on the direction of deformation, such that when the rotation is positive, assuming primary mode deflection governs, the degradation of stiffness of the whole beam results from cracking and yielding at one edge of the beam due to tensile stress, while a negative

rotation causes the other edge of the beam to degrade.

2.4.2   MDOF DAMPING

For the MDOF system, there are three types of damping that can be implemented using LPM/II:

2.4.2.1   Mass Damping

This type of damping assumes that the global damping matrix is proportional to the mass damping as given below:

$$[C] = \alpha[M] \qquad\qquad 2-9$$

Where α is the constant of proportionality. This damping matrix is usually diagonal and there is no coupling between different degrees of freedom. This formulation of the damping matrix provides different critical damping ratios for the various normal modes of vibration. The amount of damping for each mode is inversely proportional to the mode natural frequency following the relationship:

$$\delta_i = \frac{\alpha}{2\omega_i} \qquad\qquad 2-10$$

Where
δ_i :   Critical damping ratio for mode i

ω_i :   Undamped circular frequency for mode i

For modes with higher frequency, for a fixed value of α, the critical damping ratio is less than that of a lower frequency. So, mass damping is mainly a fundamental mode damper. Figure 2-7 shows the effect of mass damping on the response of a MDOF system as represented by the displacement at a height L_t of the system subjected to the excitation signal shown in Figure 2-6.

2.4.2.2 STIFFNESS DAMPING

Another type of proportional damping is stiffness damping and is defined as:

$$[C] = \beta [K] \qquad 2\text{-}11$$

Where β is the proportionality factor, this type assumes that the global damping matrix is proportional to the global stiffness matrix. This formulation is modal damping, where:

$$\delta_i = \frac{\beta \omega_i}{2} \qquad 2\text{-}12$$

So the damping ratio for a mode, is proportional to the frequency of this mode for any fixed value of β. Thus, this is mainly a higher mode damper. Figure 2-8 compares the response of the MDOF system subjected to stiffness damping compared to the undamped system.

2.4.2.3 NONUNIFORM DAMPING

This is a special form of proportional damping, where the global damping matrix is constructed in the same manner as the global stiffness matrix. The uncoupled damping matrix of each beam is proportional to the uncoupled stiffness matrix of that beam as given below:

where

$$[C]_k = \beta_k [S]_k \qquad 2\text{-}13$$

$[C]_k$:   Uncoupled damping matrix of k_{th} beam

$[S]_k$:   Uncoupled stiffness matrix of k_{th} beam

β_k :   Constant of proportionality of k_{th} beam

This form of damping provides different damping for different

2-6

beams. It has the flexibility to update the stiffness matrix and thus influence the damping matrix after some degradation of stiffness. But, it is assumed in this study that the damping of the beam elements is not proportional to the degrading stiffness of the element, but rather to the initial stiffness of each element. The damping increases if there is a degradation of stiffness, so the elements that are likely to experience more internal deformation, such as the bottom element which will have the most deformation for primary mode deflection. The effect of this type of damping is illustrated in Figure 2-9 showing the response for a system subjected to nonuniform damping compared to an undamped system.

TABLE 2-1
MATERIAL PROPERTIES OF
THE WALL PANEL

General Properties
  Material Model Parameter   =   1
  Poisson's Ratio of Masonry   = 1.6000E-01
  Thickness of Composite   = 7.6000E+00
  Weight Density of Composite   = 0.0000E-01

Compressive Properties
  Uniaxial Compressive Strength of Masonry   = 3.0000E+00
  Masonry Strain at Uniaxial Comp. Strength   = 2.2000E-03
  Shape Factor A(1), Rising Branch   = 2.0000E+00
  Shape Factor A(2), Falling Branch   = 2.0000E+00
  Shape Factor A(3), Exponential Limit   = 1.0000E-01
  Shape Factor A(4), Exponential Attach. Pt.   = 6.0000E-01
  Masonry Initial Compression Modulus   = 2.7273E+03
  Masonry Comp. Unloading Focal Point Factor   = 1.0000E+00
  Compression Damage Model No.   =   2

Tensile Properties
  Elastic Modulus of Masonry, Tension   = 3.0000E+03
  Cracking Strength of Masonry   = 1.0000E-01
  Tensile Cracking Strain of Masonry   = 3.3333E-05
  Tension Stiffening (TS) Model No.   =   2
  B(1), Exponential Limit, TS Model 2   = 0.0000E-01
  Exponent Alpha, TS Model 2   = 5.0000E-02

Reinforcement Properties
  Elastic Modulus of Reinforcement   = 2.9000E+04
  Bilinear Factor, Reinf. Plastic Modulus   = 2.0000E-02
  Plastic Modulus of Reinforcement   = 5.8000E+02
  Vertical Reinforcement Ratio   = 1.6400E-03
  Yield Stress of Vertical Reinforcement   = 6.5000E+01
  Yield Strain of Vertical Reinforcement   = 2.2414E-03
  Horizontal Reinforcement Ratio   = 1.6400E-03
  Yield Stress of Horizontal Reinforcement   = 6.5000E+01
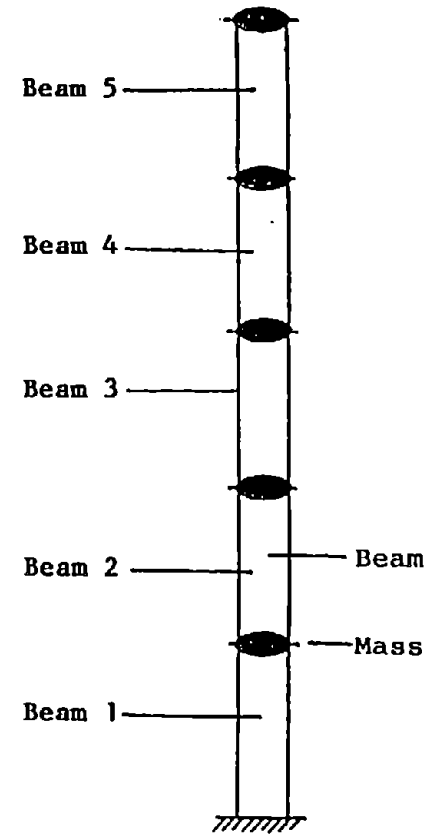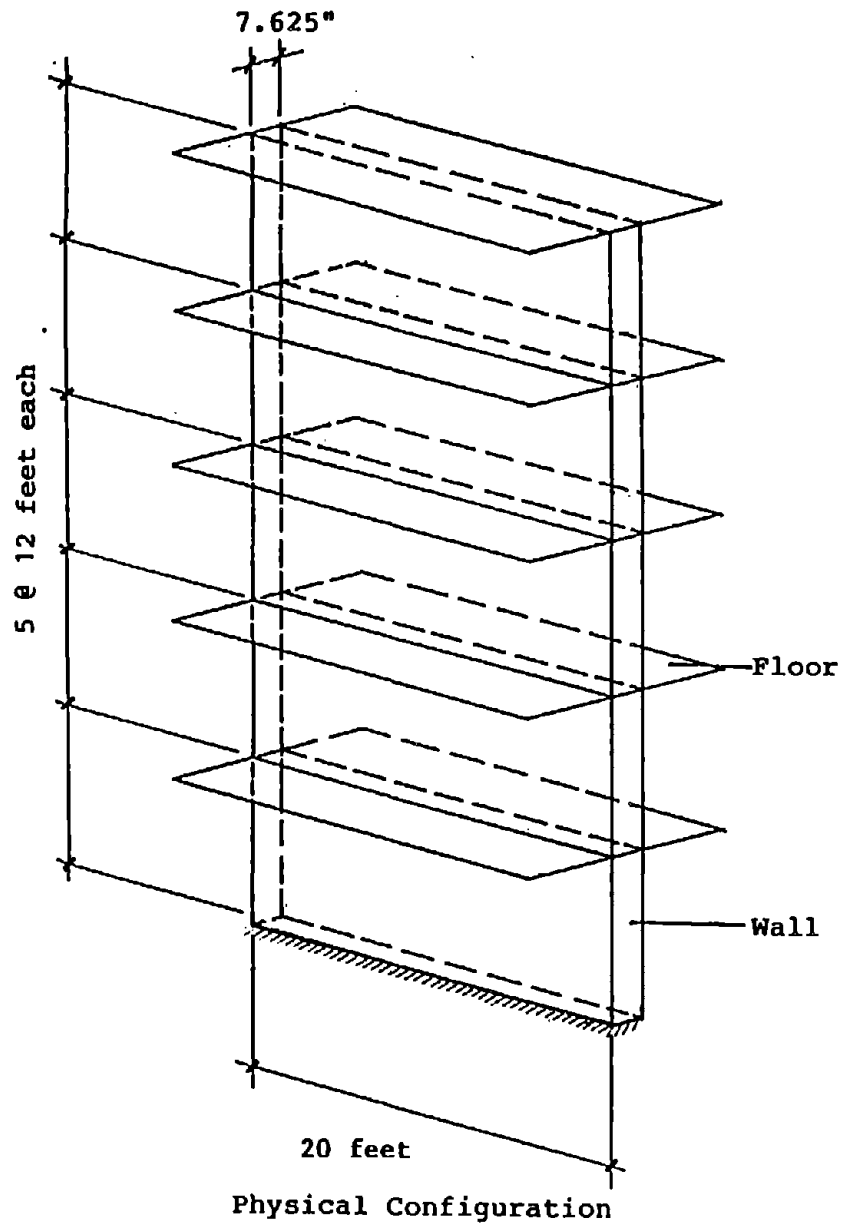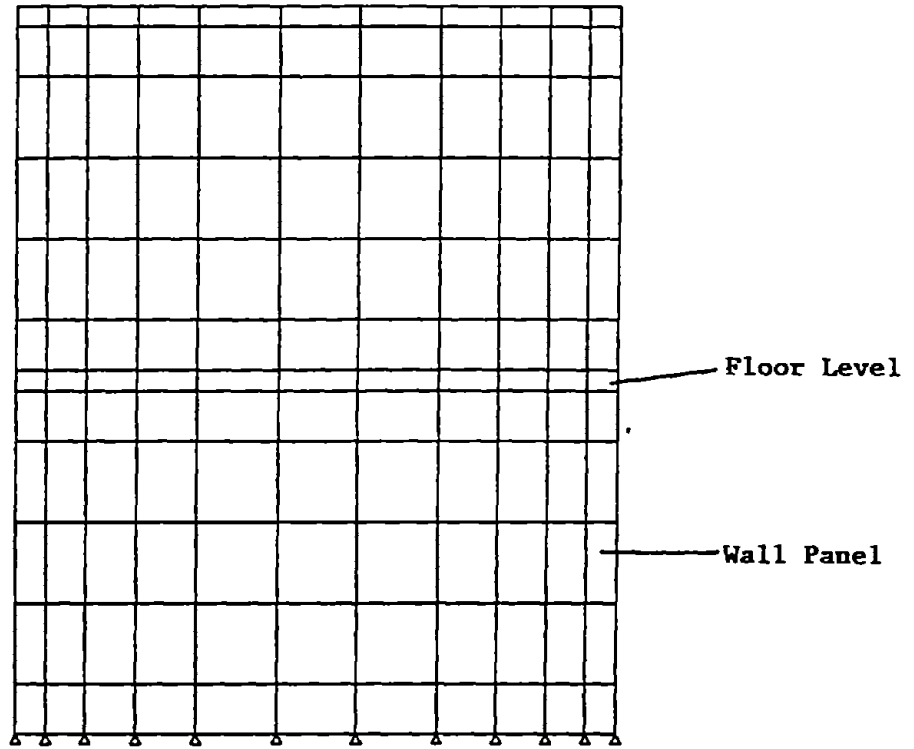 Yield Strain of Horizontal Reinforcement   = 2.2414E-03

TABLE 2-2
MATERIALS PROPERTIES OF
THE WALL AT THE FLOOR LEVEL

General Properties
Material Model Parameter   =   1
Poisson's Ratio of Masonry   = 1.6000E-01
Thickness of Composite   = 1.0000E+01
Weight Density of Composite   = 0.0000E-01

Compressive Properties
Uniaxial Compressive Strength of Masonry   = 3.0000E+00
Masonry Strain at Uniaxial Comp. Strength   = 2.2000E-03
Shape Factor A(1), Rising Branch   = 2.0000E+00
Shape Factor A(2), Falling Branch   = 2.0000E+00
Shape Factor A(3), Exponential Limit   = 1.0000E-01
Shape Factor A(4), Exponential Attach. Pt.   = 6.0000E-01
Masonry Initial Compression Modulus   = 2.7273E+03
Masonry Comp. Unloading Focal Point Factor   = 1.0000E+00
Compression Damage Model No.   =   2

Tensile Properties
Elastic Modulus of Masonry, Tension   = 3.0000E+03
Cracking Strength of Masonry   = 1.0000E-01
Tensile Cracking Strain of Masonry   = 3.3333E-05
Tension Stiffening (TS) Model No.   =   2
B(1), Exponential Limit, TS Model 2   = 0.0000E-01
Exponent Alpha, TS Model 2   = 5.0000E-02

Reinforcement Properties
Elastic Modulus of Reinforcement   = 2.9000E+04
Bilinear Factor, Reinf. Plastic Modulus   = 2.0000E-02
Plastic Modulus of Reinforcement   = 5.8000E+02
Vertical Reinforcement Ratio   = 1.6400E-03
Yield Stress of Vertical Reinforcement   = 6.5000E+01
Yield Strain of Vertical Reinforcement   = 2.2414E-03
Horizontal Reinforcement Ratio   = 5.2000E-02
Yield Stress of Horizontal Reinforcement   = 6.5000E+01
Yield Strain of Horizontal Reinforcement   = 2.2414E-03

2-9

7.625"

5 @ 12 feet each

—Floor

—Wall

20 feet

Physical Configuration

Beam 5

Beam 4

Beam 3

Beam 2 — —Beam

—Mass

Beam 1

Dynamic Model

FIGURE 2-1

Floor Level

Wall Panel

FIGURE 2-2   FINITE ELEMENT MESH FOR TWO PANELS

L   L

P_1

V

P_2

x

Loading Configuration

Δx_1

M

1   2

Δy_2

Y

x

θ
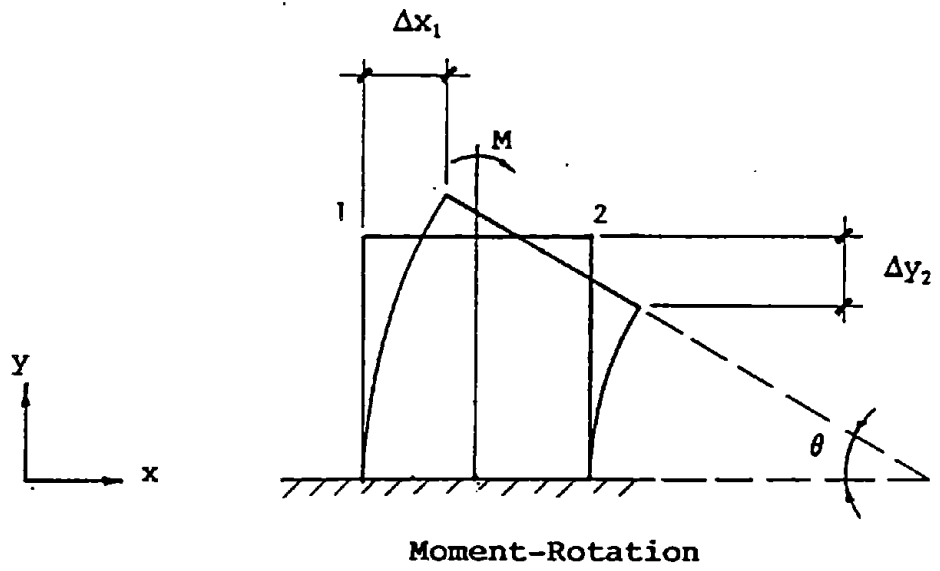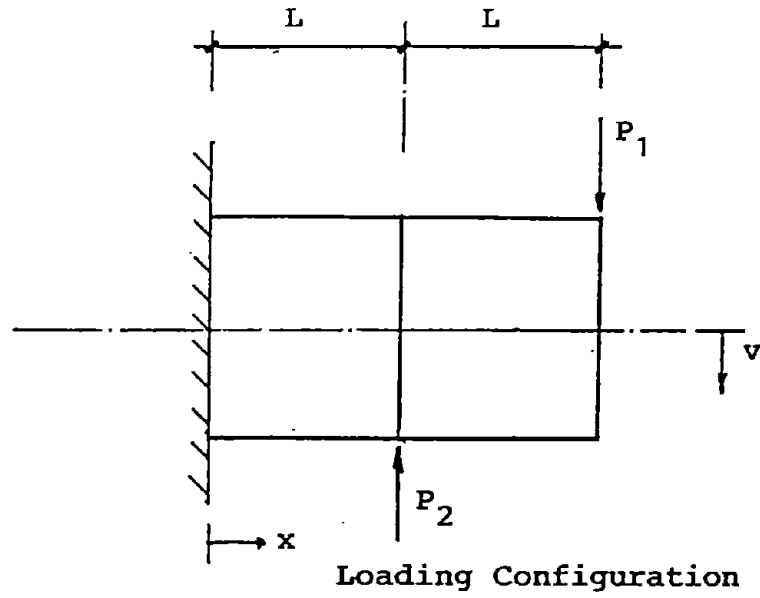
Moment-Rotation

FIGURE 2-3   LOADING AND DEFORMATION OF TWO-PANEL SYSTEM

2-12
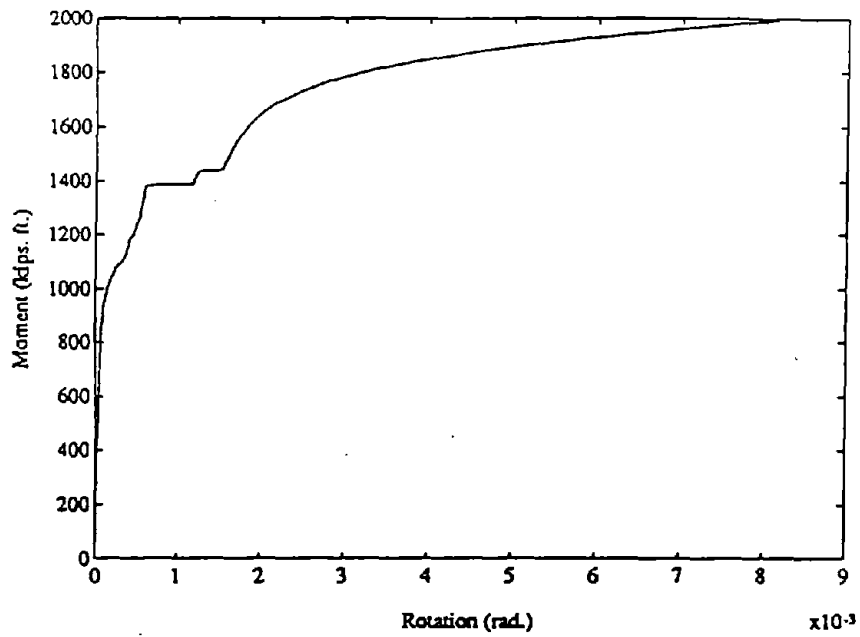
FIGURE 2-4 MOMENT ROTATION RELATIONSHIP FOR A WALL BEAM ELEMENT
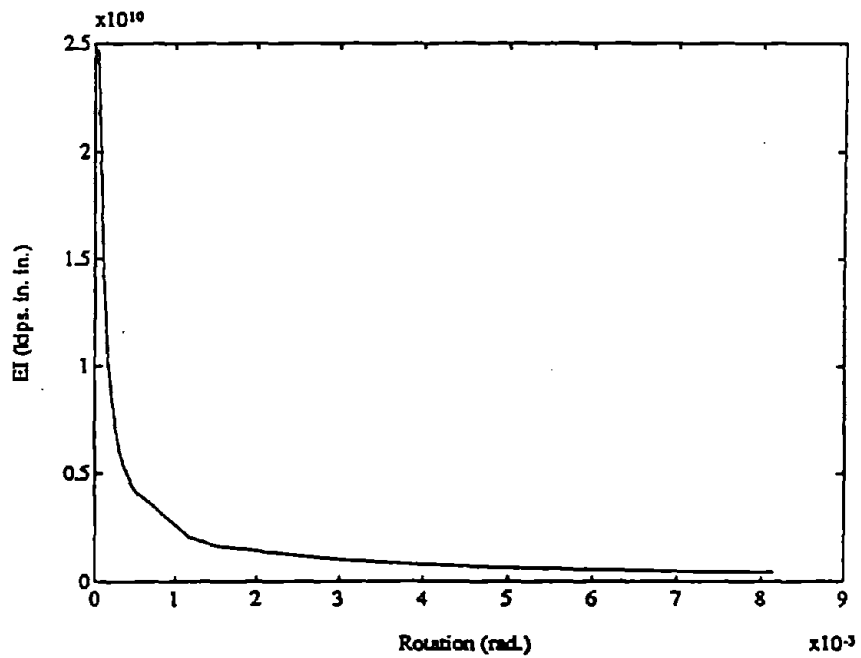
FIGURE 2-5 EI ROTATION RELATIONSHIP FOR A WALL BEAM ELEMENT

2-13
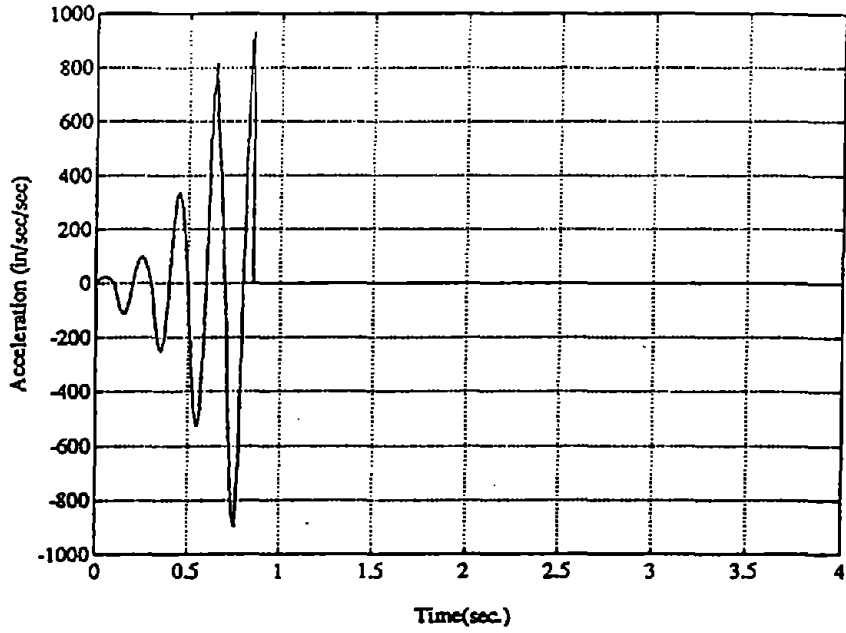
FIGURE 2-6   BASE EXCITATION SIGNAL
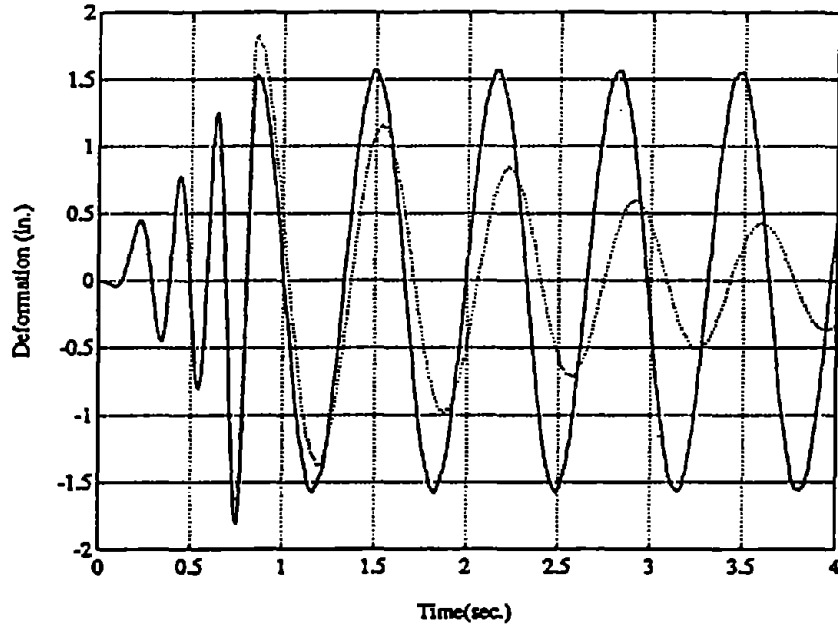
FIGURE 2-7   MDOF RESPONSE WITH ZERO DAMPING AND MASS
DAMPING OF $\alpha_m=0.95$
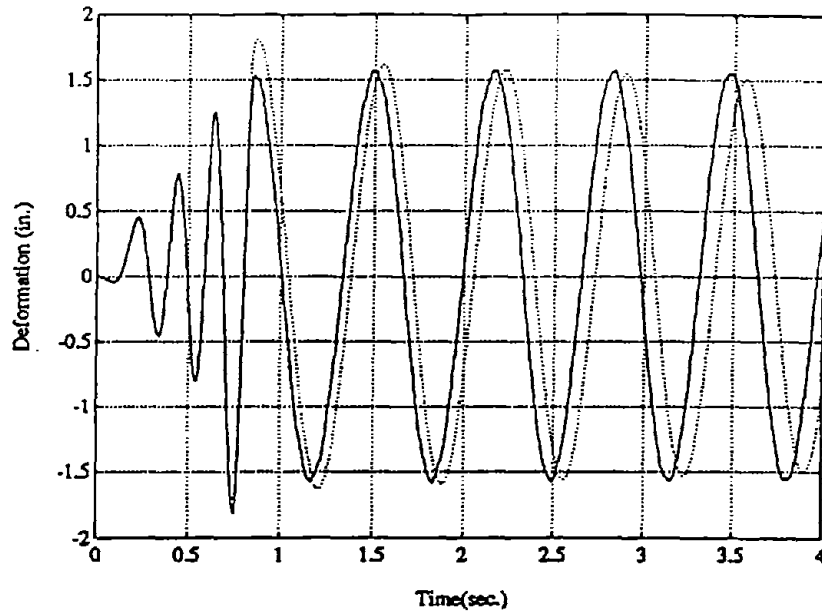
FIGURE 2-8 MDOF RESPONSE WITH ZERO DAMPING AND STIFFNESS
DAMPING OF $\beta=0.0007$
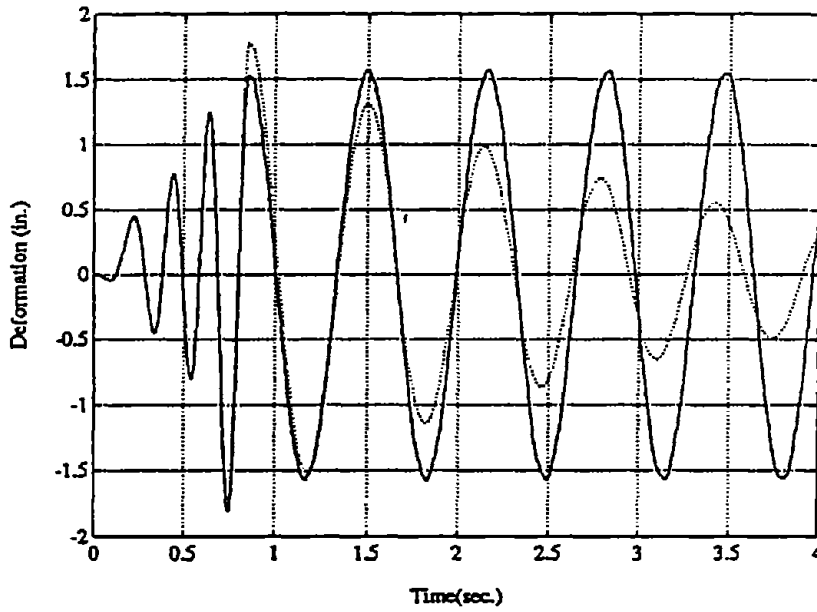
FIGURE 2-9   MDOF RESPONSE WITH ZERO DAMPING AND ELEMENT
DAMPING OF $\beta_k=0.0006$

SECTION 3

SPRING SYSTEM: HYSTERESIS MODEL

3.1 INTRODUCTION

The analysis of the nonlinearity of experimental test data of
reinforced masonry and reinforced concrete structures subjected to
cyclic loading suggests that a model is needed which has the
complexity to represent the physical behavior of the structure and
the capability to match the experimental response. This model has
the capability to produce analytical results that replicate the
experiments and thus improve the understanding of the dynamic
response of the reinforced concrete or masonry structures to
various dynamic loadings. In this chapter, the modified spring 11
(Appendix A, LPM/I, Kariotis, 1992) is adopted as the spring
system. The characteristics of this spring are described herein.
The performance of this spring under cyclic loading is demonstrated
for small and large deformations, emphasizing its stiffness
degradation and damping.

3.2 FORCE-DEFORMATION RELATIONSHIP

The stiffness obtained for the five story wall that represents the
multi-degree-of-freedom system was defined in terms of the moment
at the base versus the deformation at a particular height that is
to be defined later. The moment at the base can be a result of any
combination of loading at various levels of the structure.   A
triangular load configuration as shown in Figure 3-1 is adopted to
produce a deflection mode similar to the primary mode of vibration
of the structure. The load at each floor level is proportional to
the height of the floor. The moment at the base is equivalent to:

$$M = \sum_{r=1}^{N} F_r \times H_r \qquad\qquad 3-1$$

where

F_r :   Force at level r

H_r : Height at level r

N : Total number of floors

The force-deformation relationship describing a spring for an equivalent SDOF system represented by a single mass, M_e at an equivalent height, L_e is the single force F_e at that height as shown in Figure 3-1. This force would produce an equivalent base moment to the moment produced by triangular loading. Further description of the force-deformation relationship is presented in the next section.

3.3 HYSTERESIS MODEL

The general rules of the spring system are designed to simulate the actual response of the structure. The main phases that describe the cyclic behavior are loading, unloading and reloading. Initial loading follows the virgin envelope as would be determined by monotonic loading. This envelope was obtained from a monotonic test using a nonlinear finite element analysis program FEM, (Ewing, 1990). Triangular loading as shown in Figure 3-1 was used to apply loading on the mesh shown in Figure 3-2. Figures 3-3 and 3-4 show the virgin envelope representing the force-deformation relationship of this system as obtained from the finite element analysis. Figure 3-3 shows the moment as calculated using Equation 3-1 versus the lateral displacement at the top of the wall. Figure 3-4 shows the force F_e at a height L_e versus the lateral displacement X at the same height. This figure shows the comparison of the actual envelope obtained from FEM analysis to the LPM/I spring model.

The virgin envelope is defined in three regions; the first is an exponential curve modeling the transformation from elastic linear uncracked behavior to nonlinear post-yield behavior. The remaining two segments of straight lines describing the region of pre-peak compressive strain phase. Unloading follows a line that has a slope defined in terms of the initial stiffness, the peak force and the maximum deformation of the spring as follows:

$$K_u = K_i \left[\frac{F_p}{K_i E_{max}} \right]^\tau$$

where

K_u	:	Unloading Stiffness
K_i	:	Initial Stiffness
E_{max}	:	Maximum previous deformation
τ	:	Exponent. Ranges between 0.5 - 0.8 for concrete and masonry

The exponent τ controls the unloading slope where a higher value of τ indicates a steeper unloading path as shown in the variation of the unloading path in Figure 3-5. Reloading is defined in two phases depending on the sign of the deformation. The first region is defined between the zero force crossing and the deformation zero crossing as shown in Figure 3-5. In this region the force and deformation have opposite signs, and the reloading slope has a low value in this region that is dependent on the unloading stiffness and the pinching force. The pinching force is a principal factor in the amount of damping of the system since it influences the size of the loop. The second region of the reloading phase follows a straight line between the origin and the force on the stabilized envelope corresponding to the maximum deformation of the spring in the same direction. The stabilized envelope defines the maximum force in the spring at a displacement that has been reached in previous cycles. The value of this force depends on the maximum deformation in the history of the spring in the same direction, it is modeled as a fraction of the virgin envelope force for the same displacement. This fraction varies between unity at zero deformation to a user defined value ζ at the peak force. ζ usually varies between 0.7 - 0.9. This factor is significant since it controls the variations of reloading stiffness and the amount of energy dissipation under cyclic loading. The response of an SDOF system implementing this type of spring is controlled by two main components; stiffness degradation and energy dissipation.

3.3.1   Stiffness Degradation

The stiffness of the spring at any particular deformation is defined as the secant stiffness. Generally, the virgin envelope controls the magnitude and the rate of degradation of the stiffness for a monotonic test. Cyclic loading causes a different rate of degradation of stiffness. The stabilized curve indicates that an additional loss of stiffness is encountered on recycling to the same internal deformation in the spring. The system's natural frequency evaluated using the final stiffness of the degraded system compared to the natural frequency of the system with undegraded stiffness gives an indication of the amount of degradation. It also provides means of comparisons between a MDOF system and an equivalent SDOF system.

3.3.2   ENERGY DISSIPATION

This component is highly sensitive to many parameters. It is difficult to obtain from a dynamic test. The variation of the amount of energy loss in each cycle makes it difficult to implement an average value in a non-hysteretic model. The energy loss per cycle can be expressed in terms of an equivalent viscous damping coefficient, or more conveniently, it is expressed in terms of the critical damping ratio as (Clough, 1975):

$$\delta = \frac{W_D}{4\pi W_s} \qquad\qquad 3\text{-}3$$

where:

δ :   Critical damping ratio

W_s :   Area under the force-displacement diagram.

W_D :   Total area within a complete loop.

Figure 3-6 demonstrates W_s and W_D. W_D is the energy loss per cycle. W_s is a measure of the work done by the spring such that:

W_s = $\frac{1}{2} Kx^2$.

The quantity of energy dissipated in a cyclic variation with the

3-4

unloading slope is represented in Figure 3-7 as a variation of the critical damping ratio with τ - the unloading exponent. A lower value of τ indicates a steeper unloading path. Figure 3-7 shows the damping ratio for two cycles with a maximum displacement of 3 inches. The first cycle represents the virgin state of the spring while the second cycle shows damping for the stabilized curve. Equation 3-2 shows that a smaller τ will produce a steeper unloading slope. This will increase the area within the loop thus increasing W_D while keeping W_S constant, thus increasing the critical damping ratio. Figure 3-8 shows an increase in the damping for higher pinch force. An increase in the pinch force produces a larger area within the cycle, W_D, while leaving leaving W_S unchanged and subsequently increasing the critical damping ratio. There is very little variation in the amount of energy dissipation with the variations of the stabilized curve ratio as shown in Figure 3-9, since the increase in the stabilized force introduces relatively comparable increases in both W_D and W_S. Tables 3-1 and 3-2 show the variation of damping as a function of the maximum deformation of the spring for various displacement combinations. For typical spring parameters, the amount of damping increases with the maximum displacement as shown in Table 3-2, where the damping for 6 inches of maximum displacement is greater than the damping of smaller displacements, for both the first and second cycles. The damping for a cycle depends also on the maximum deformation the spring has experienced previously. This is shown in Table 3-2. A second cycle of 3 inches that had a previous cycle of 6 inches, had higher damping than that shown for two successive cycles of 3 inches. This is also illustrated in Figure 3-10. This is due to degradation of stiffness that causes W_s to decrease more severely than the W_D, since W_D represented by the total area within the loop and are controlled by three variables, namely; the degraded stiffness, the unloading slope and the pinch force, while W_S is controlled by the degraded stiffness only. Thus, for a larger displacement the reloading stiffness degrades and is more influenced than the unloading slope, and the pinch force is not affected. One important aspect of damping in hysteresis models is

3-5

that damping forces start taking effect once unloading starts. There is no damping forces during loading on the virgin state of the spring.

A displacement sequence is generated to further understand the damping of hysteresis loops. This displacement sequence is shown in Figure 3-11. Two springs with their characteristics listed in Table 3-3 are subjected to this displacement sequence and their force-deformation plots are shown in Figures 3-12 and 3-13. The critical damping ratios for each cycle are presented in Table 3-4 for springs that have low damping and have typical damping.

3.4   SDOF DAMPING

The hysteresis loops of the SDOF system cause nonuniform damping. Each cycle has a different damping that is dependent on the maximum deformation as well as the history of the spring. To investigate the effects of hysteresis damping of the SDOF system an acceleration signal, shown in Figure 3-11, is applied as base excitation to displace the mass. The free vibration response of the mass is monitored. Figure 3-14 shows the relative displacement of the mass for two springs with different characteristics. One spring has minimum damping while the other has a higher value that is representative of a more typical structure. The percentage of critical damping ratios of both springs are estimated for each cycle using the logarithmic decrement method, so:

$$\delta = \frac{1}{2\omega} \ln\left(\frac{x1}{x2}\right) \qquad\qquad 3\text{-}4$$

where

δ	:	Fraction of critical damping ratio
x1	:	The peak of a cycle
x2	:	The peak of the following cycle

The damping ratios as percentages of the critical damping are listed in Table 3-5 for each cycle.

TABLE 3-1

DAMPING AS A PERCENTAGE OF CRITICAL DAMPING
FOR VARIOUS TWO-CYCLE DISPLACEMENTS.
SPRING PARAMETERS: F_{pin}=0.1 KIPS, ζ=0.99, AND γ=0.999.
LOW DAMPING SPRING

DISPLACEMENT (IN.)		DAMPING PERCENTAGE	
1ST CYCLE	2ND CYCLE	1ST CYCLE	2ND CYCLE
0.3	0.3	14.3	6.4
0.7	0.7	16.3	5.5
1.0	1.0	16.3	5.0
3.0	3.0	13.7	2.6
6.0	6.0	13.3	1.6
6.0	3.0	13.3	1.6
6.0	1.0	13.3	1.6
3.0	1.0	13.7	2.7
3.0	6.0	13.7	8.2

TABLE 3-2

DAMPING AS A PERCENTAGE OF CRITICAL DAMPING
FOR VARIOUS TWO-CYCLE DISPLACEMENTS. SPRING PARAMETERS:
F_{pin}=5.0 KIPS, ζ=0.75, AND γ=0.5
HIGH DAMPING SPRING

DISPLACEMENT (IN.)		DAMPING PERCENTAGE	
1ST CYCLE	2ND CYCLE	1ST CYCLE	2ND CYCLE
0.3	0.3	17.7	10.5
0.7	0.7	22.5	12.7
1.0	1.0	23.6	13.4
3.0	3.0	24.6	14.9
6.0	6.0	25.9	15.9
6.0	3.0	25.9	18.0
6.0	1.0	25.9	33.5
3.0	1.0	24.6	19.7
3.0	6.0	24.6	20.5

TABLE 3-3

MATERIAL PROPERTY DATA FOR
NONLINEAR SPRING

SPRING 1 (LOW DAMPING)

SPRING INITIAL STIFFNESS, K1 (S1)	=	3.600E+02
GAP	=	0.000E-01
SPRING CONSTANT, EP1	=	2.350E+00
PEAK DEFORMATION, EP2	=	6.306E+00
1st BREAK POINT FORCE, FP1	=	4.252E+01
2nd BREAK POINT DEFORMATION, FP2	=	4.758E+01
PINCH FORCE, FPIN	=	1.000E-03*
UNLOADING CONSTANT GAM	=	9.990E-01*
POST PEAK COEFFICIENT BET	=	2.000E-01
STRENGTH DEGRADATION CONSTANT ZET	=	9.990E-01*
MAXIMUM DEFORMATION (EM)	=	2.000E+01
SHEAR ENVELOPE DISP	=	0.000E-01
VELOCITY EXPONENT FOR CV, EXPCV	=	0.000E-01
COULOMB DAMPING COEFFICIENT, CC	=	0.000E-01
FORCE TIME HISTORY NUMBER FOR CC	=	0.000E-01
NONLINEAR SPRING NUMBER FOR CC	=	0.000E-01
UNUSED COEFFICIENT	=	0.000E-01
TAU (ENVEL. CONSTANT)	=	9.000E-01
KAPPA (ENVEL. CONSTANT)	=	2.000E-01

SPRING 2 (TYPICAL DAMPING)

SPRING INITIAL STIFFNESS, K1 (S1)	=	3.600E+02
GAP	=	0.000E-01
SPRING CONSTANT, EP1	=	2.350E+00
PEAK DEFORMATION, EP2	=	6.306E+00
1st BREAK POINT FORCE, FP1	=	4.252E+01
2nd BREAK POINT DEFORMATION, FP2	=	4.758E+01
PINCH FORCE, FPIN	=	1.500E-00*
UNLOADING CONSTANT GAM	=	9.000E-01*
POST PEAK COEFFICIENT BET	=	2.000E-01
STRENGTH DEGRADATION CONSTANT ZET	=	8.000E-01*
MAXIMUM DEFORMATION (EM)	=	2.000E+01
SHEAR ENVELOPE DISP	=	0.000E-01
VELOCITY EXPONENT FOR CV, EXPCV	=	0.000E-01
COULOMB DAMPING COEFFICIENT, CC	=	0.000E-01
FORCE TIME HISTORY NUMBER FOR CC	=	0.000E-01
NONLINEAR SPRING NUMBER FOR CC	=	0.000E-01
UNUSED COEFFICIENT	=	0.000E-01
TAU (ENVEL. CONSTANT)	=	9.000E-01
KAPPA (ENVEL. CONSTANT)	=	?.000E-01

*Variable properties affecting the damping.

TABLE 3-4

DAMPING AS A PERCENTAGE OF CRITICAL DAMPING
FOR DISPLACEMENT SEQUENCE. SPRING 1 PARAMETERS:
F_{pin}=0.1 KIPS, $\digamma$=0.99, AND γ=0.999. LOW DAMPING.
SPRING 2 PARAMETERS: F_{pin}=5.0 KIPS, $\digamma$=0.75, AND γ=0.5
HIGH DAMPING

NO.	CYCLE DISPLACEMENT (IN.)	DAMPING PERCENTAGE SPRING 1	SPRING 2
1	1.0	16.1	18.1
2	1.0	4.8	7.32
3	2.0	8.9	11.9
4	2.0	3.1	6.9
5	3.0	6.7	9.7
6	3.0	2.3	7.0
7	4.0	5.4	8.3
8	4.0	1.9	7.4
9	5.0	4.2	6.8
10	5.0	1.5	7.6
11	6.0	3.3	6.0
12	6.0	1.1	7.9
13	5.0	1.1	7.9
14	4.0	1.1	8.0
15	3.0	1.1	8.2
16	2.0	1.1	8.5
17	1.0	1.1	9.9

TABLE 3-5

PERCENTAGE OF CRITICAL DAMPING FOR SUCCESSIVE
CYCLES OF SPRING SYSTEMS EVALUATED USING
THE LOGARITHMIC DECREMENT METHOD

CYCLE NO.	DAMPING PERCENTAGE SPRING 1	SPRING 2
1	4.0	8.2
2	4.3	9.9
3	4.3	11.1
4	4.3	19.3

F5

F4

F3

F2

F1

M

H1 H2 H3 H4 H5

MDOF Triangular Loading

F_e

M_e

X

L_e

Equivalent SDOF

M_e

Spring

Dynamic Model
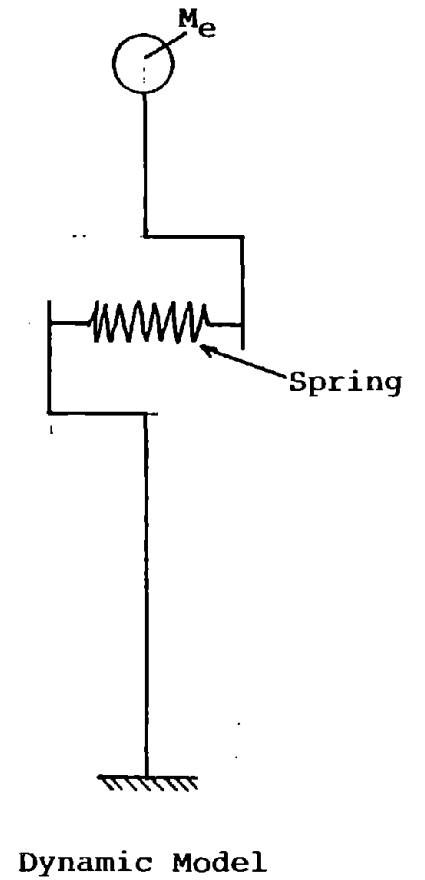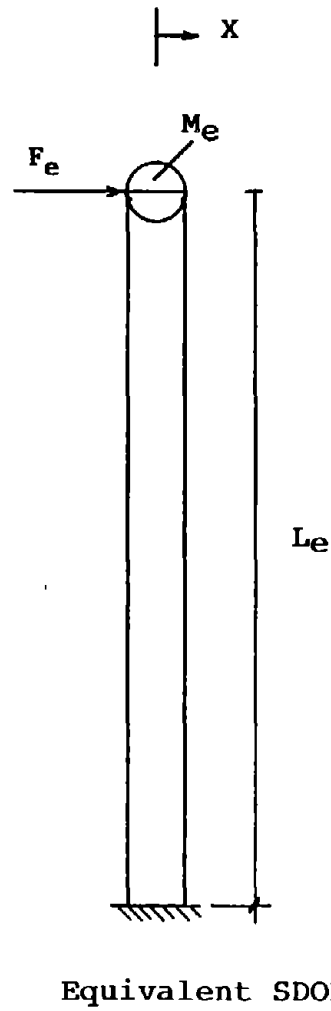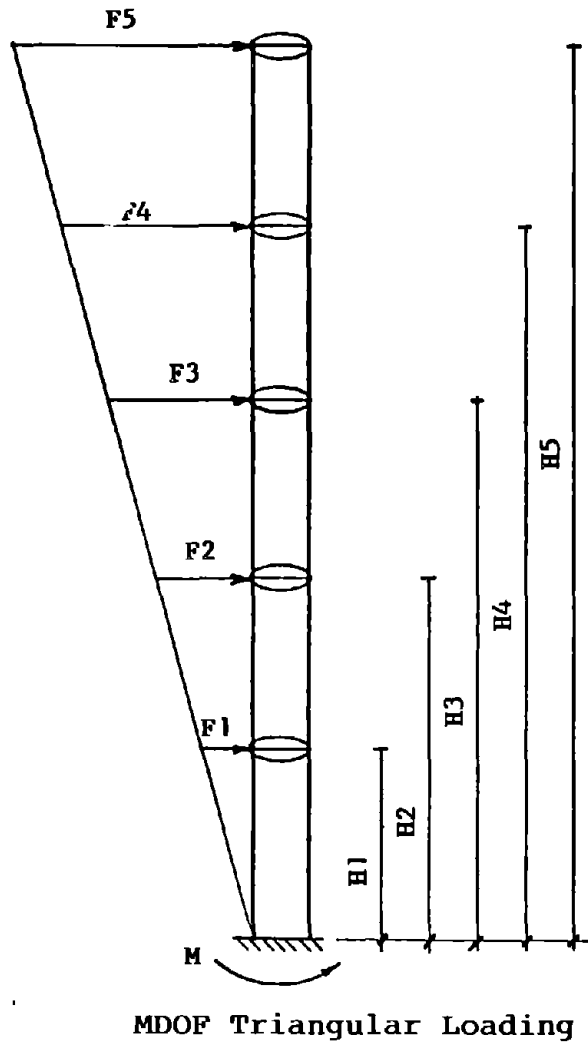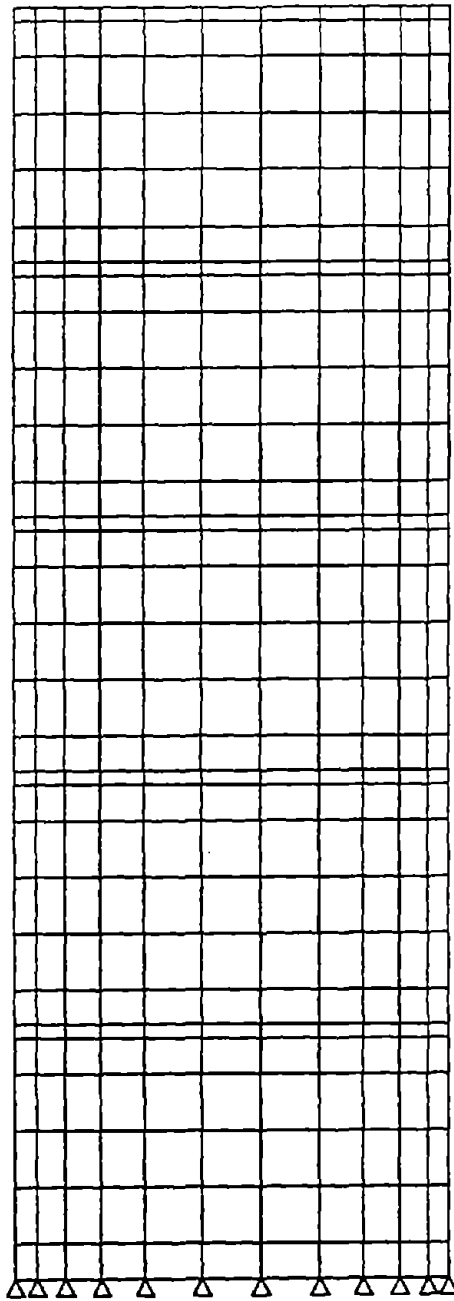
FIGURE 3-1

FIGURE 3-2 FINITE ELEMENT MESH FOR THE FIVE-STORY WALL
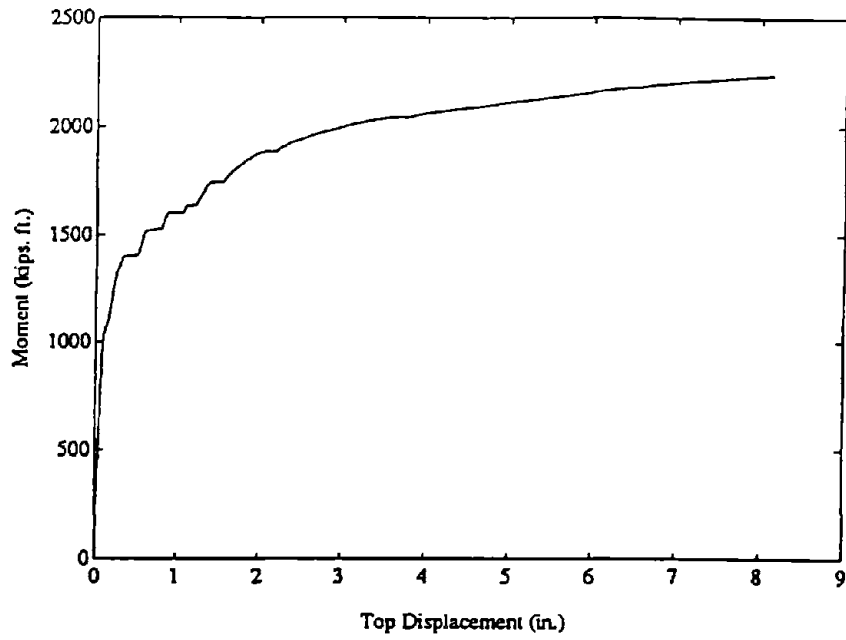
FIGURE 3-3   BASE MOMENT VS. TOP DISPLACEMENT FOR THE WALL
                    USING TRIANGULAR LOADING
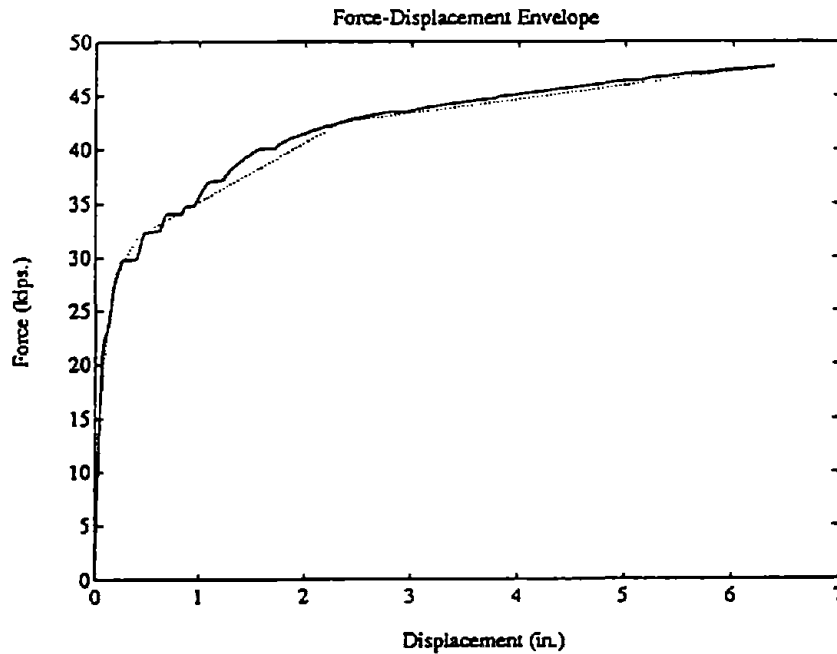
FIGURE 3-4   MONOTONIC VIRGIN ENVELOPE FOR THE WALL RELATING THE
                    FORCE AND DISPLACEMENT OF THE SPRING SYSTEM AT
                    HEIGHT L_c.   SOLID LINE REPRESENTS THE FEM ENVELOPE

3-12
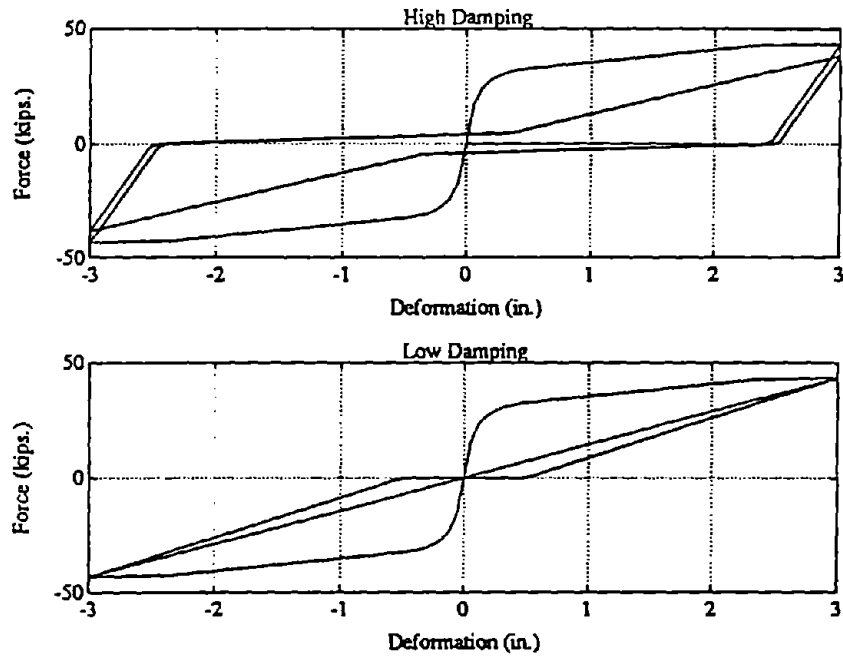
FIGURE 3-5   THE EFFECT OF THE VARIATION OF THE SPRING
CHARACTERISTICS ON THE BEHAVIOR OF THE SPRING
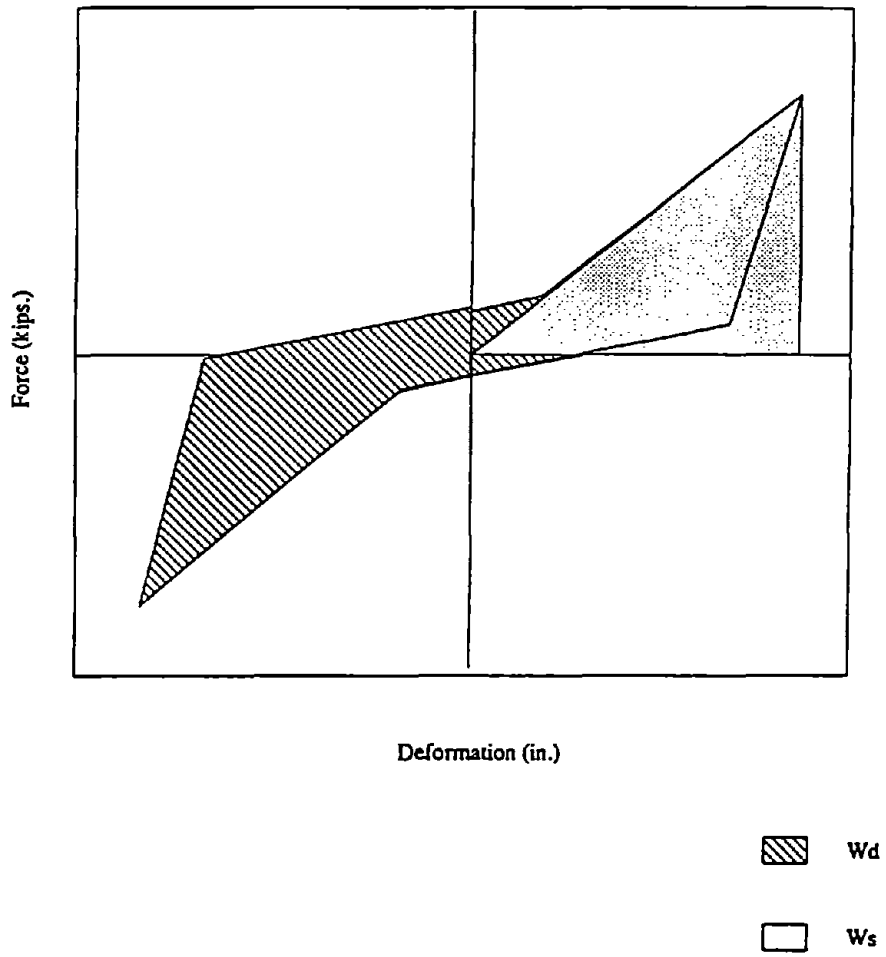
FIGURE 3-6   THE DAMPER AND SPRING ENERGY FOR EVALUATION OF
CRITICAL DAMPING RATIO FROM HYSTERESIS LOOPS
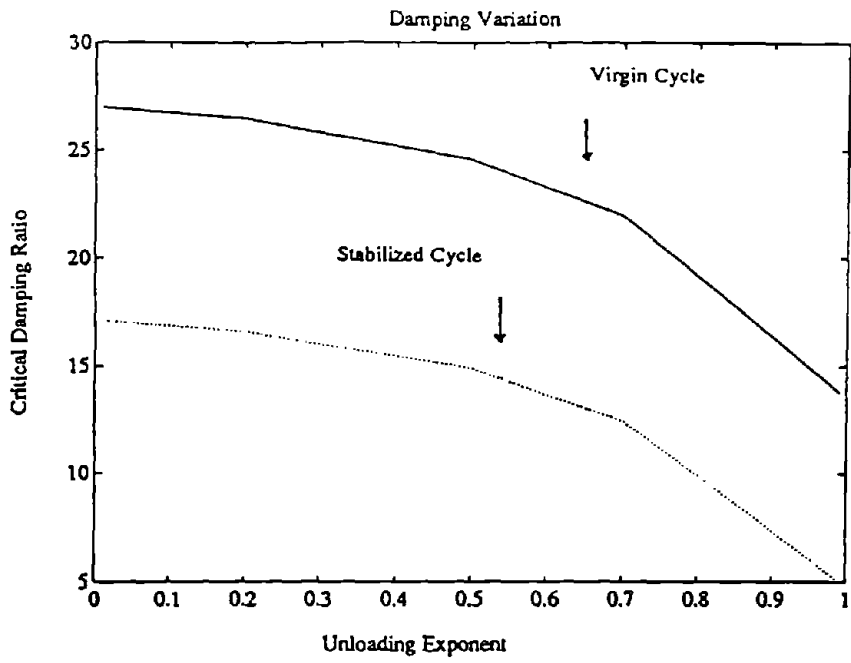
FIGURE 3-7   VARIATION OF DAMPING WITH UNLOADING SLOPE EXPONENT τ
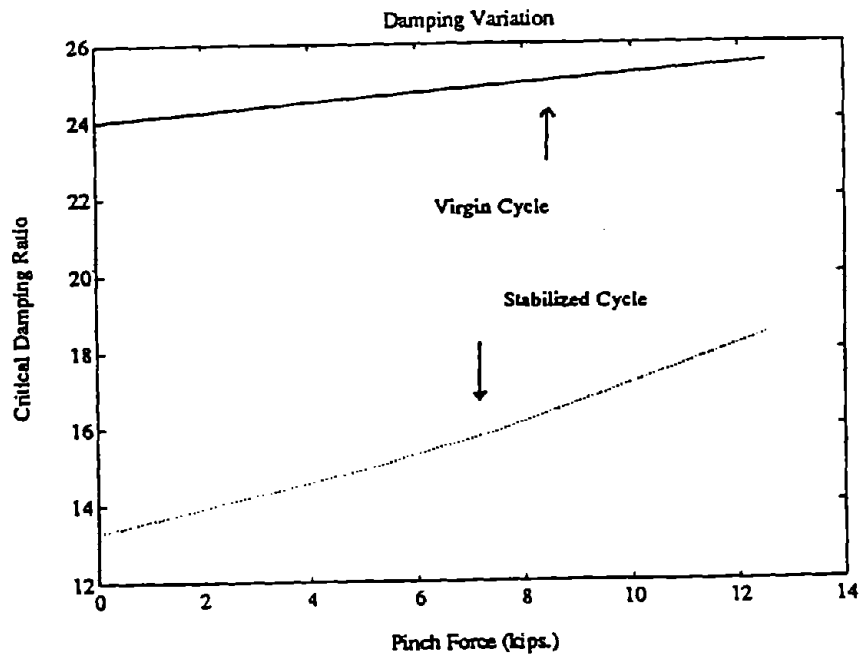
FIGURE 3-8   VARIATION OF DAMPING WITH PINCH FORCE F_{pin}

3-15
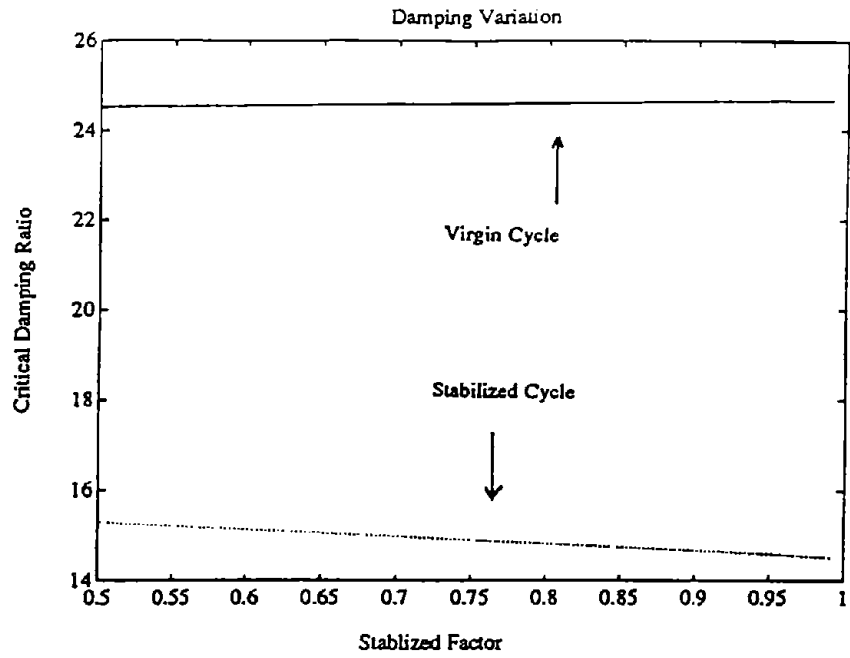
Damping Variation

FIGURE 3-9   VARIATION OF DAMPING WITH STABILIZED CURVE FACTOR ζ

Force-Deformation
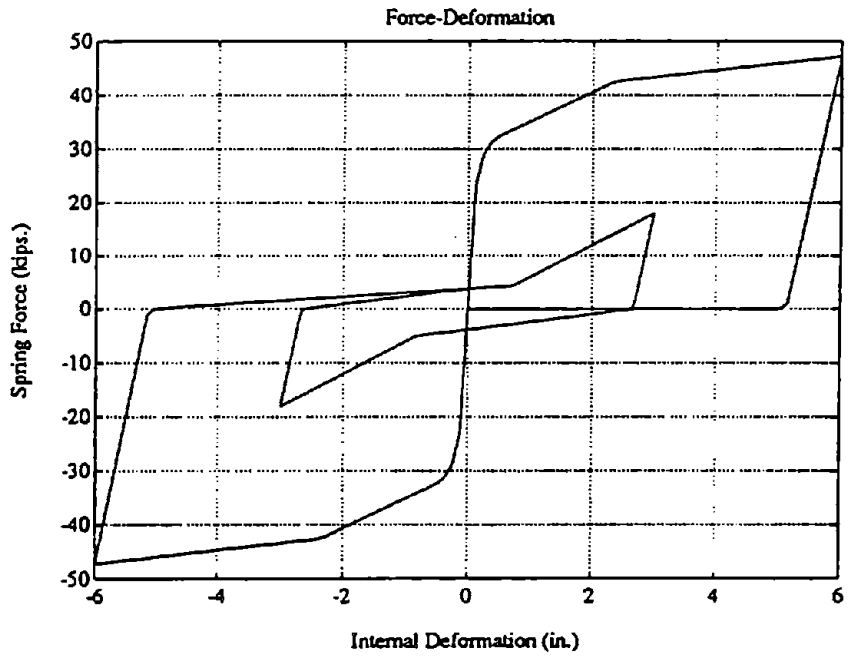
FIGURE 3-10   TWO CONSECUTIVE CYCLES OF 6 AND 3 INCHES RESPECTIVELY

Displacement Sequence for Spring
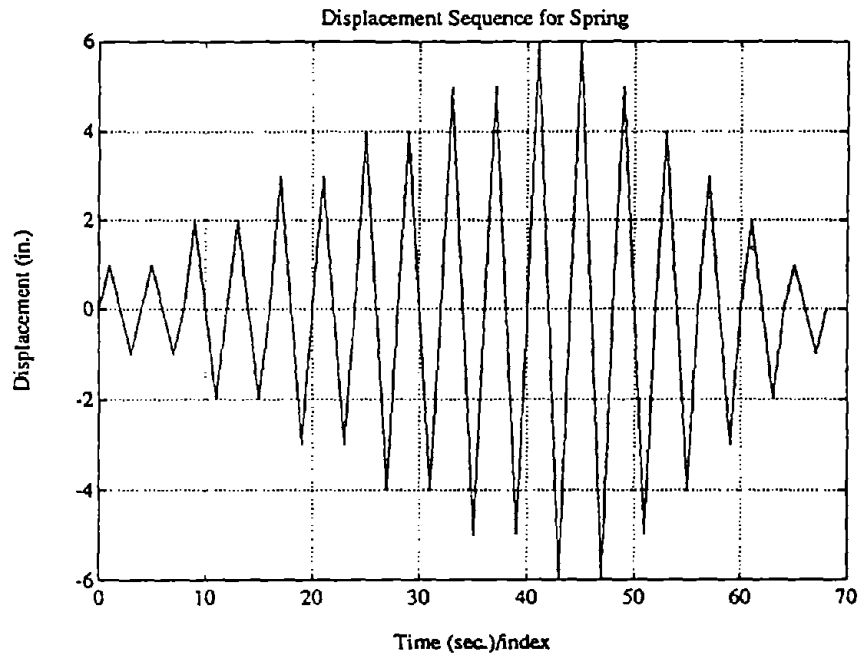
FIGURE 3-11   DISPLACEMENT SEQUENCE FOR SPRING SYSTEM

Force-Deformation
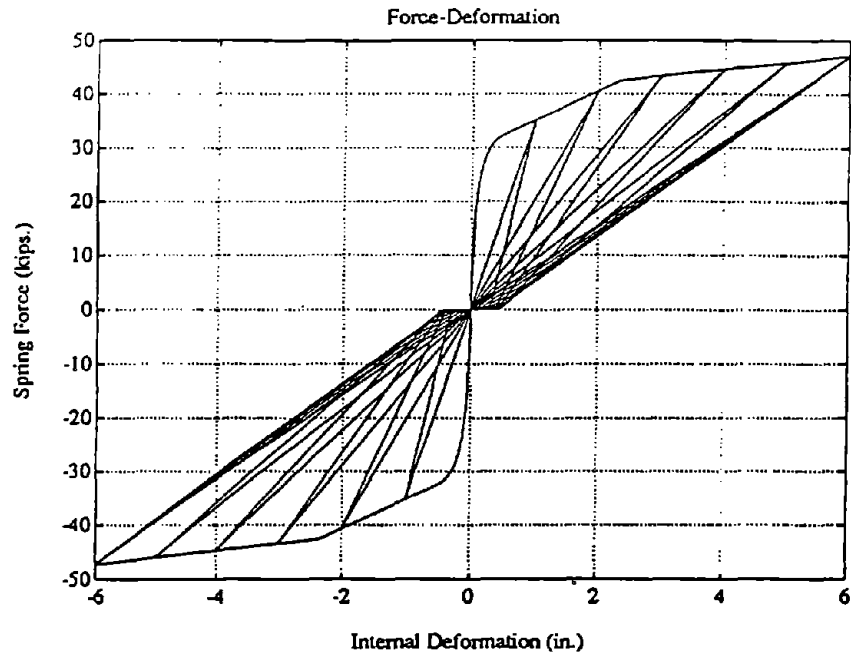
FIGURE 3-12   SPRING CYCLES WITH LOW DAMPING CHARACTERISTICS

Force-Deformation
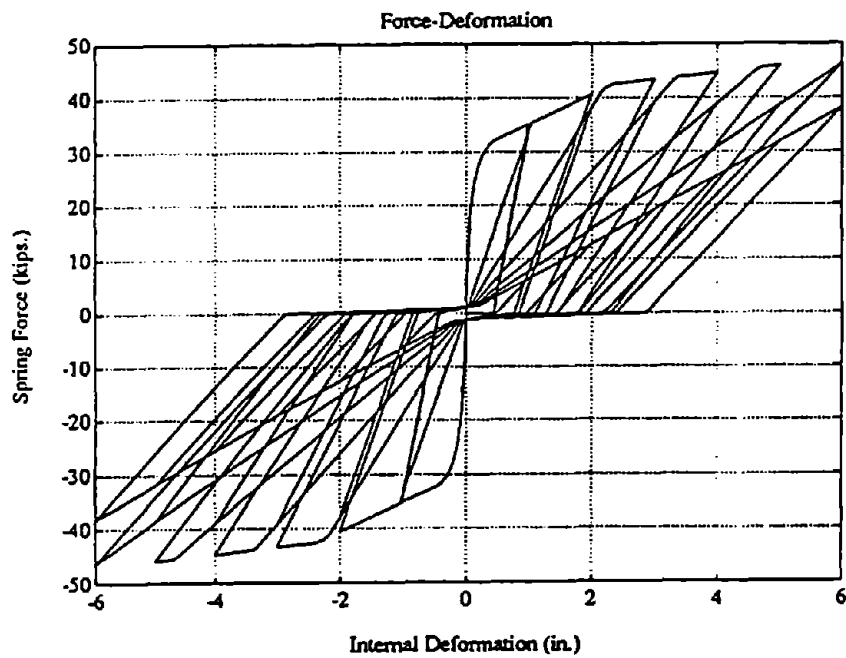
FIGURE 3-13   SPRING CYCLES WITH HIGH DAMPING CHARACTERISTICS

3-18
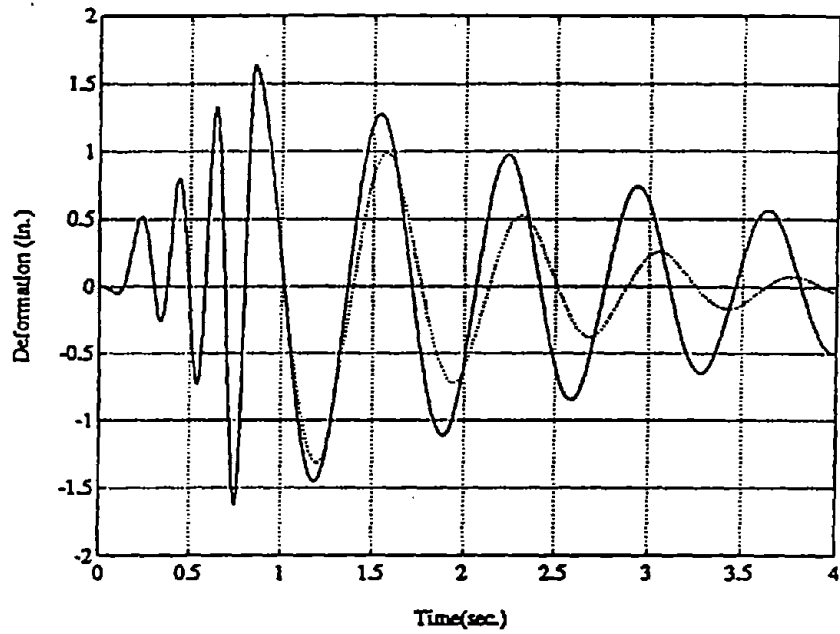
FIGURE 3-14   SDOF RESPONSE FOR TWO DIFFERENT SPRING SYSTEMS
               EXHIBITING LOW AND HIGH DAMPING. LOW DAMPING
               SOLID LINE

SECTION 4

EQUIVALENT MODEL

4.1 INTRODUCTION

This chapter introduces the two models being compared, a multi-degree-of-freedom system representing five story structure, and an equivalent single-degree-of-freedom Q-model. The behavior and responses of both models are presented in this section. Various excitations and material nonlinearities were implemented in this investigation.

4.2 Q-MODEL

The MDOF model as described in Section 2 has five lumped masses connected by beam elements with degrading stiffness as shown in Figure 2-5. This system is subjected to ground motions with acceleration $\ddot{X}_g$. This is equivalent to a set of forces applied at each mass equivalent to $M\ddot{X}_g$.

The differential equations of motion for an undamped MDOF system can be expressed as:

$$[M][\ddot{X}] + [K][X] = [F] \qquad\qquad 4\text{-}1$$

where
M	:	Mass matrix
K	:	Stiffness matrix
X	:	Response vector
F	:	External force vector

An equivalent SDOF model representing equation 4-1 can be expressed in several ways. Biggs (1964) derived a simple expression describing the equivalent system as:

$$\alpha_m M_e \ddot{X} + \alpha_l Kx = \alpha_l F_t \qquad\qquad 4\text{-}2$$

where

α_l : $[\Sigma^N_{r=1} \; F_i \phi_i]/F_t$

α_m : $[\Sigma^N_{r=1} \; M_i \phi^2_i]/M_t$

M_t :   Total mass

x :   Relative displacement of equivalent mass

K :   Stiffness of original system

F_t :   Total external force

F_i .:   External force at level i

M_i :   Mass at level i

ϕ_i :   Mode shape coefficient at level i with top displacement normalized to unity.

The external force is represented by ground motion. This is equivalent to a set of forces applied at each mass so:

$$F_i = M_i \ddot{X}_g \qquad\qquad 4\text{-}3$$

and

$$F_t = \sum^N_{r=1} M_i \ddot{X}_g = M_t \ddot{X}_g \qquad\qquad 4\text{-}4$$

so Equation 4-2 becomes:

$$M_e \ddot{X} + Kx = -M_t \ddot{X}_g \qquad\qquad 4\text{-}5$$

where

$$M_e = [\alpha_m/\alpha_l] M_t \qquad\qquad 4\text{-}6$$

M_e is the equivalent mass of the SDOF system. It is a function of the distribution of masses and the mode shape coefficients of the selected mode. For structures subjected to earthquakes, the

deflected shape of the MDOF system is closely matched with the primary mode of the structure. M_e will be located at a height L_e, where:

$$L_e = \sum_{r=1}^{N} M_i \phi_i h_i / \sum_{r=1}^{N} M_i \phi_i \qquad \text{4-7}$$

where N is number of floors.

The ground motion for the MDOF system is equivalent to $M\ddot{X}_g$. This will produce a moment at the base equivalent to:

$$\text{Moment} = \sum_{r=1}^{N} M_r \ddot{X}_g H_r \qquad \text{4-8}$$

This moment should be equivalent to the moment calculated for the equivalent SDOF system. Ground motion applied to the SDOF system is equivalent to a force $M_e \ddot{X}_g$ applied at a height L_e from the base, so the moment is equivalent to:

$$\text{Moment} = M_e \ddot{X}_g L_e \qquad \text{4-9}$$

In order to obtain equal moment at the base of the two systems, the SDOF and the MDOF models, we introduce a factor for the ground motion, such that:

$$C[M_e \ddot{X}_g L_e] = \sum_{r=1}^{N} M_r \ddot{X}_g H_r \qquad \text{4-10}$$

or

$$C = \sum_{r=1}^{N} M_r H_r / M_e L_e \qquad \text{4-11}$$

The stiffness is determined from the moment deflection

4-3

relationship, such that the term Kx represents the spring system forces. This is evaluated by applying a triangular load on the MDOF system such that the load of each level is proportional to the height of that level. This system of forces produces a moment at the base which is equivalent to a force at L_e multiplied by L_e. The equivalent force is conveniently located at the equivalent mass level, such that:

$$F = \text{Moment}/L_e \qquad\qquad 4-12$$

The deformation has to be at the same height as the force L_e. It can be evaluated either by directly monitoring the displacement at L_e if it coincides with a floor level, or by linear interpolation if L_e is between levels. The stiffness is defined as the force necessary to produce a unit displacement at level L_e, which is illustrated by the force-deformation plot in Figure 3-4.

4.3 APPLICATION EXAMPLE

The MDOF system described in Section 2 is adopted as an application example. The linear system has the following properties:

$$m = \frac{30}{386.4} = 0.0776 \ \text{k-sec}^2/\text{inch.} \qquad\qquad 4-13$$

$$[\phi]_1^T = [0 \quad 0.06 \quad 0.22 \quad 0.45 \quad 0.72 \quad 1.0] \qquad\qquad 4-14$$

α_m and α_L as defined by Equation 4-2 are:

$$\alpha_m = 0.3544 \qquad\qquad 4-15$$

$$\alpha = 0.4904 \qquad\qquad 4-16$$

so:

$$M_e = 0.2804 \ k\text{-}sec^2/inch.$$
4-17

and:

$$L_e = 47.088 \ feet$$
4-18

The beams rigidity EI, is a function of the deformation and is defined in Figure 2-5.

The validity of the Q-model representation was examined for the linear system by assuming that the beams have a non-degrading properties (i.e. constant EI). The stiffness of the MDOF is equivalent to:

The SDOF stiffness defined as the force necessary to produce a unit displacement at height L_e is:

$$K = \frac{3EI}{L^3} = \frac{3 \ x \ 2.45 \ x \ 10^9}{(47.1 \ x \ 12)^3} = 40.7 \ k/inch.$$
4-20

$$EI = 2.45 \ x \ 10^9 \ k\text{-}inch.^2$$
4-19

Using these values the response of both the MDOF and the SDOF systems are shown in Figure 4-1. The second graph on the plots shows the difference between the two responses.

SDOF
DEFLECTION OF EQUIVALENT MASS

MDOF
DEFLECTION AT Le
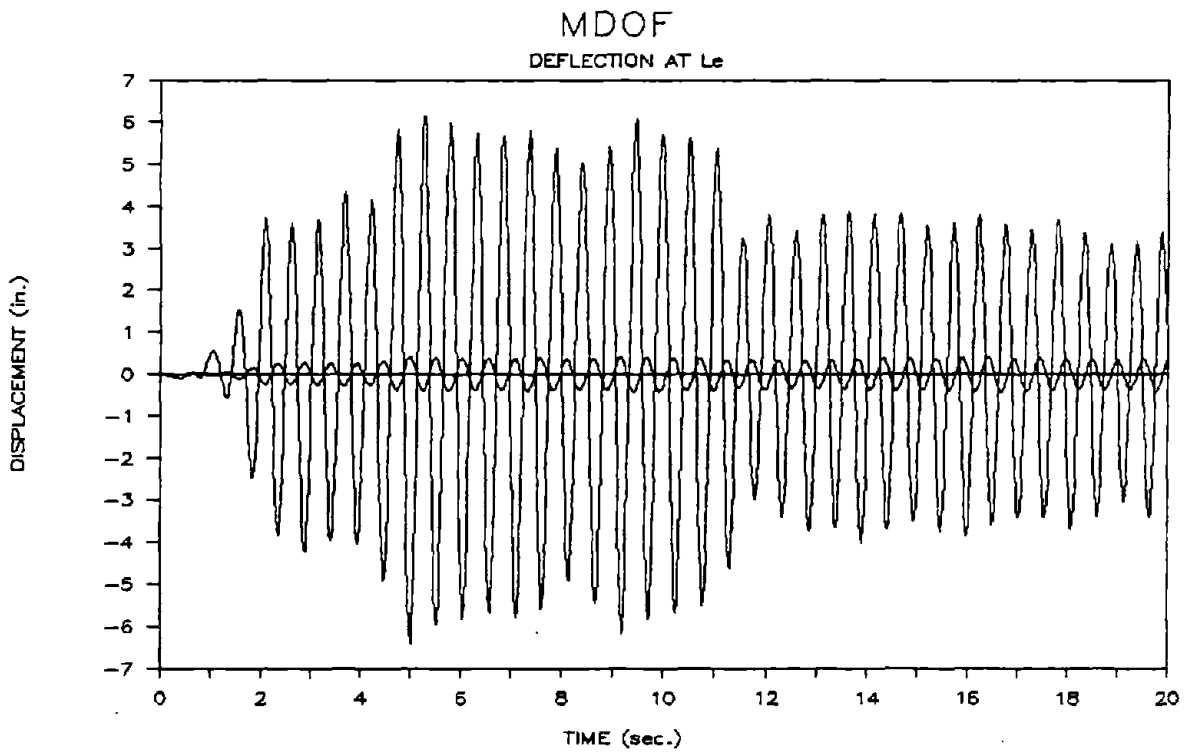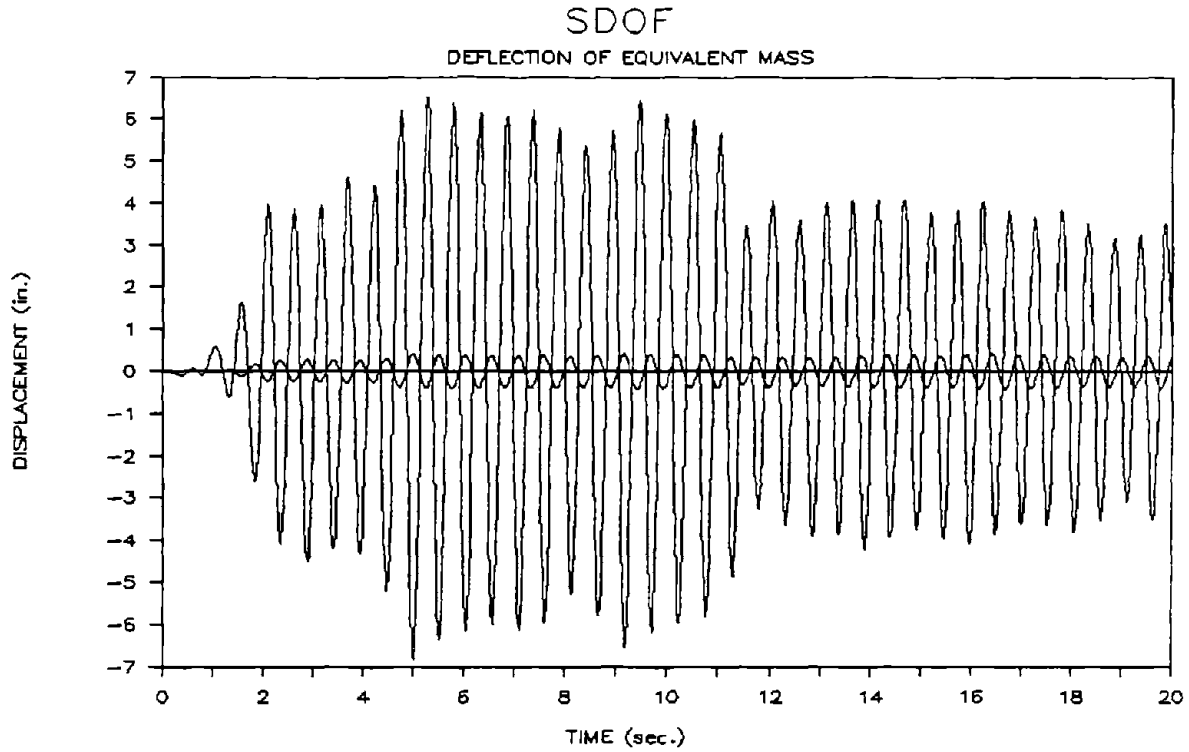
**FIGURE 4-1   RESPONSE OF MDOF SYSTEM AND AN
EQUIVALENT Q-MODEL**

4-6

SECTION 5
RESULTS

5.1 INTRODUCTION

The response of the MDOF and SDOF systems are compared in this chapter. Two loading conditions are used to excite the models. The displacement at the equivalent height, L_e, was monitored and plotted. Three types of damping of the MDOF system were used; mass damping, stiffness damping and element damping.

5.2 FREE VIBRATION RESPONSE

Both systems are subjected to a ground motion acceleration as shown in Figure 5-1 to give them an initial displacement, then released to vibrate freely. The response of the MDOF system is compared to the response of the SDOF system and is illustrated in Figures 5-2, 5-3 and 5-4. The plots show the deflection of the MDOF system at a height, L_e, and the deflection of the mass of the SDOF Q-model.

Figure 5-2 shows the response of lightly damped SDOF systems compared to undamped MDOF responses. There was a slight difference in the period of free vibration. This variation was due to the fact that the SDOF system had damping implemented within the spring system, however small it was, it influenced the response. Also the damping in the SDOF system introduces a damped period of vibration, which is longer than the undamped period.

The effect of mass damping on the MDOF system is shown in Figure 5-3. The SDOF system is lightly damped, while the MDOF system has a factor of proportionality, α, equal to 0.95. This is equivalent to:

$$[C] = 0.95[M]$$

This produces a diagonal uncoupled damping matrix equivalent to 0.95 M at each DOF. The damping can be translated as modal damping

5-1

where:

$$\alpha = 2\omega_i \delta_i \qquad\qquad\qquad 5-1$$

So, an α value of 0.95 is equivalent to modal damping of:

$$\delta_i = \frac{0.425}{\omega_i} \qquad\qquad\qquad 5-2$$

Where δ_i is the critical damping ratio for mode i. The angular frequency ω is a function of the system's stiffness and mass. The stiffness of the MDOF system degrades, thus reducing the frequency and increasing the critical damping ratio. Table 5-1 shows the damping ratio calculated using the logarithmic decrement method for both the SDOF system with low damping and the MDOF system with mass damping. It is clear that beyond the first cycle, the damping is constant and is approximately equal to 5%. This represents a 5% damping of the first mode for the degraded stiffness model. Table 5-2 shows the percentage of critical damping as obtained from Equation 5-2, where ω_i is evaluated based on the MDOF system initial undegraded stiffness and the final degraded state of stiffness.

Generally the amount of damping depends on the maximum displacement in the SDOF and the MDOF systems. For the SDOF the structural damping is a more appropriate representation as it follows the behavior of the hysteresis loops. In the MDOF system, the physical damping problem is more complicated than the simple representations of damping currently adopted.

Stiffness proportional damping has an opposite effect on the modal damping ratios than the mass damping. It damps the higher modes more than the lower modes. The direct effect on the response of the MDOF system is shown in Figure 5-4. The proportionality factor is 0.0007. The critical damping ratios are shown in Table 5-3. The modal critical damping ratios as evaluated using Equation 5-2 are shown in Table 5-4, where the natural frequencies are evaluated using the initial stiffness and the final stiffness of the degraded system. From the plot, it is clear that stiffness damping smoothes

the deformation graph, or filters out most of the high frequency content. This type of damping does not influence the overall response since the contributions of the higher modes to the deflected shape is usually small. However, it would influence other parameters that are strongly related to higher modes, such as floor acceleration and inter-story shears.

Element damping as defined earlier is constant throughout the degradation stages. It is defined in terms of the elements initial stiffness. The top deformation is mainly primary mode deflection, so the damping of the higher elements has little influence on the total displacement, and the damping of the lower two elements which suffer the most stiffness degradation and the highest amount of internal deformation, is enough to obtain the same response, or the same top deformation.

The effect of uniform damping is shown in Figure 5-5 for β_κ of 0.0006, where κ is defined in Equation 4-6. The damping in the lower elements influences the primary mode deflection while damping the upper elements influences the higher modes.

5.3 RESPONSE TO GROUND MOTIONS

The response of both the SDOF and MDOF to ground motion records are shown. The SDOF responses for two spring systems with the characteristics shown in Table 3-3 were monitored. The MDOF system was subjected to the same set of ground motions and the responses were monitored for the systems having no damping and with mass damping. The amount of mass damping was estimated from the response of the SDOF system.

The damping of the SDOF is hysteretic damping. It can be represented by a percentage of critical damping for each individual cycle as explained in Section 3. The MDOF mass damping is a constant form of damping. It acts on loading and unloading and is equivalent to modal damping. For a degrading system, mass damping

produces a higher value of modal damping as the system degrades since the frequency decreases and Y_i as defined by Equation 5-2 increases.

The main differences between hysteretic and mass damping are:

1. Hysteretic damping is activated on unloading, while mass damping forces take affect at all times.

2. Hysteretic damping takes in affect the degradation of stiffness and the percentage of critical damping stays relatively uniform. Mass damping stays constant and is not affected by stiffness degradation. An estimate of the final stiffness is necessary to determine the adequate amount of mass damping in order to provide adequate amount of damping to represent the loss of energy in the system.

The following steps were used to estimate the appropriate amount of mass damping:

1. The SDOF spring 2 is subjected to a displacement sequence and the critical damping ratio is calculated for each individual cycle. Figure 5-6 shows the hysteretic loops and the critical damping ratio for all cycles. The damping of the virgin cycle is ignored because it only occurs once and any subsequent cycles have a different amount of damping than the virgin cycle. An average critical damping ratio of 6.87 is estimated.

2. The secant stiffness of the spring defined as the force divided by the displacement is estimated from the virgin envelope described in Section 3. R_d is the ratio of the secant stiffness for a particular displacement divided by the initial stiffness k_i. For d = 1,2, and 3 inches. R_d is:

3. The frequency of a system ω is related to the stiffness

5-4

$$R_1 = \frac{30}{360} = 0.083$$

$$R_2 = \frac{17.3}{360} = 0.048$$

$$R_3 = \frac{13}{360} = 0.036$$

such as:

$$\omega \; \alpha \; \sqrt{k}$$

The frequency change due to the changes of stiffness corresponding to R_1, R_2 and R_3 are:

$$\frac{\omega_1}{\omega_I} = \sqrt{0.083} = 0.29$$

$$\frac{\omega_2}{\omega_I} = \sqrt{0.048} = 0.22$$

$$\frac{\omega_3}{\omega_I} = \sqrt{0.036} = 0.19$$

Where ω_I corresponds to the frequency of the initial system.

4. The MDOF system has an initial frequency of primary mode of vibration equal to:

$$\omega_1 = 0.29 \; x \; 38.0 = 11.0 \; (rad./sec.)$$

$$\omega_I = 38.0 \; (rad./sec.)$$

so:

$$\omega_2 = 0.22 \; x \; 38.0 = 8.4 \; (rad./sec.)$$

$$\omega_3 = 0.19 \; x \; 3.80 = 7.2 \; (rad./sec.)$$

5. The mass damping for a system that has a one inch average displacement and a critical damping ratio of 6.87% for the primary mode

$$\alpha_{m1} = 2\gamma_i \; \omega_i$$
$$= 2 \; x \; 0.0687 \; x \; 11 = 1.51$$

Similarly $\alpha_{m2} = 1.15$

and $\qquad \alpha_{m3} = 0.99$

This mass damping is based on the frequency of the degraded system.

6. Mass damping would induce damping on loading and unloading of the MDOF system. The SDOF has damping on unloading only. The values obtained in the previous step should be halved to provide an average damping force. A set of mass damping values equivalent to $\omega_m = 0.76$, 0.58 and 0.5 are used in the following analysis.

The ground motions applied to both the SDOF and the MDOF systems are listed in Table 5-5. A scaling factor C2 is applied to all records of the ground motions. Figure 5-7a and b through 5-15a and b present the response of both systems to nine ground motions. Figure 5-7a shows the scaled ground motion acceleration in the top plot. The second plot is the SDOF response with low damping spring (spring 1), as defined in Table 3-3. The third plot is the MDOF response with no damping. The top plot of Figure 5-7b shows the response of the SDOF system with a spring (spring 2) of typical damping as defined in Table 3-3. The MDOF responses are shown in the following three plots with mass damping of 0.76, 0.56 and 0.5

respectively. The plots shown in Figure 5-8a and b through Figure 5-15a and b present the same sequence of plots for different ground motions.

The final degraded stiffness ratios of the beams shown in Figure 2-1, are presented in Table 5-6. The natural frequencies of the MDOF system were calculated based on the final stiffness and are presented in Tables 5-7 and 5-8. Table 5-9 shows the critical damping ratio for the primary mode of MDOF systems based on the initial and final stiffness. The maximum absolute displacement for all different cases of all ground motions are shown in Table 5-10.

TABLE 5-1

PERCENTAGE OF CRITICAL DAMPING FOR SUCCESSIVE
CYCLES OF SDOF AND MDOF SYSTEMS   FOR MASS
DAMPING OF 0.95.   EVALUATED USING
THE LOGARITHMIC DECREMENT METHOD

CYCLE NO.	DAMPING PERCENTAGE	
	SPRING 1	MDOF
1	4.0	7.2
2	4.4	5.0
3	4.4	5.6
4	4.4	5.0

TABLE 5-2

EQUIVALENT MODAL DAMPING AS EVALUATED
FROM EQUATION 5-2 BASED ON THE
INITIAL AND FINAL STIFFNESS OF
THE MDOF SYSTEM

MODE NO.	DAMPING PERCENTAGE	
	INITIAL	FINAL
1	1.12	5.21
2	0.17	0.60
3	0.06	0.20
4	0.03	0.11
5	0.02	0.06

TABLE 5-3

EQUIVALENT MODAL DAMPING AS EVALUATED
FROM EQUATION 5-2 BASED ON THE
INITIAL AND FINAL STIFFNESS OF
THE MDOF SYSTEM

| MODE | DAMPING PERCENTAGE | |
NO.	INITIAL	FINAL
1	1.33	0.33
2	8.51	2.78
3	24.12	8.18
4	46.6	15.94
5	69.41	27.24

TABLE 5-4

PERCENTAGE OF CRITICAL DAMPING FOR
SUCCESSIVE CYCLES OF SDOF AND MDOF SYSTEMS
FOR STIFFNESS DAMPING OF 0.0007.
EVALUATED USING THE LOGARITHMIC DECREMENT METHOD

| CYCLE | DAMPING PERCENTAGE | |
NO.	SPRING 1	MDOF
1	4.0	0.82
2	4.4	0.38
3	4.4	0.32
4	4.4	0.33

TABLE 5-5

GROUND MOTIONS FOR LPM RUNS

NO.	NAME	DURATION	C1	C2
1	El Centro E-W	53.0	0.9255	1.7875
2	El Centro N-S	53.0	0.6777	1.3145
3	Pine Union 140	29.0	0.8622	1.7067
4	Cruickshank Rd 230	34.0	0.7632	1.4951
5	James Road 140	29.0	0.7126	1.3893
6	Kern County 69	54.0	1.4080	2.8648
7	Cruickshank Rd 140	34.0	0.6157	1.2024
8	Brawley Airport 315	37.0	1.0644	2.0738
9	Keystone Road 140	39.0	0.9485	1.8501

C1: Scaling Factor for ZPA 0.2g.
C2: Scaling Factor for ZPA 0.4g.

TABLE 5-6

RATIO OF FINAL DEGRADED STIFFNESS
TO INITIAL STIFFNESS

GROUND MOTION	BEAM 1	BEAM 2	BEAM 3	BEAM 4	BEAM 5
1	0.0152	0.1202	0.6757	0.9997	1.0000
2	0.0219	0.1202	0.2259	0.9506	1.0000
3	0.0219	0.1202	0.4430	0.9997	1.0000
4	0.0197	0.1202	0.2088	0.9997	1.0000
5	0.0289	0.1651	0.3809	0.9854	1.0000
6	0.0197	0.1202	0.3993	0.9997	1.0000
7	0.0414	0.1202	0.4697	0.9997	1.0000
8	0.0414	0.1202	0.2855	0.9506	1.0000
9	0.0239	0.1202	0.1651	0.7950	1.0000
MEAN	0.0260	0.1252	0.3615	0.9645	1.0000

TABLE 5-7

NATURAL FREQUENCIES OF MDOF
BASED ON THE FINAL DEGRADED STIFFNESS (RAD/SEC)

GROUND MOTION	1ST MODE	2ND MODE	3RD MODE	4TH MODE	5TH MODE
1	6.01	90.28	291.87	621.90	1411.66
2	7.09	88.05	268.04	579.34	1186.71
3	7.12	95.28	297.50	617.31	1320.64
4	6.75	85.49	258.70	574.09	1182.62
5	8.16	104.61	313.23	652.06	1305.54
6	6.77	92.39	286.53	609.92	1299.24
7	9.41	107.22	342.89	645.29	1336.72
8	9.36	100.73	320.04	620.27	1229.82
9	7.33	84.34	258.02	549.72	1107.73
INITIAL	38.08	243.18	689.02	1331.55	1983.02

TABLE 5-8

RATIO OF THE NATURAL FREQUENCIES OF
THE MDOF BASED ON THE FINAL DEGRADED
STIFFNESS DIVIDED BY THE INITIAL FREQUENCIES.

GROUND MOTION	1ST MODE	2ND MODE	3RD MODE	4TH MODE	5TH MODE
1	0.16	0.37	0.42	0.47	0.71
2	0.19	0.36	0.39	0.44	0.60
3	0.19	0.39	0.43	0.46	0.67
4	0.18	0.35	0.38	0.43	0.60
5	0.21	0.43	0.45	0.49	0.66
6	0.18	0.38	0.42	0.46	0.66
7	0.25	0.44	0.50	0.48	0.67
8	0.25	0.41	0.46	0.47	0.62
9	0.19	0.35	0.37	0.41	0.56
MEAN	0.20	0.39	0.42	0.46	0.64

TABLE 5-9

PERCENTAGE OF CRITICAL DAMPING OF THE
FIRST MODE OF VIBRATION AS EVALUATED BASED
ON THE FINAL DEGRADED STIFFNESS FOR VARIOUS
GROUND MOTIONS AND THE INITIAL STIFFNESS

GROUND MOTION	FREQ. (RAD/SEC)	MD=0.76	MD=0.58	MD=0.5
1	6.01	6.32	4.82	4.16
2	7.09	5.36	4.09	3.53
3	7.12	5.34	4.08	3.51
4	6.75	5.63	4.30	3.71
5	8.16	4.65	3.55	3.06
6	6.77	5.61	4.28	3.69
7	9.41	4.04	3.08	2.66
8	9.36	4.06	3.10	2.67
9	7.33	5.18	3.95	3.41
MEAN		5.13	3.92	3.38
INITIAL	38.08	1.00	0.76	0.66

TABLE 5-10

MAXIMUM DEFLECTION OF MODEL SUBJECTED TO
NINE GROUND MOTIONS. MDOF MODEL HAS
STIFFNESS DAMPING =0.0002, AND MASS DAMPING

GM No.	SDOF LOW DAMP	SDOF TYP. DAMP	MDOF NO DAMP	MDOF MD=0.76	MDOF MD=0.58	MDOF MD=0.5
1	4.78	4.65	5.42	4.60	4.77	5.42
2	5.64	4.16	4.81	3.21	3.52	3.75
3	6.91	4.98	5.97	3.15	3.66	3.35
4	4.53	4.53	4.43	5.47	5.69	5.86
5	3.29	4.13	3.59	2.51	2.75	2.96
6	7.45	3.90	8.53	3.78	4.07	4.10
7	22.01	4.29	7.41	2.58	2.57	3.78
8	3.67	2.98	3.27	2.57	2.68	2.82
9	21.36	5.74	5.38	3.44	3.68	6.25
MEAN	8.85	4.37	5.42	3.48	3.71	4.25
SD	6.98	0.72	1.61	0.95	0.97	1.20
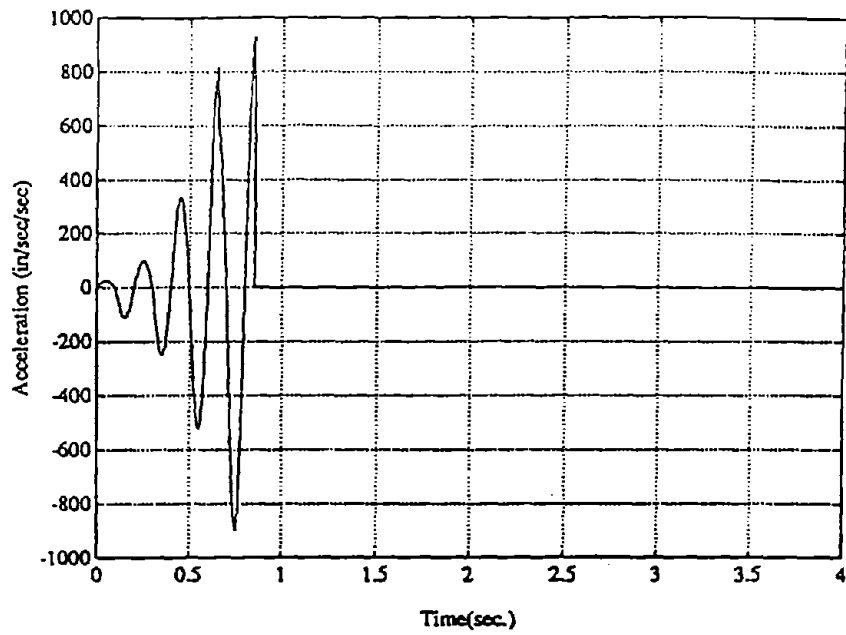
FIGURE 5-1   BASE EXCITATION
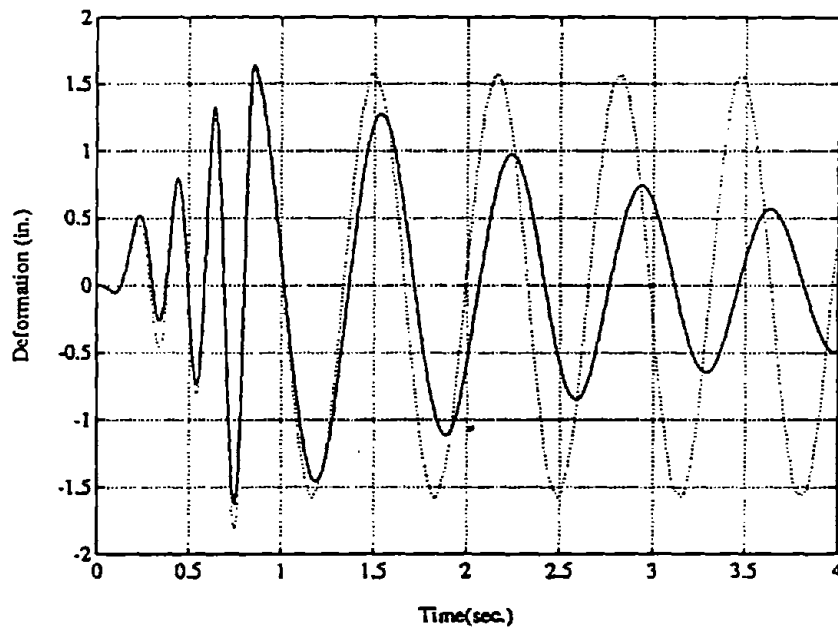
FIGURE 5-2   NON-DAMPED MDOF RESPONSE COMPARED TO SDOF Q-MODEL
                RESPONSE WITH LOW DAMPING.   SDOF: SOLID LINE

5-13
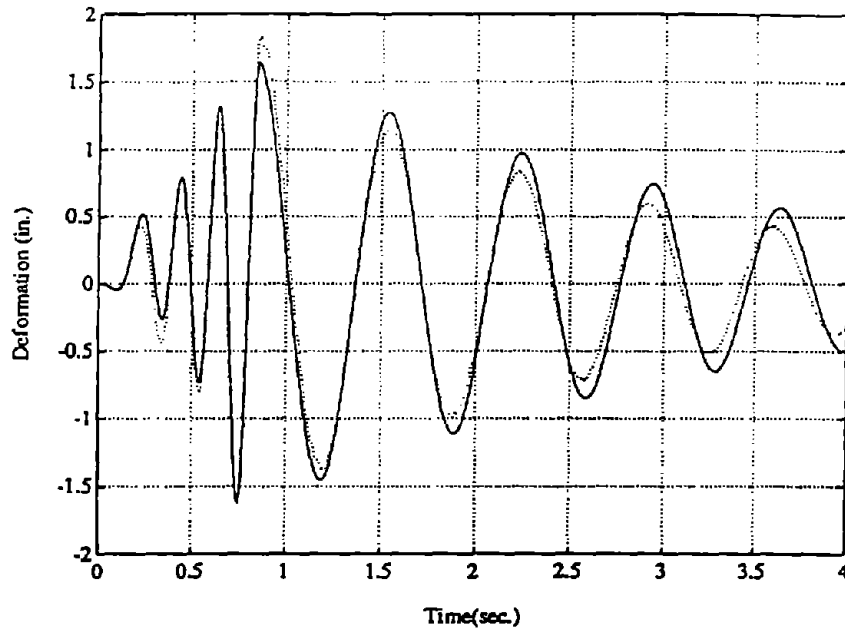
FIGURE 5-3   MASS DAMPED MDOF RESPONSE COMPARED TO SDOF Q-MODEL
               RESPONSE WITH LOW DAMPING. SDOF: SOLID LINE
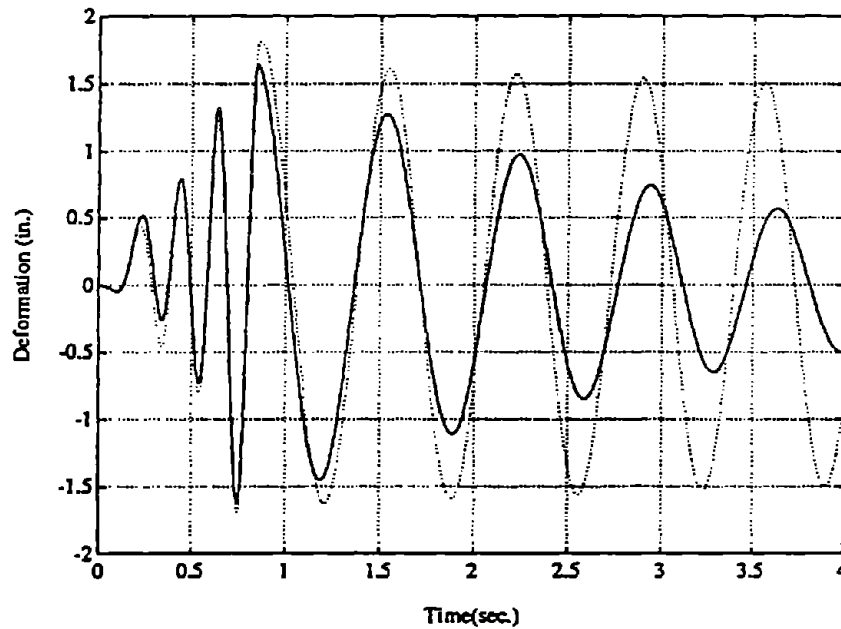
FIGURE 5-4   STIFFNESS DAMPED MDOF RESPONSE COMPARED TO SDOF
             Q-MODEL RESPONSE WITH LOW DAMPING. SDOF: SOLID LINE
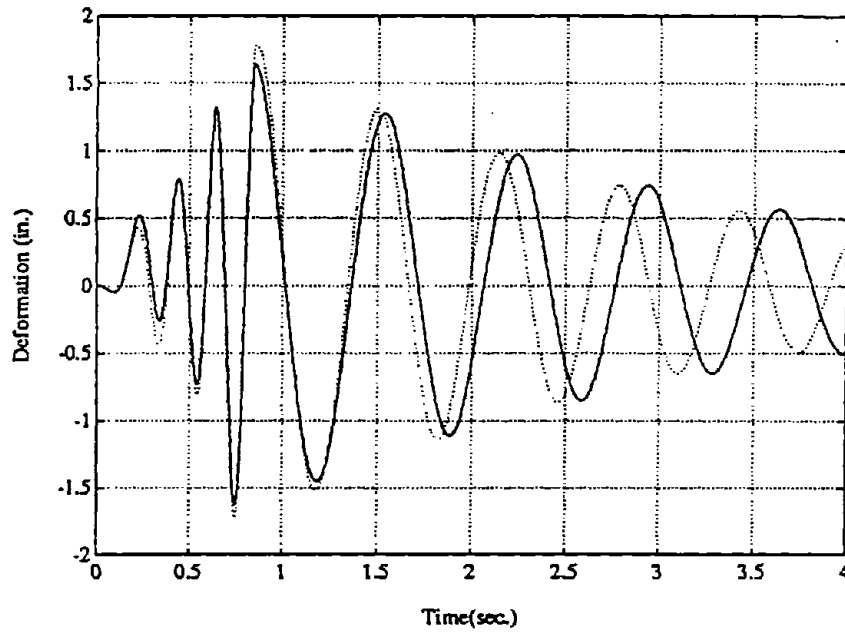
FIGURE 5-5   ELEMENT DAMPED MDOF RESPONSE COMPARED TO SDOF
              Q-MODEL RESPONSE WITH LOW DAMPING.   SDOF:
              SOLID LINE

5-15

SDOF
TYPICAL DAMPING HYSTERETIC LOOPS
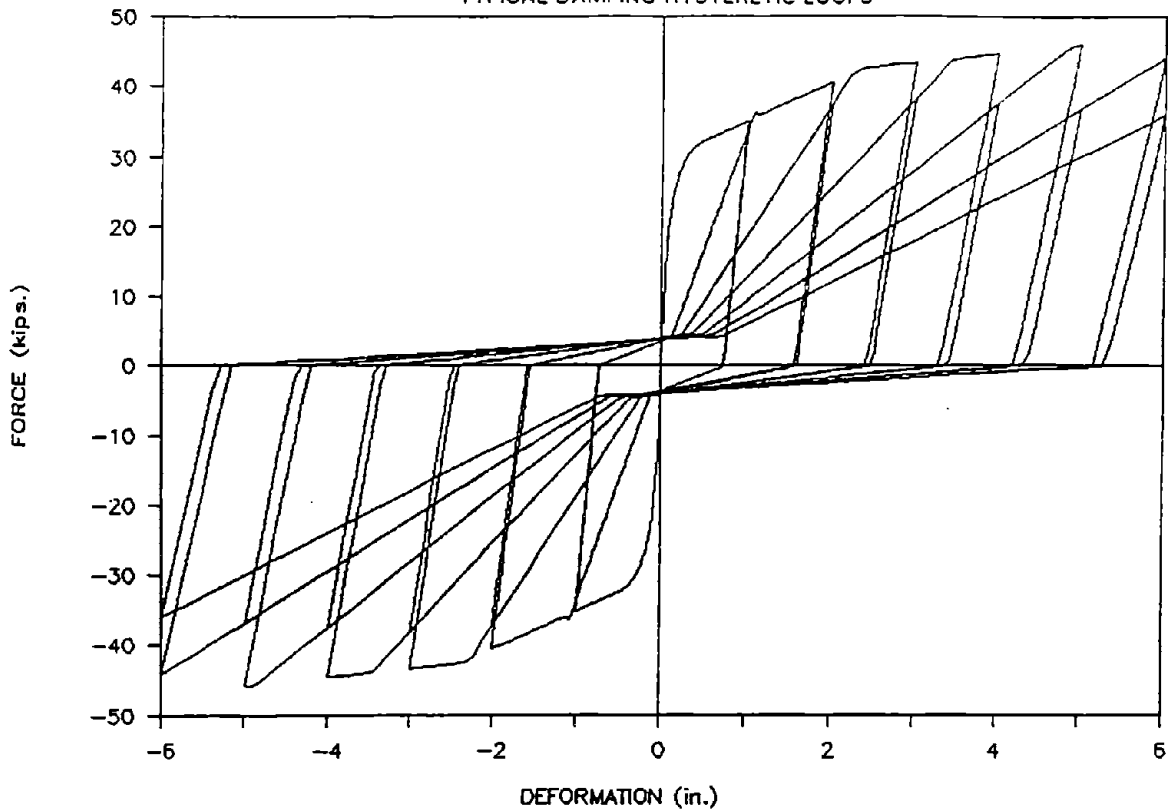
CYCLE No.	DISP. (IN)	CRITICAL DAMP. (%)	
1	1	17.6	
2	1		6.8
3	2	11.3	
4	2		6.4
5	3	9.2	
6	3		6.5
7	4	7.7	
8	4		6.9
9	5	6.3	
10	5		7.2
11	6	5.5	
12	6		7.4
MEAN		9.65	6.87

FIGURE 5-6   EQUIVALENT CRITICAL DAMPING RATIOS FOR EACH HYSTERETIC LOOP OF SPRING 2

GROUND MOTION # 1
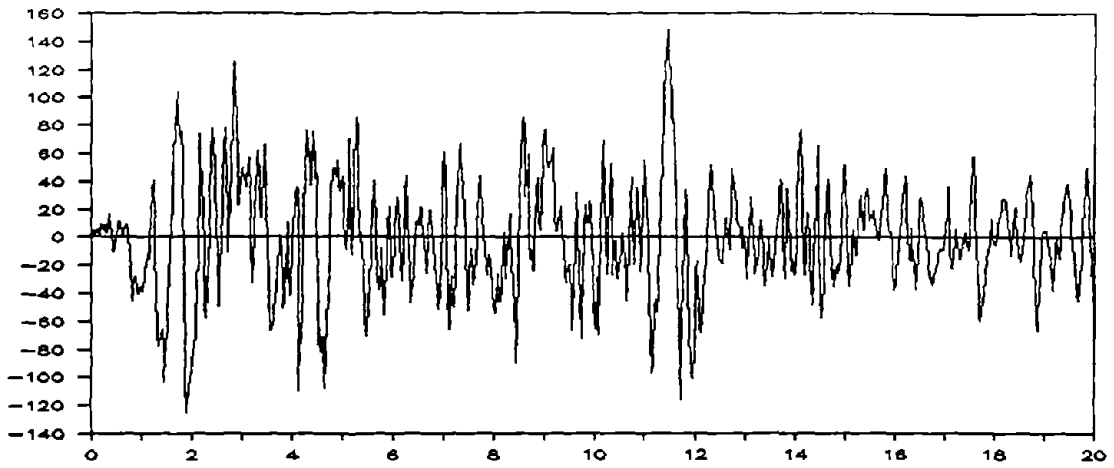
GROUND MOTION 1

SDOF. LOW DAMPING
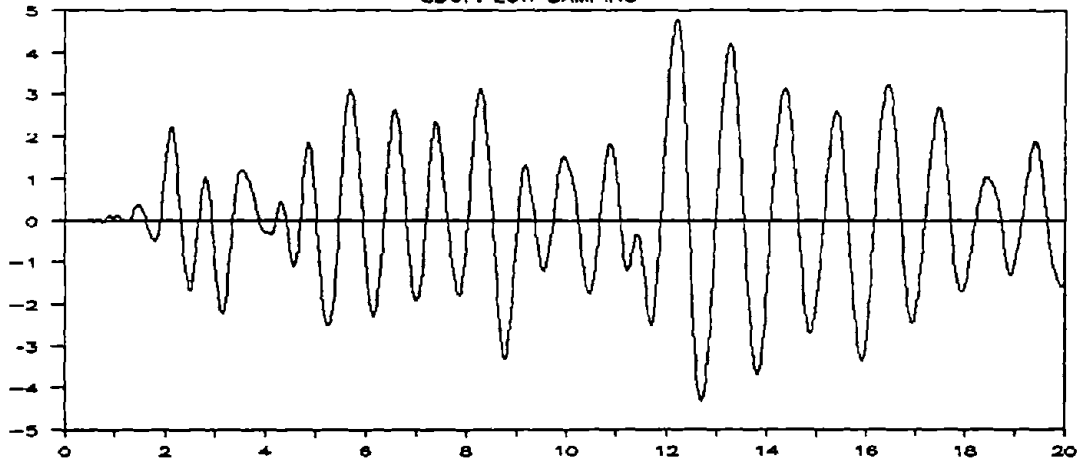
MDOF. NO DAMPING
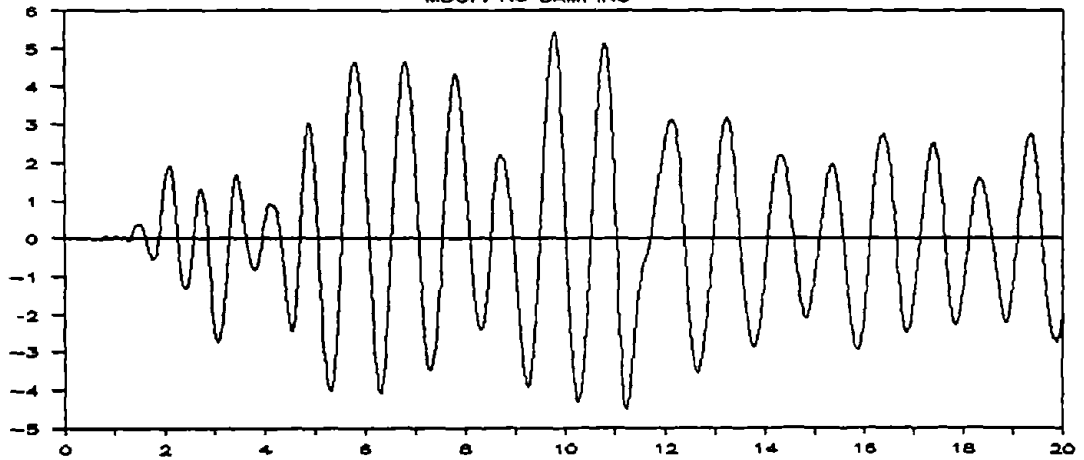
FIGURE 5-7a
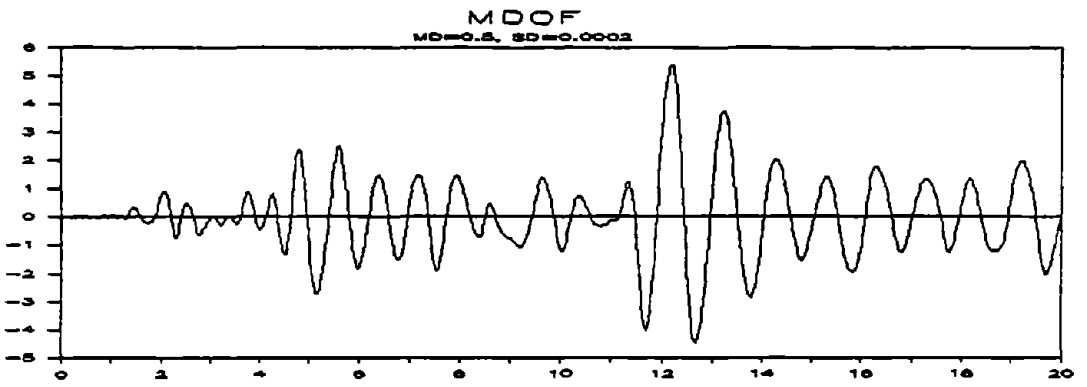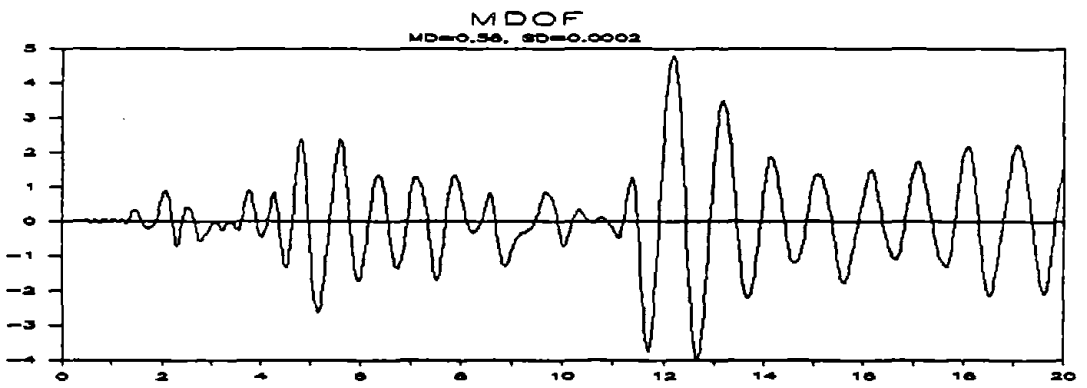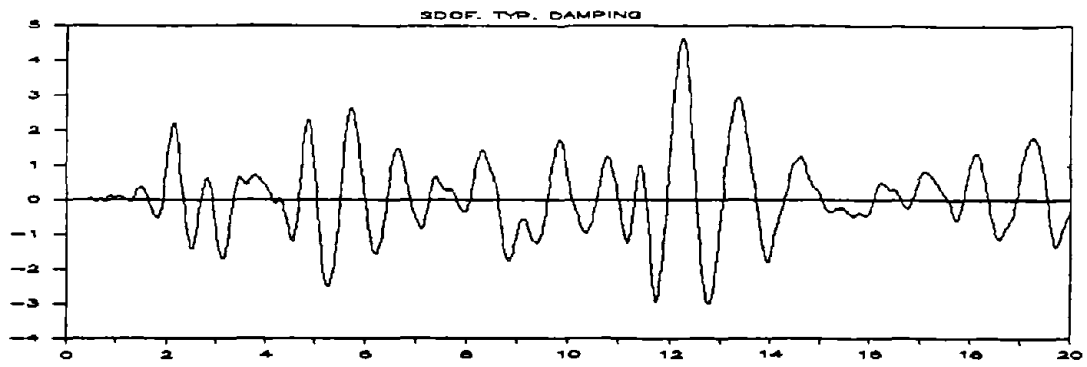
FIGURE 5-7b

GROUND MOTION # 2
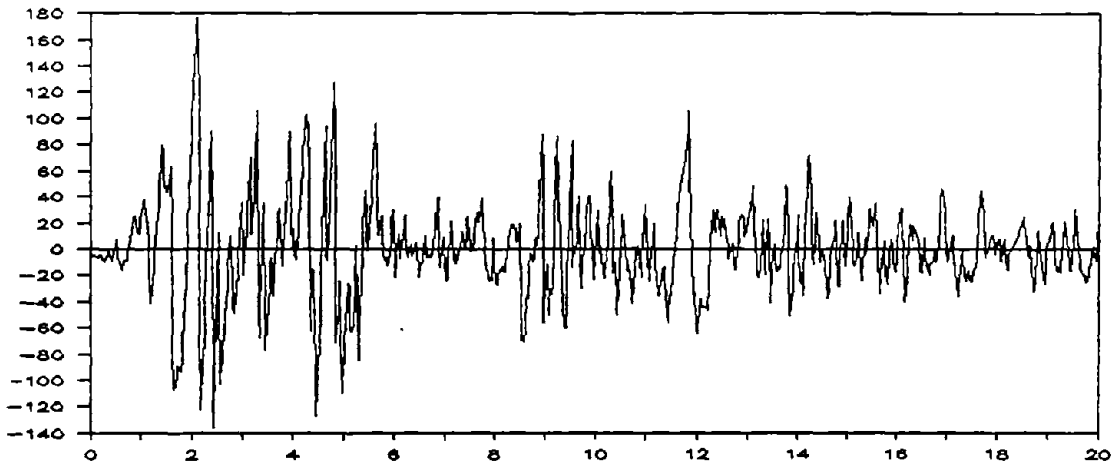
GROUND MOTION 2

SDOF. LOW DAMPING

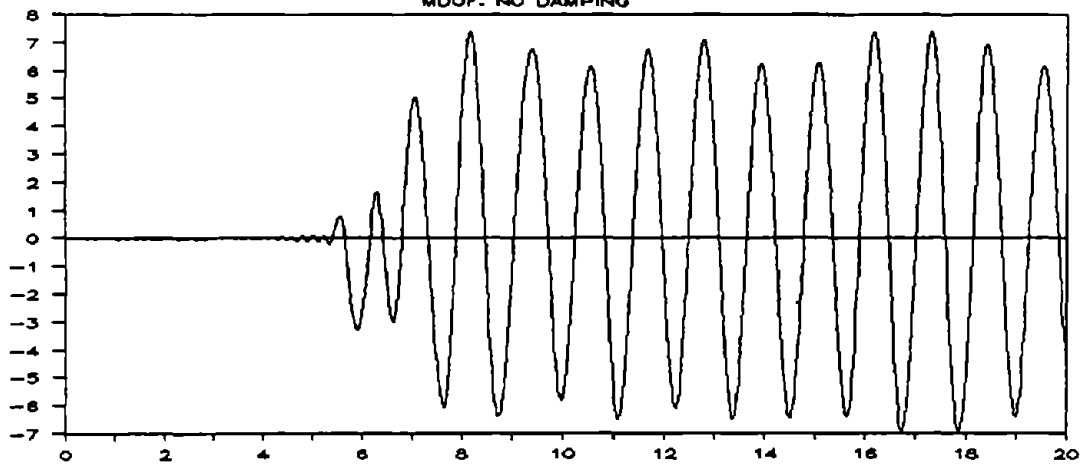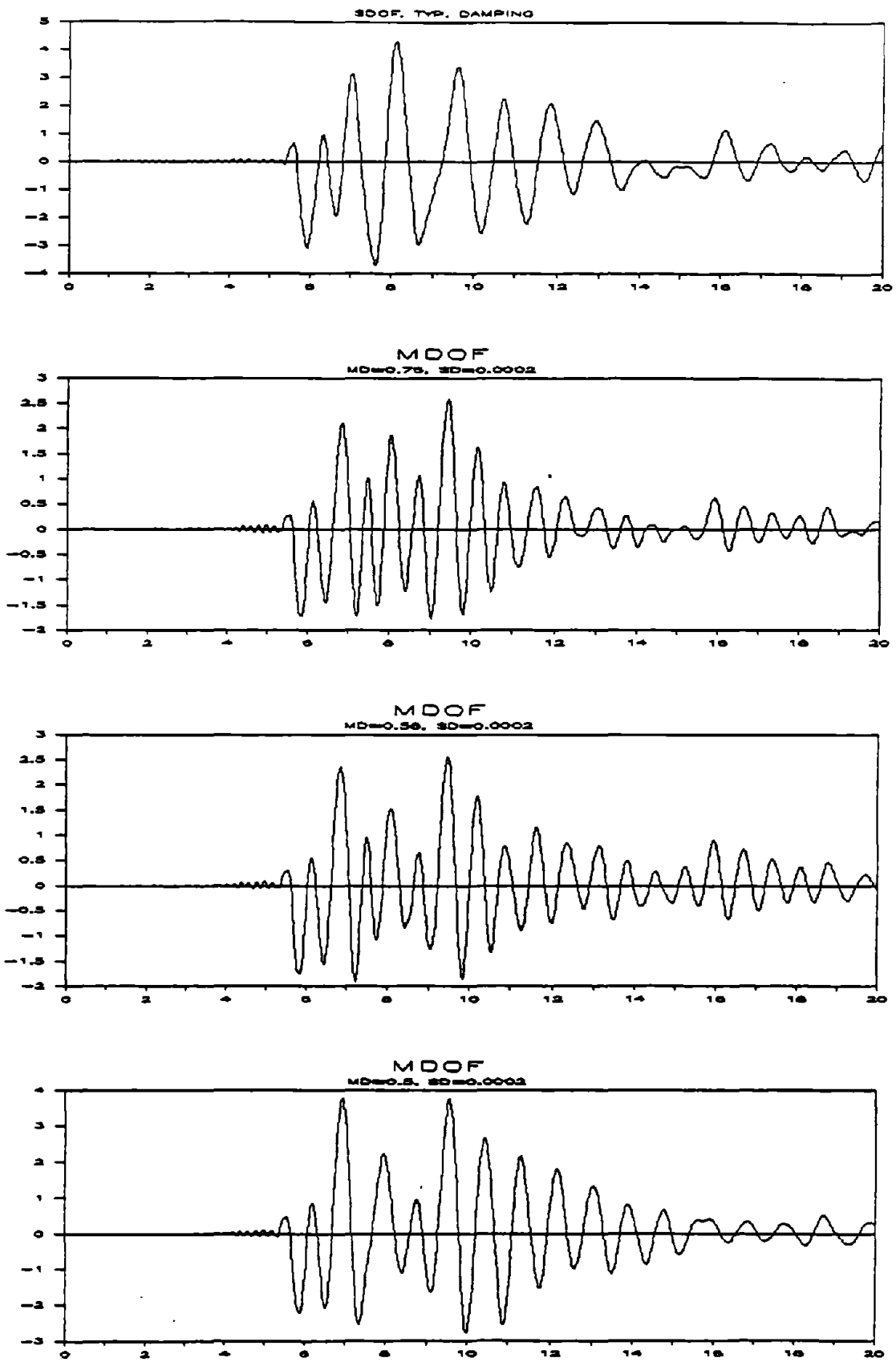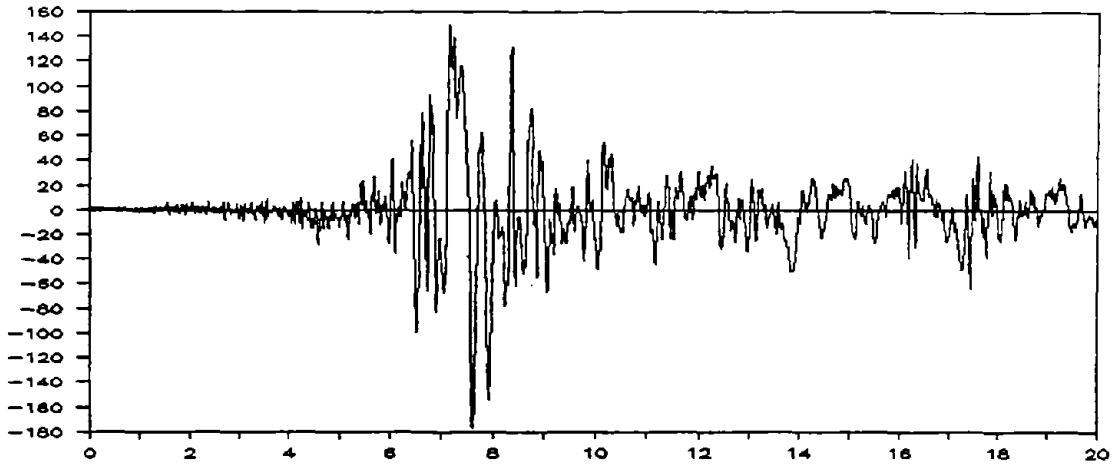MDOF. NO DAMPING

FIGURE 5-8a

SDOF, TYP. DAMPING

MDOF
MD=0.75, SD=0.0002
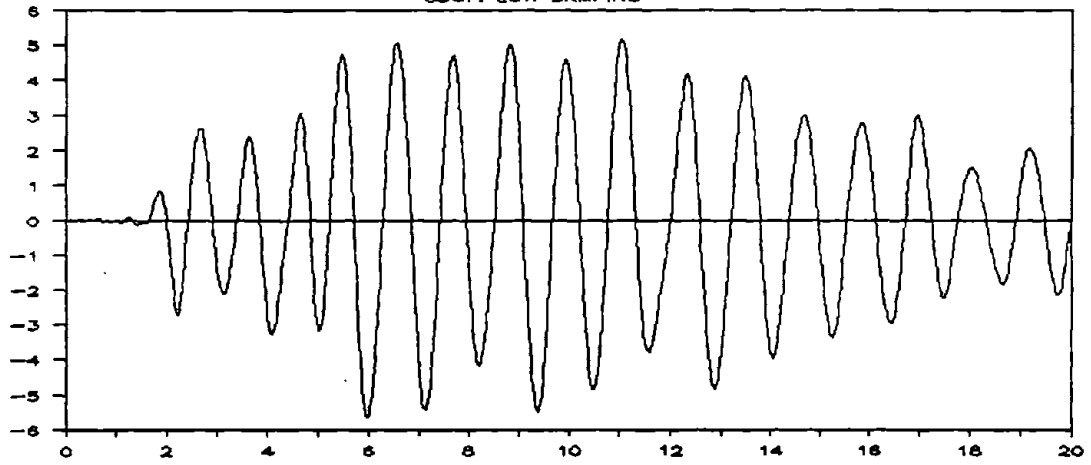
MDOF
MD=0.58, SD=0.0002
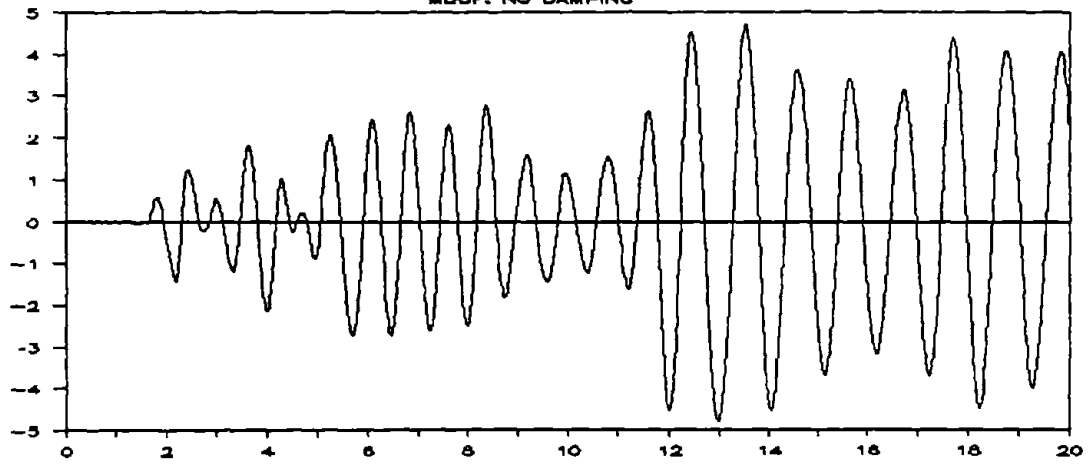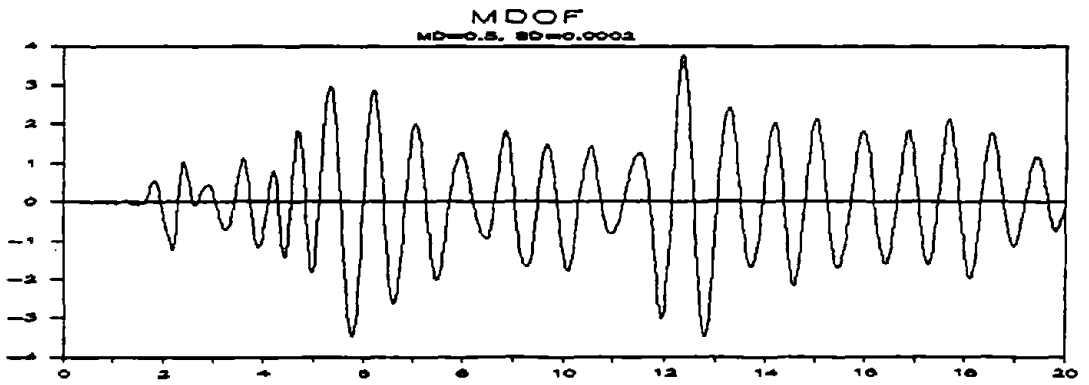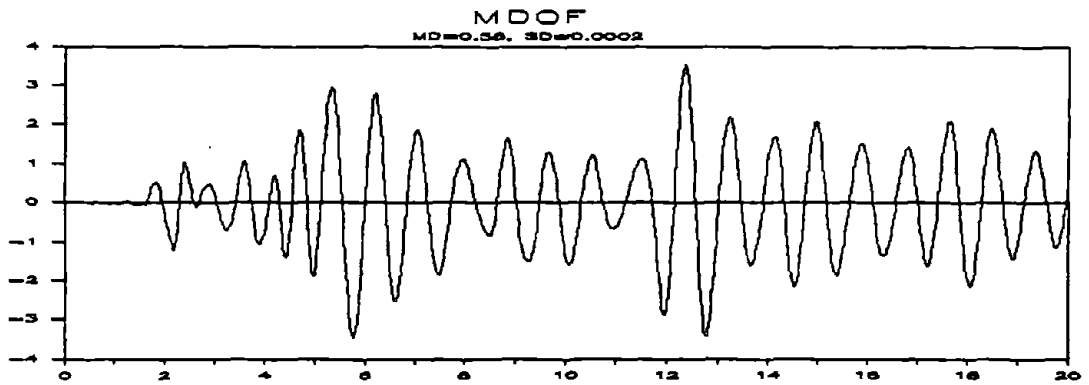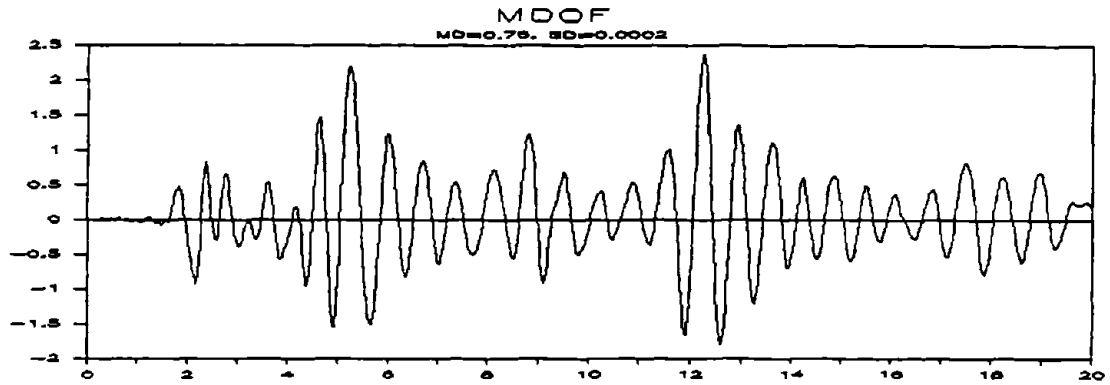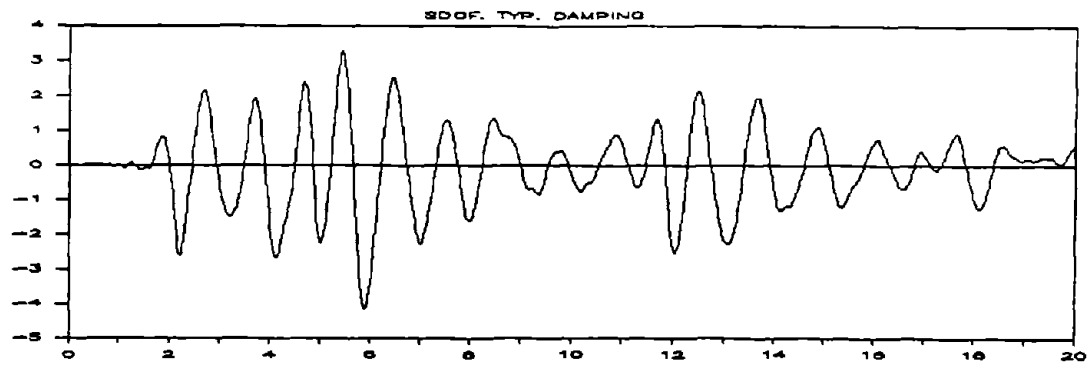
MDOF
MD=0.5, SD=0.0002

FIGURE 5-8b

GROUND MOTION # 3
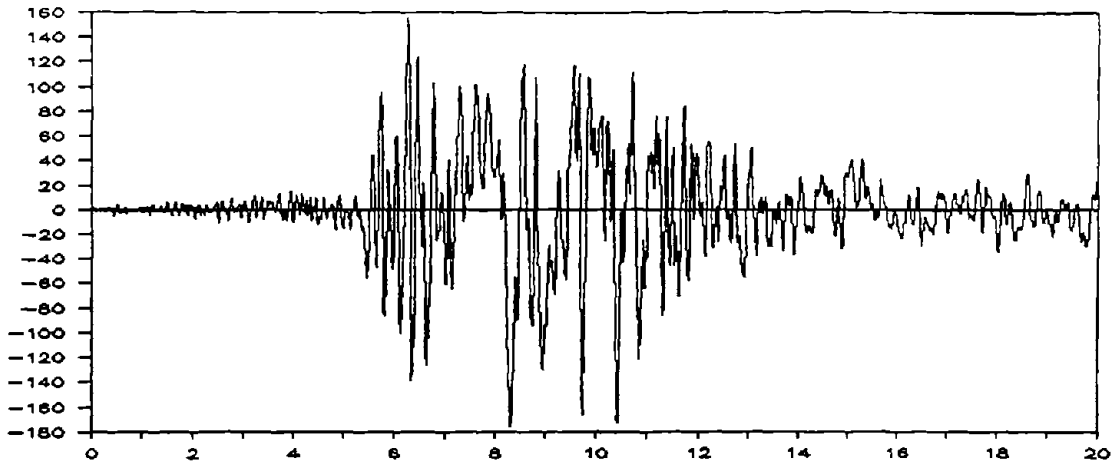
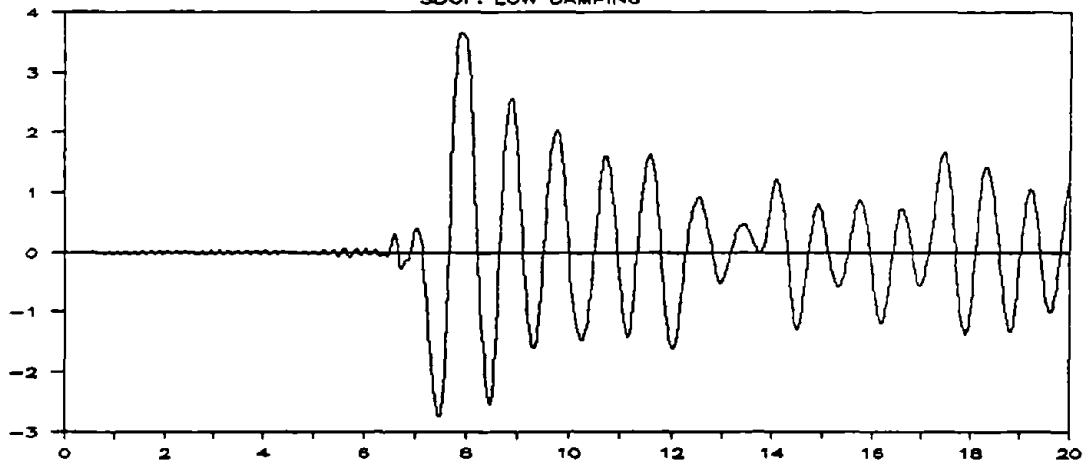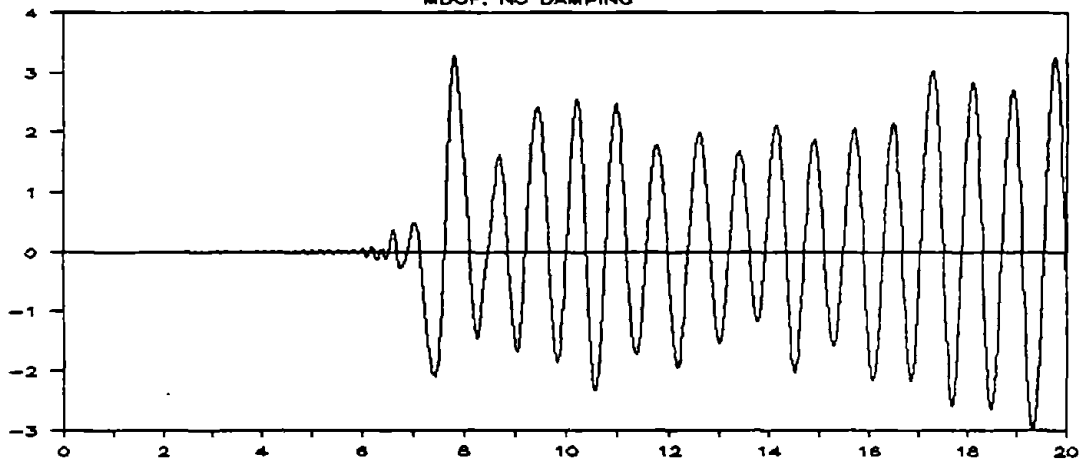GROUND MOTION 3

SDOF. LOW DAMPING
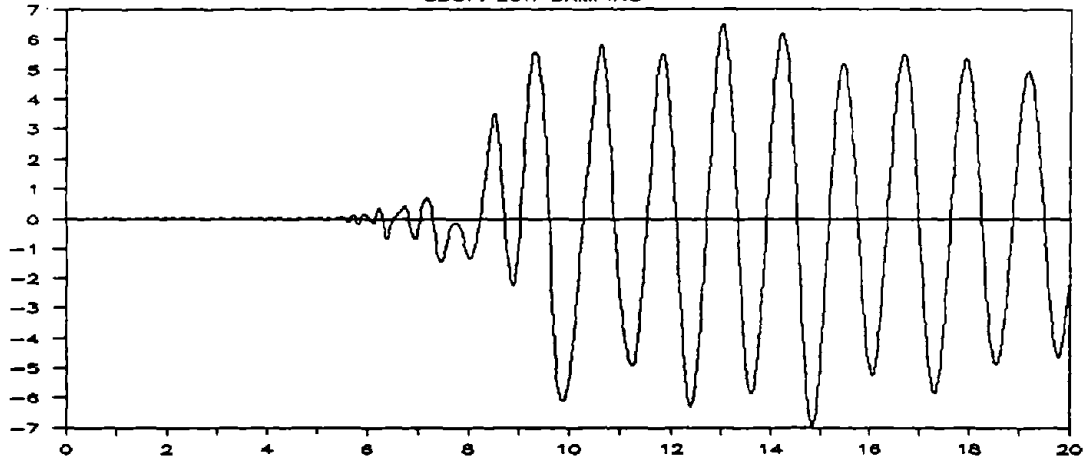
MDOF. NO DAMPING
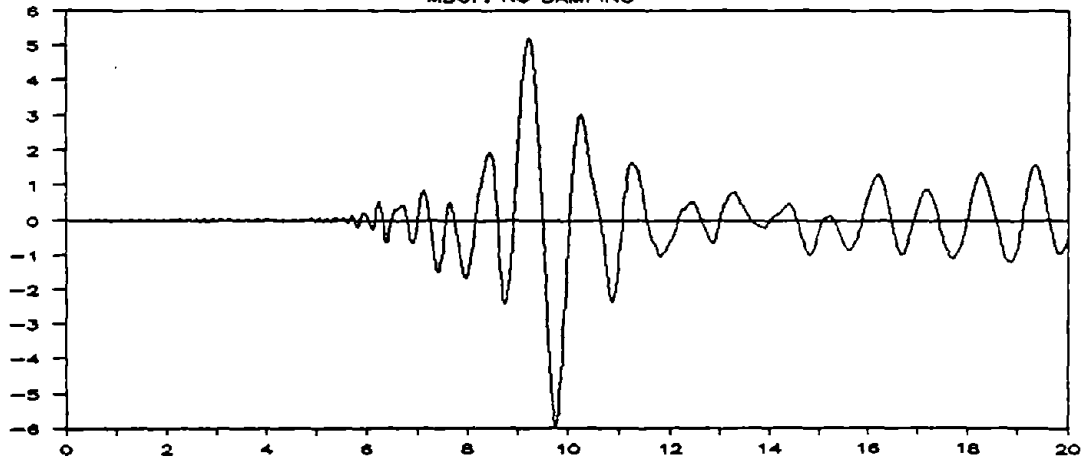
FIGURE 5-9a
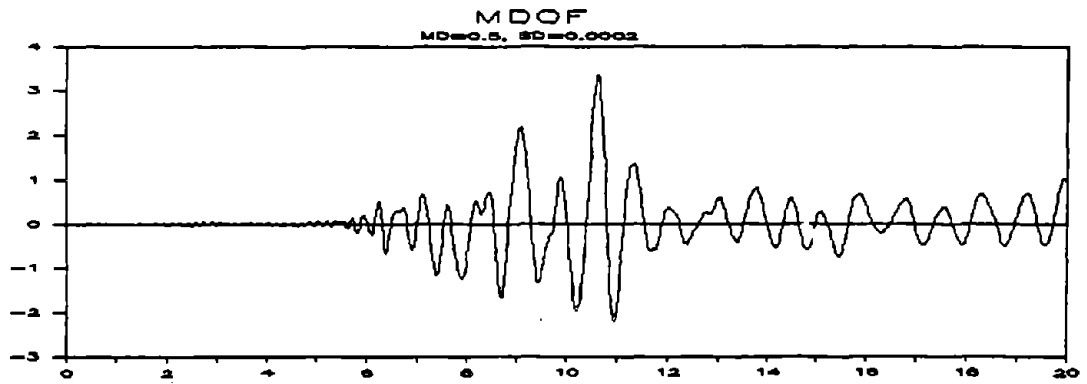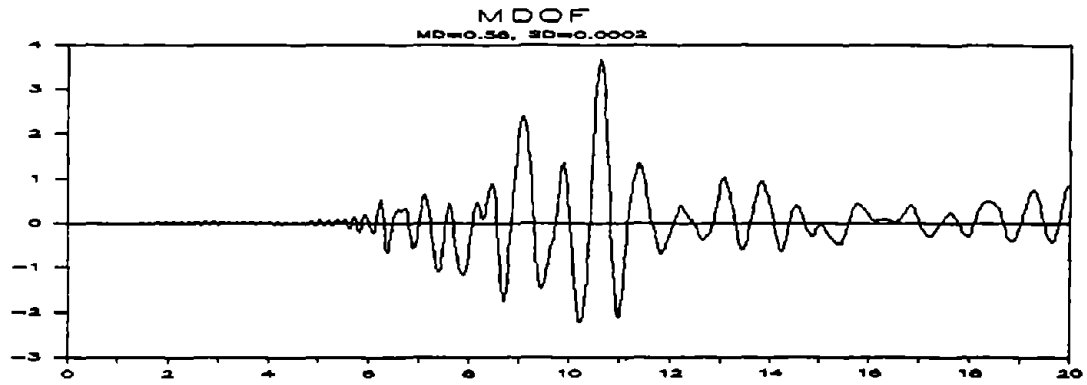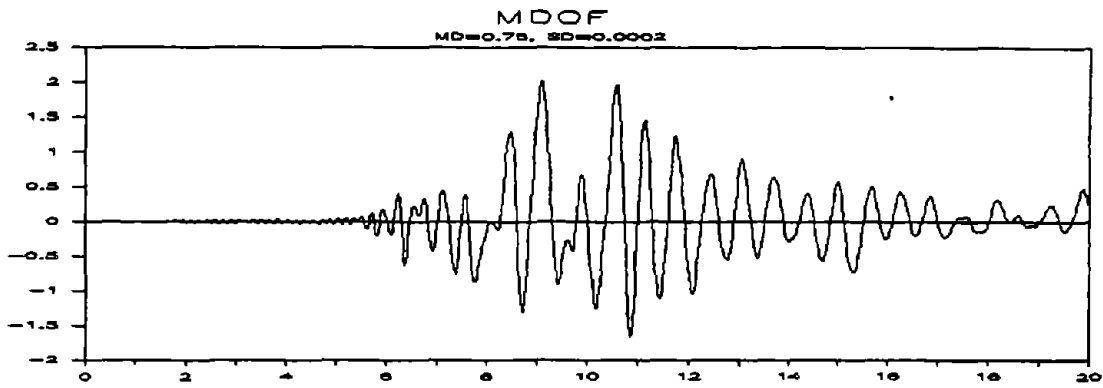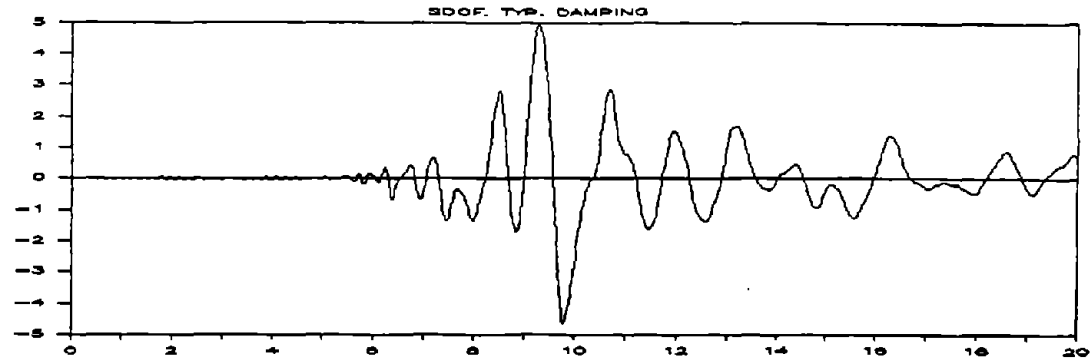
FIGURE 5-9b

GROUND MOTION # 4
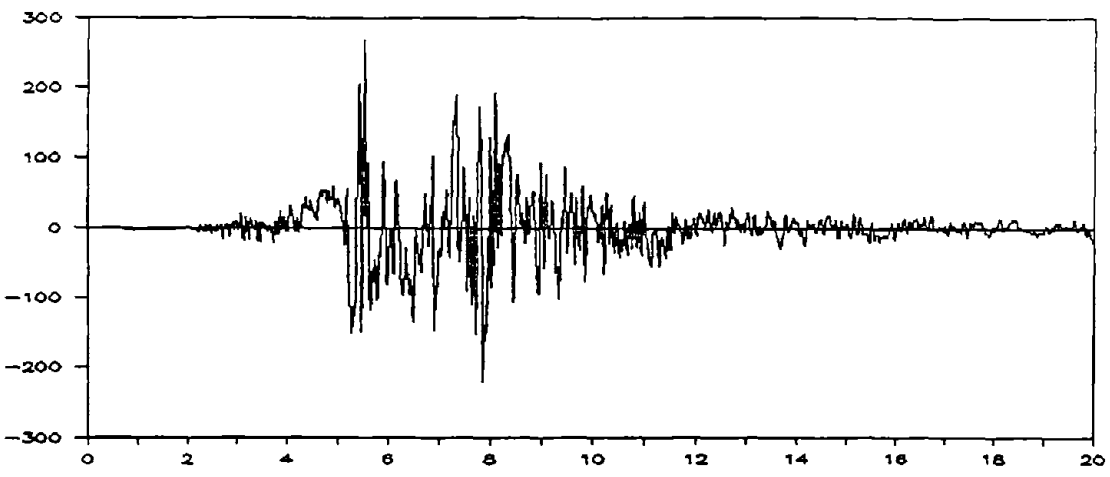
GROUND MOTION 4

SDOF. LOW DAMPING
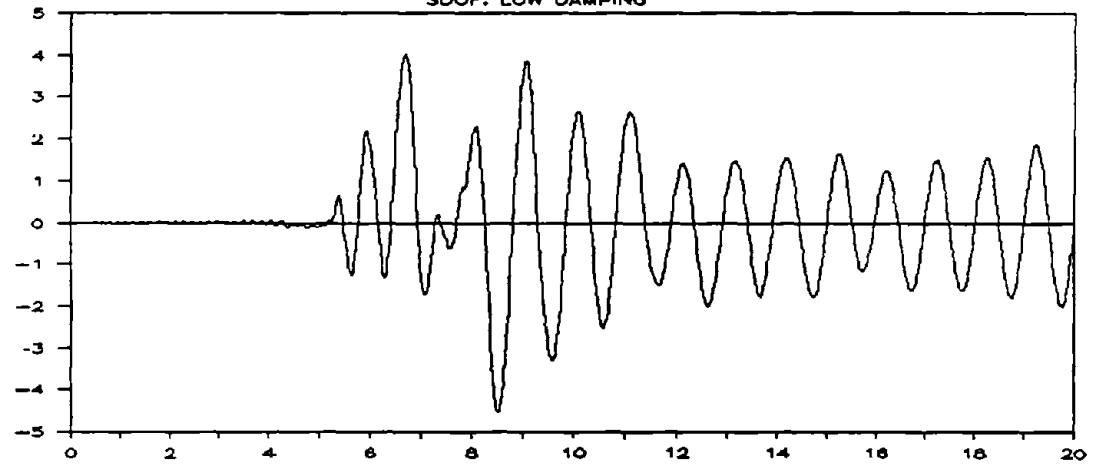
MDOF. NO DAMPING
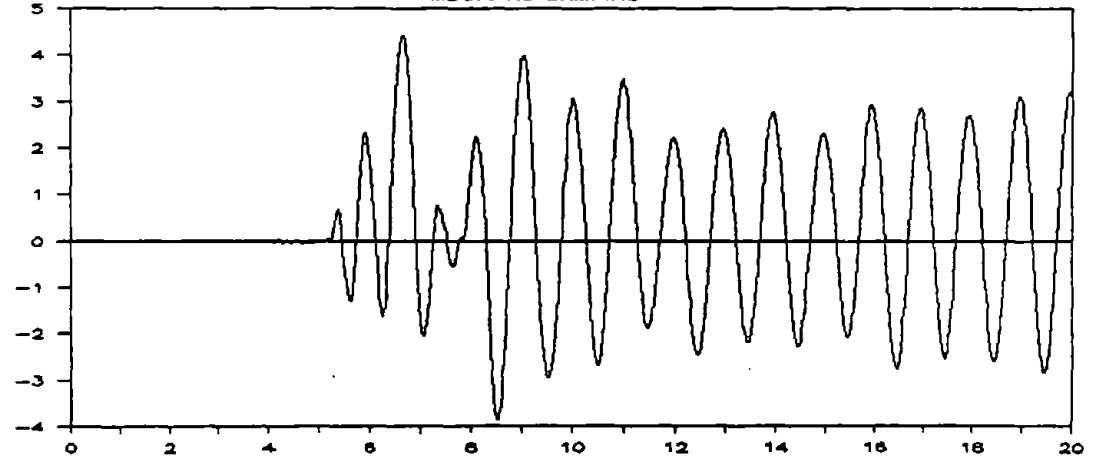
FIGURE 5-10a
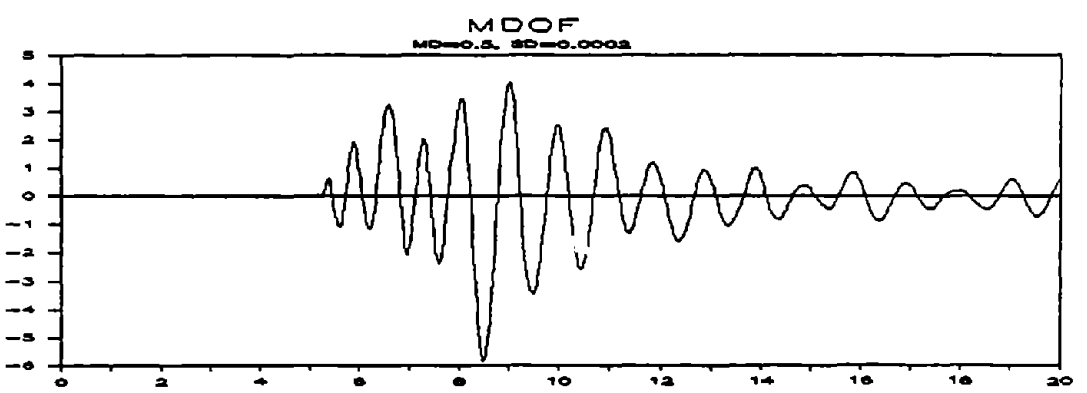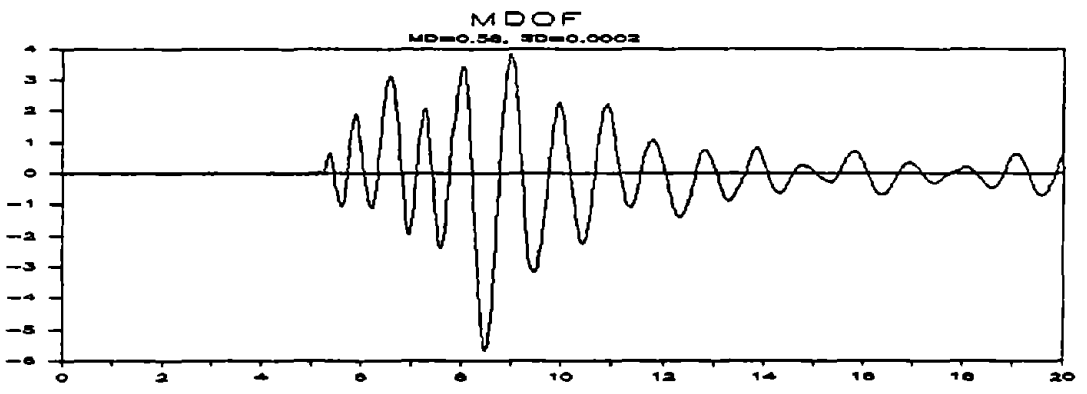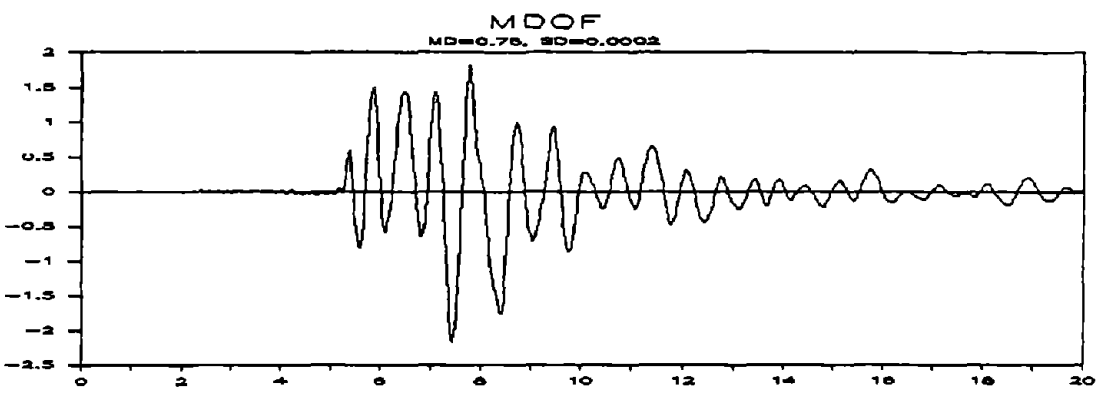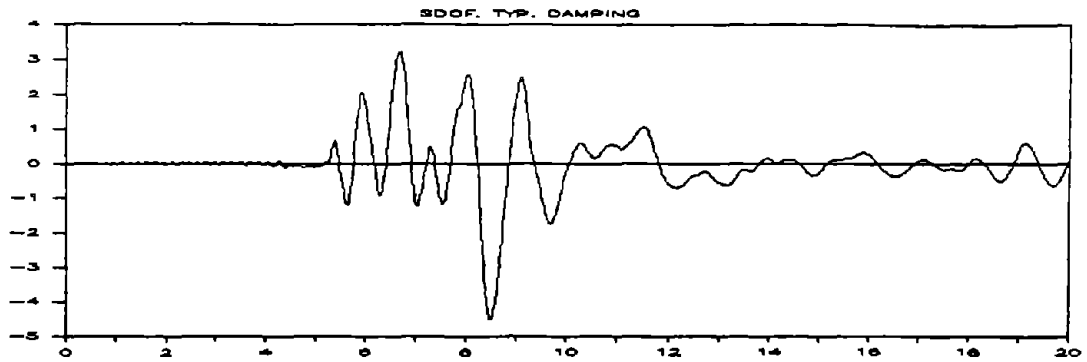
FIGURE 5-10b

GROUND MOTION # 5
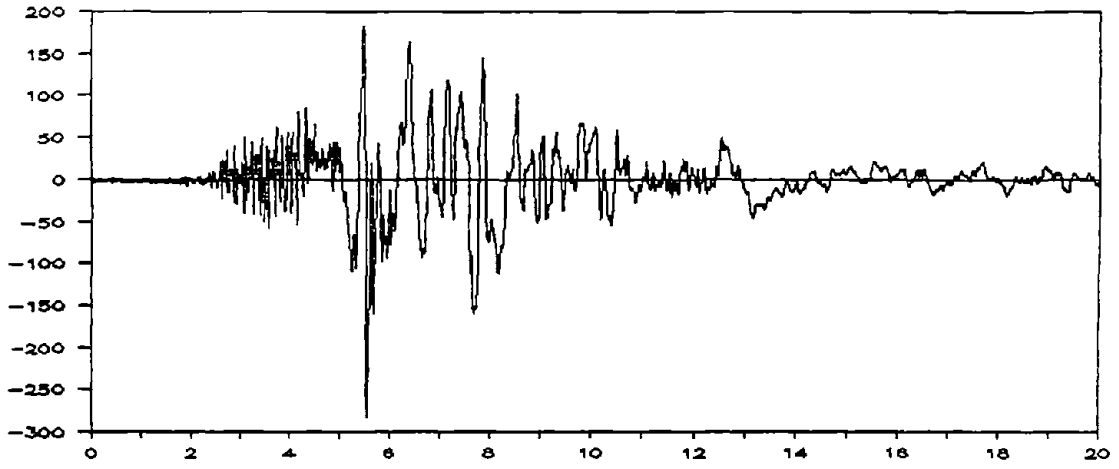
GROUND MOTION 5

SDOF. LOW DAMPING
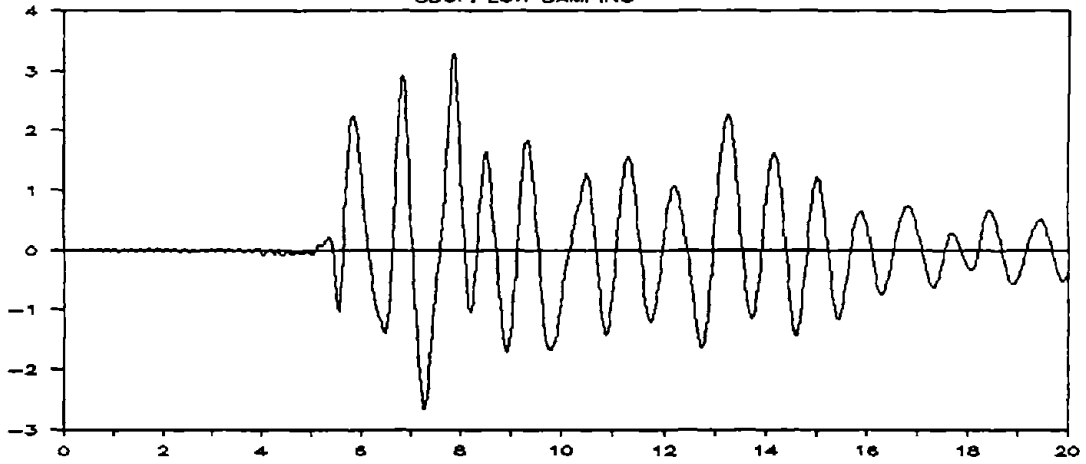
MDOF. NO DAMPING
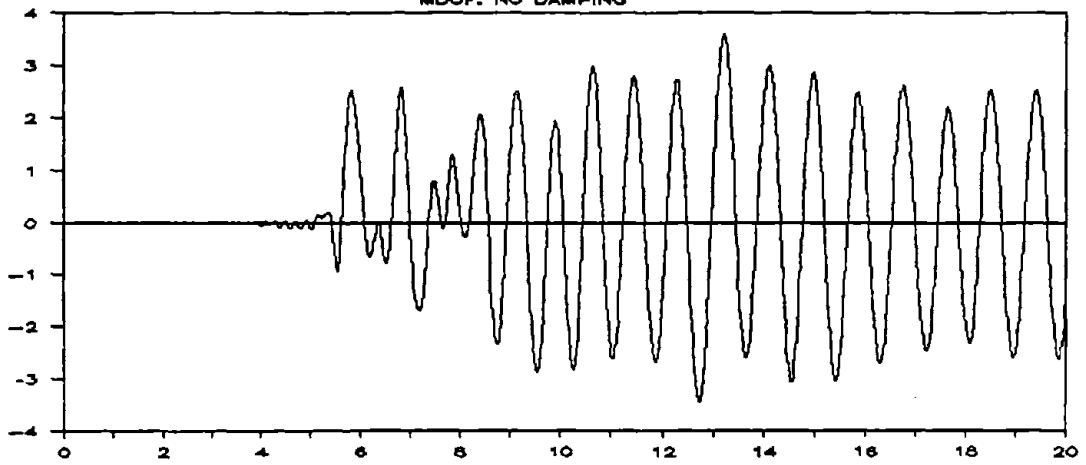
FIGURE 5-11a
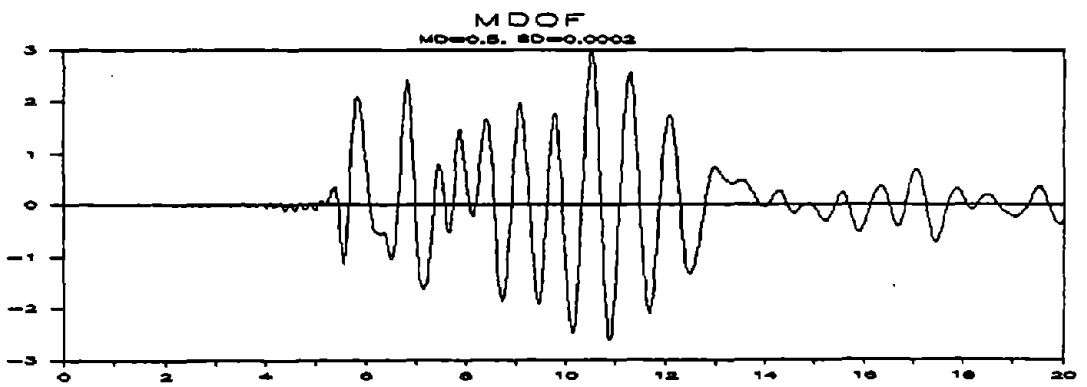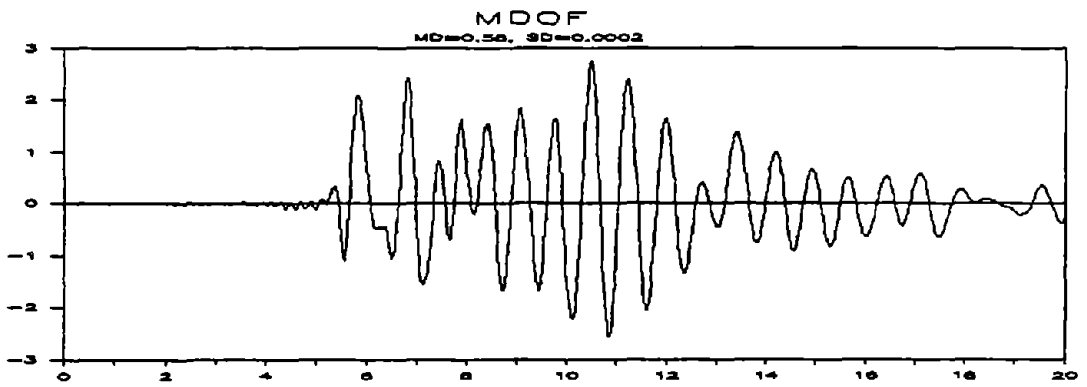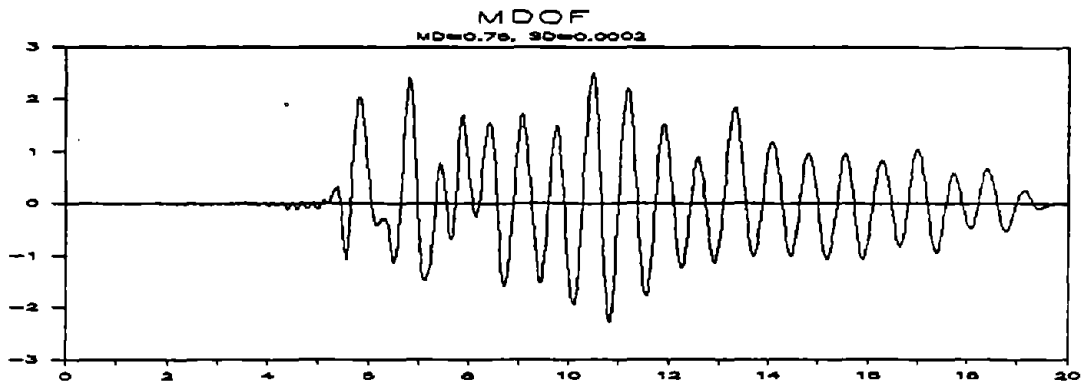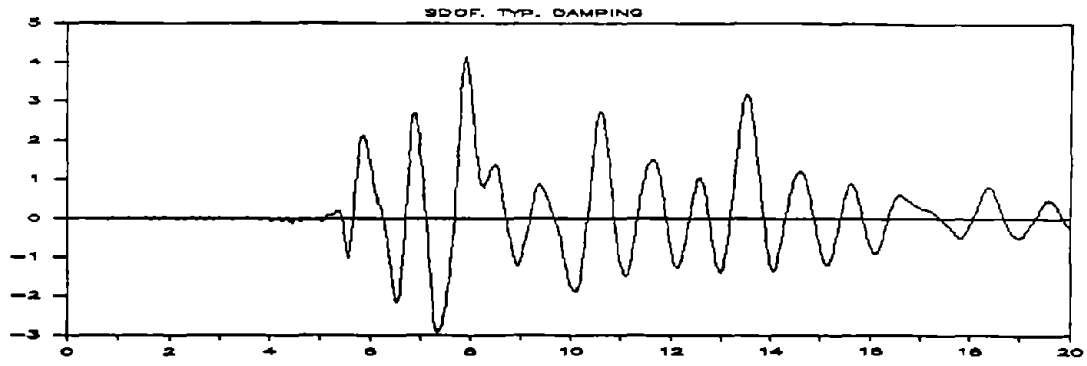
FIGURE 5-11b

GROUND MOTION # 6
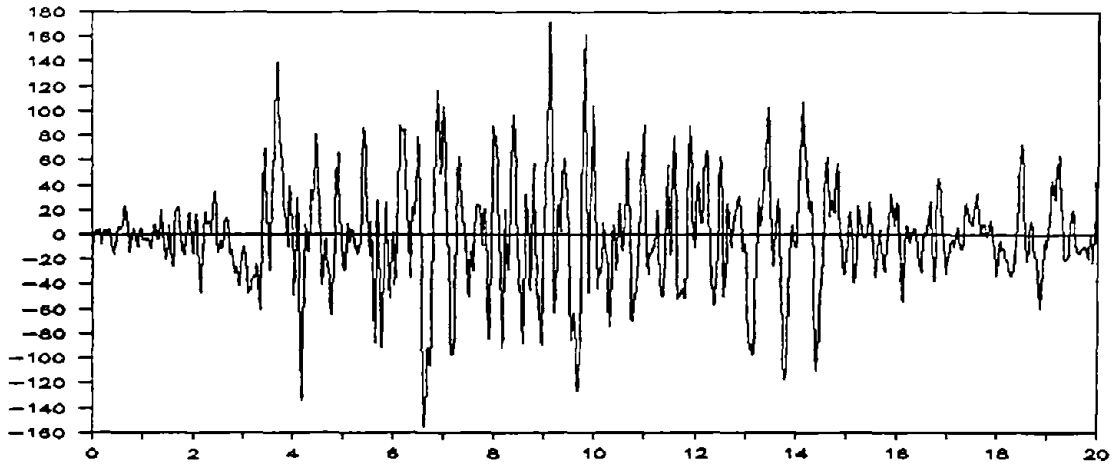
GROUND MOTION 6
SDOF. LOW DAMPING
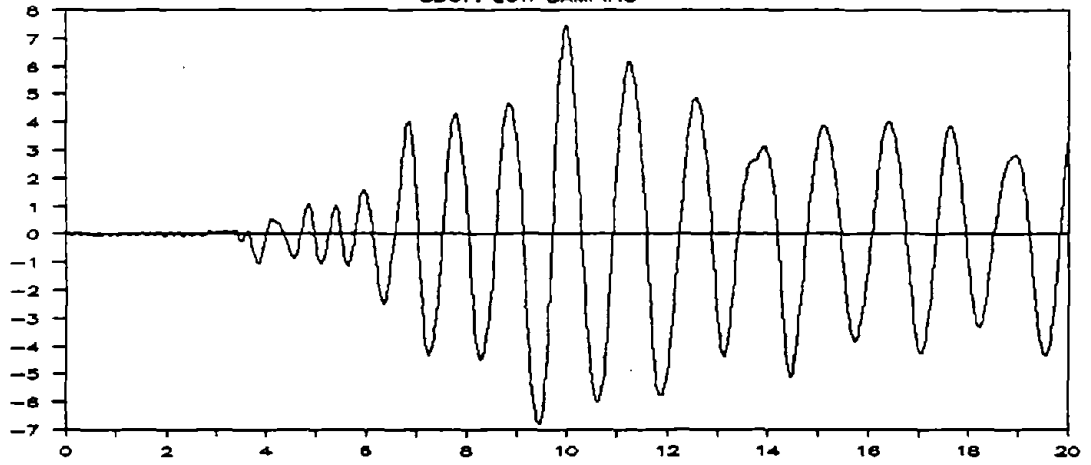
MDOF. NO DAMPING
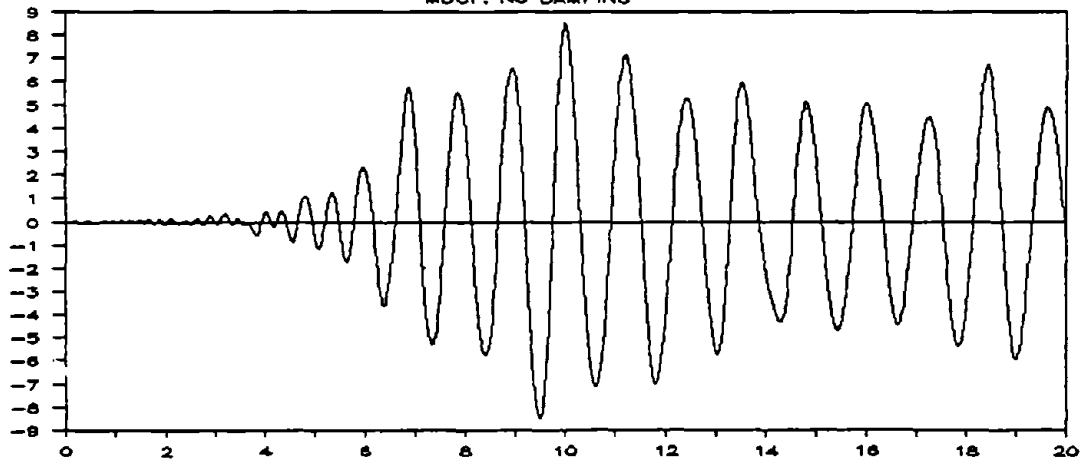
FIGURE 5-12a
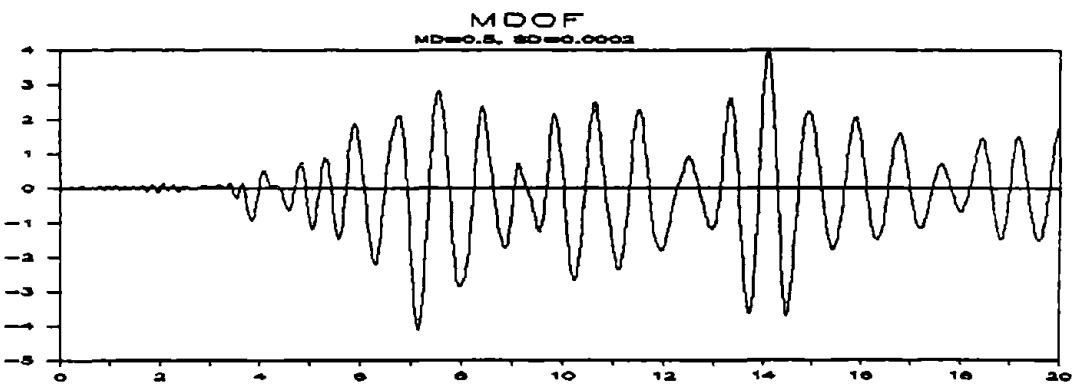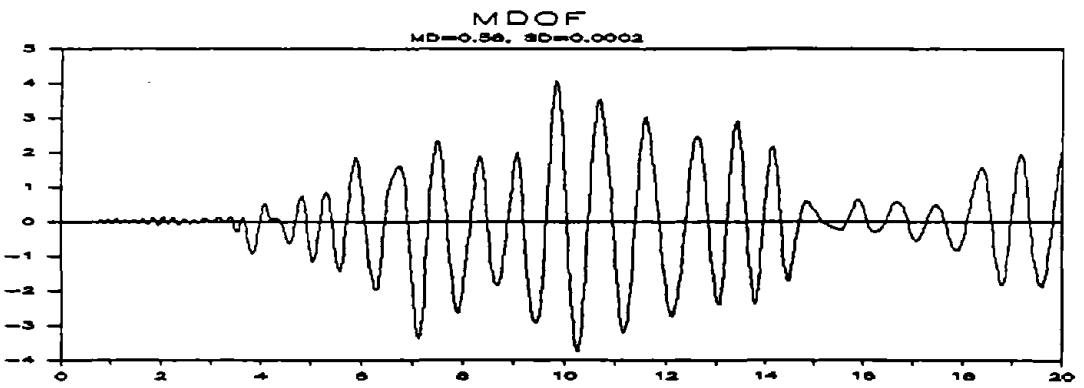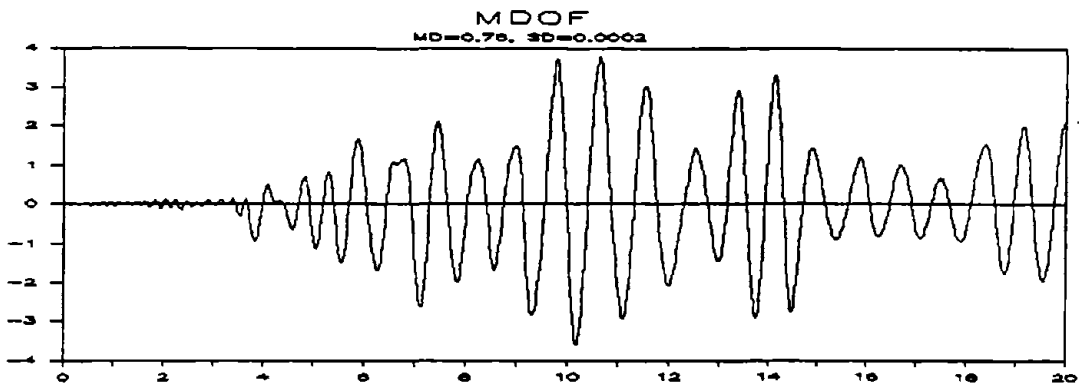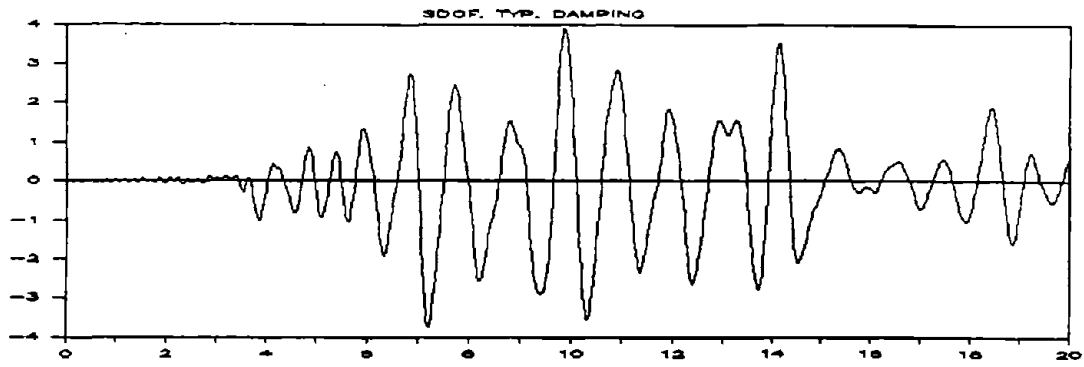
FIGURE 5-12b

GROUND MOTION # 7
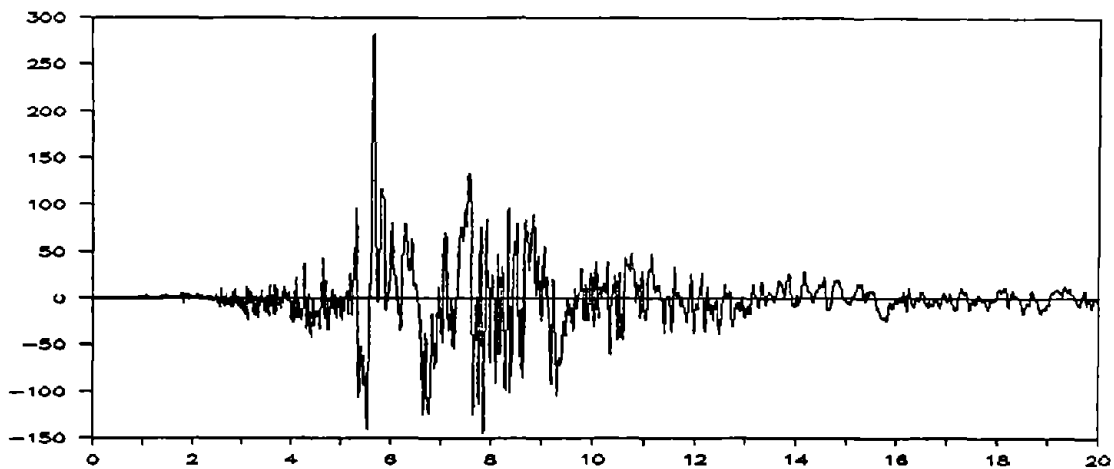
GROUND MOTION 7

SDOF. LOW DAMPING
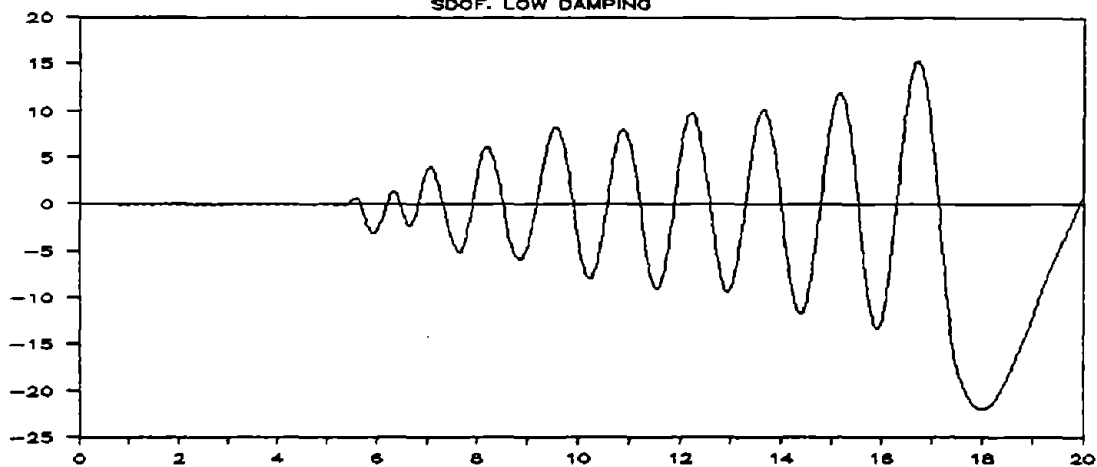
MDOF. NO DAMPING

FIGURE 5-13a

FIGURE 5-13b

GROUND MOTION # 8

GROUND MOTION 8

SDOF. LOW DAMPING

MDOF. NO DAMPING

FIGURE 5-14a
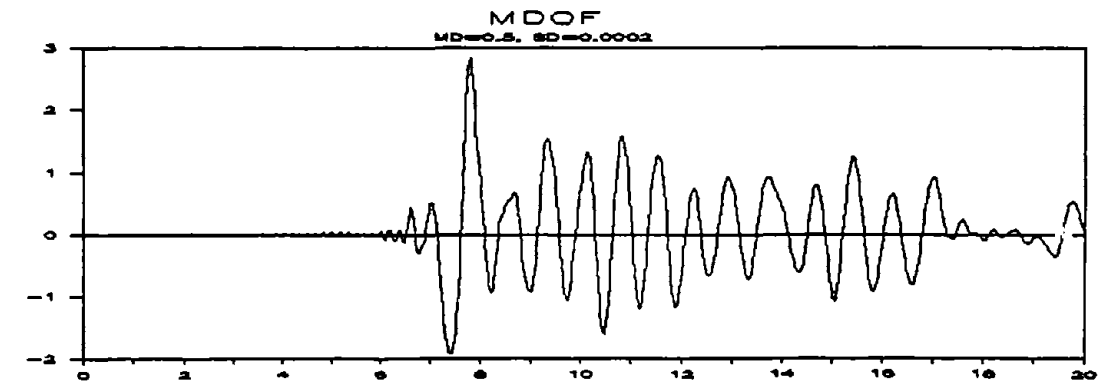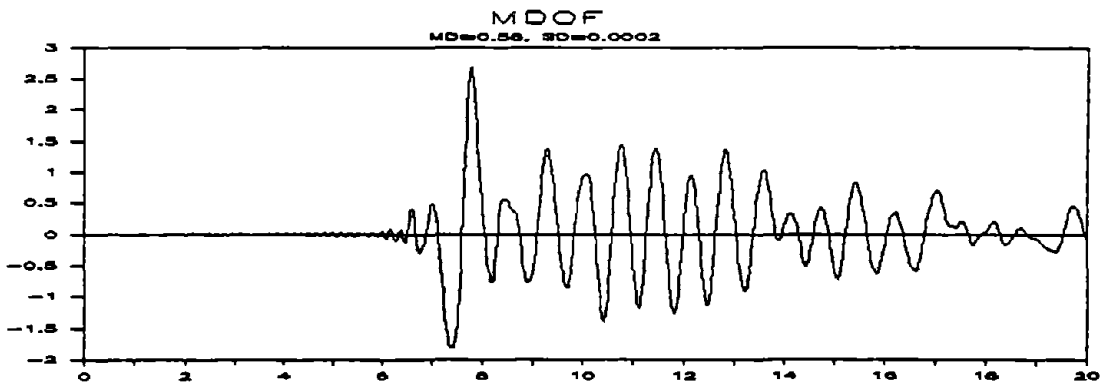
FIGURE 5-14b

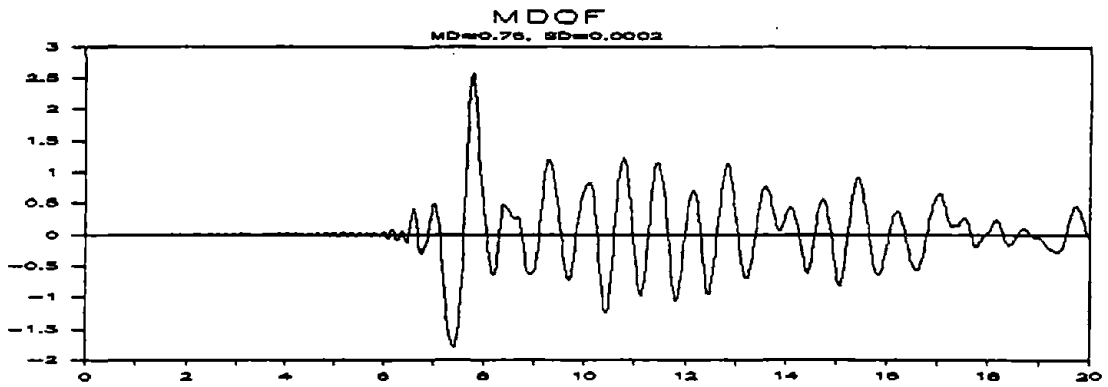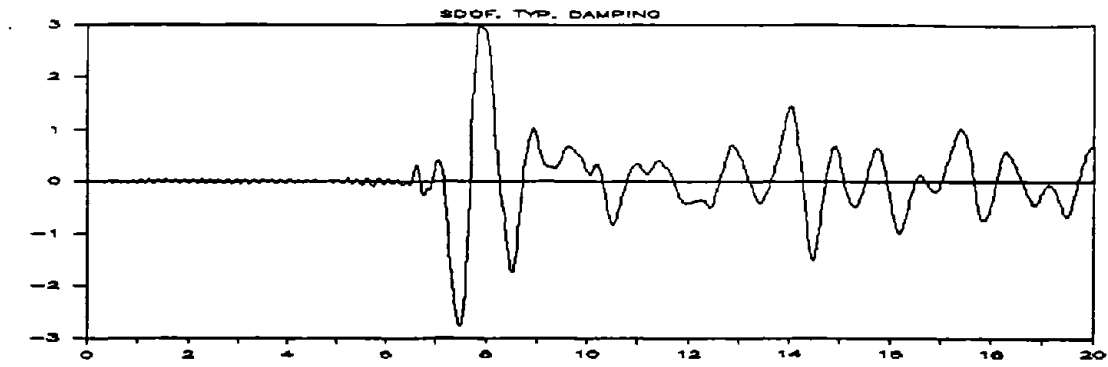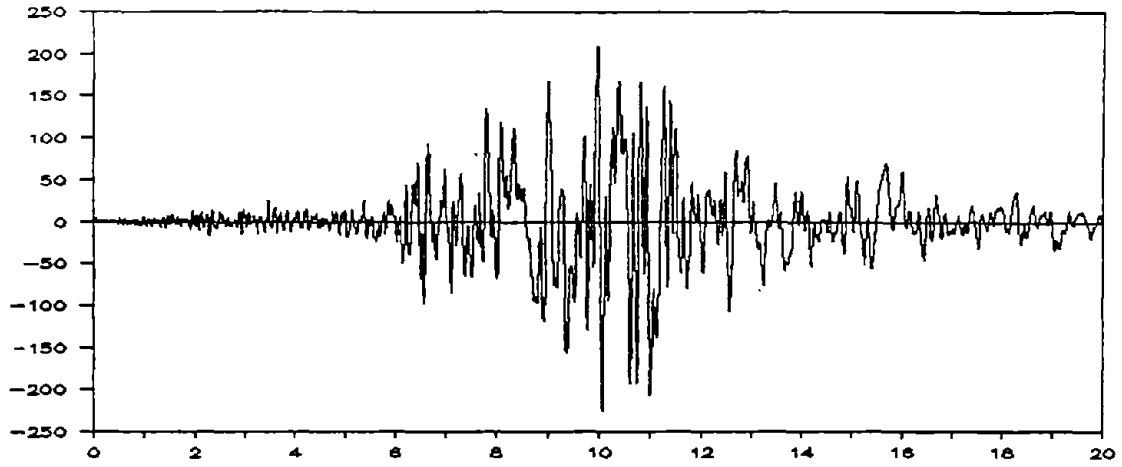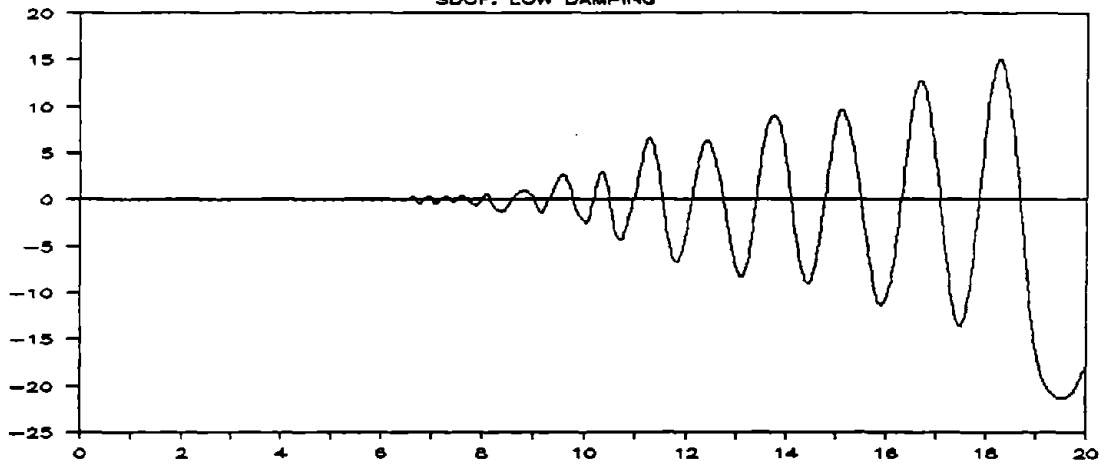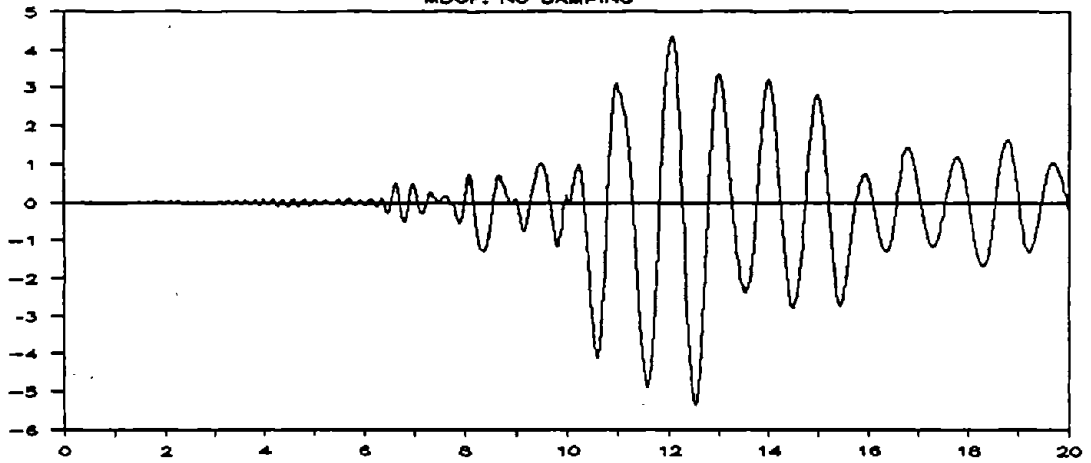## GROUND MOTION # 9

GROUND MOTION 9

SDOF. LOW DAMPING

MDOF. NO DAMPING

FIGURE 5-15a

3DOF. TYP. DAMPING

MDOF
MD=0.76. SD=0.0002
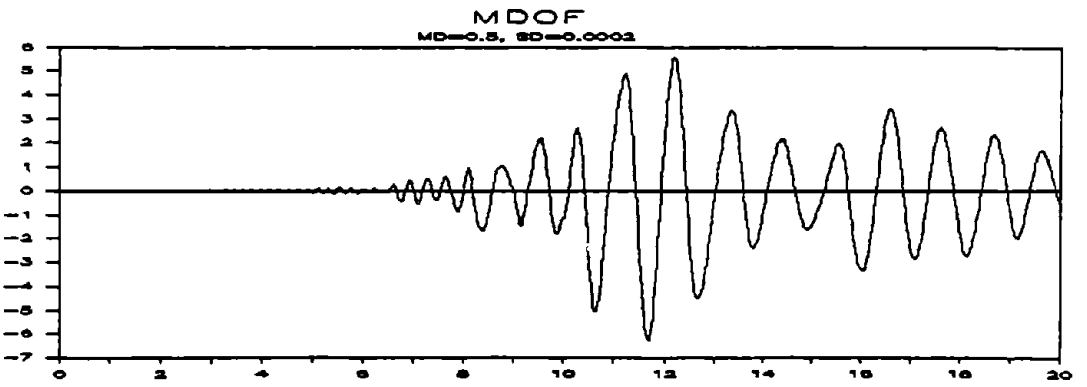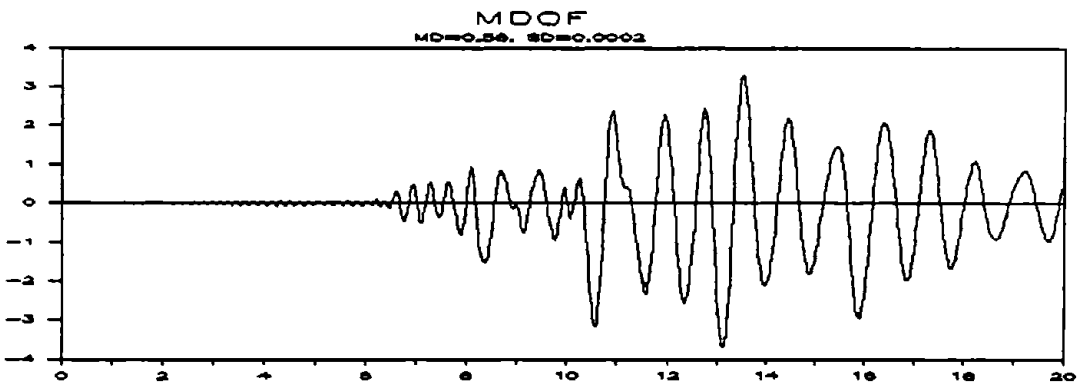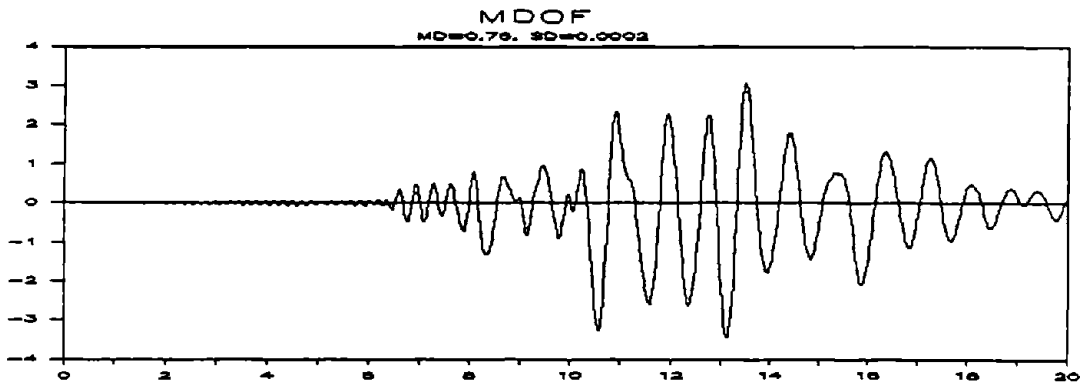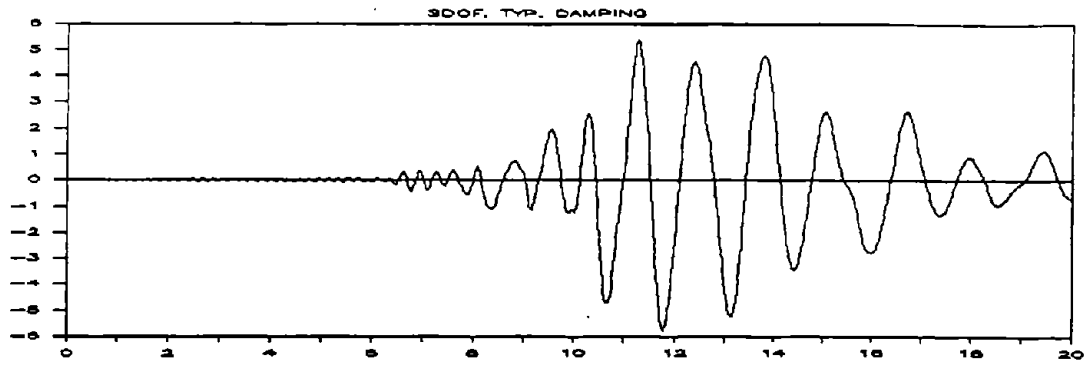
MDOF
MD=0.56. SD=0.0002

MDOF
MD=0.5. SD=0.0002

FIGURE 5-15b

SECTION 6

CONCLUSIONS

The studies have shown that nonlinear MDOF models with specified
damping can simulate the top displacement of a multi-story shear
wall as calculated by a nonlinear SDOF model with hysteretic
damping. The studies have also shown that simulation of the
response of a SDOF model with hysteretic damping to a specific
ground motion, ie. a recorded ground motion, is dependent on the
user's choice of damping values and of the combination of mass and
stiffness damping.

Figures 5-7a and b through Figures 5-15a and b show that the
damping needed for a full simulation of hysteretic damping is
dependent on the sequence of energy pulses. A single large pulse
followed by a train of smaller pulses will not be accurately
modeled by the MDOF model. The apparent reason is the hysteretic
model has no damping on the initial loading and a large quantity of
energy dissipation upon unloading. Subsequent cycles will have
small quantities of energy dissipation. The MDOF model has damping
on the initial pulse and will predict a smaller peak response to
the initial pulse. As its damping is selected from hysteretic
response of the SDOF to a second displacement to the displacement
attained at the first cycle, the MDOF model is under-damped for the
subsequent smaller cycles and responds in a manner somewhat similar
to a forced vibration. Figure 5-11b and Figure 5-13b illustrate
this behavior. The damped SDOF model, without damping on the
initial loading pulse has larger deformation and thus a
significantly lower stiffness when subjected to the following
pulses.

The ground motions that have a longer duration of high intensity
shaking, such as GM 1, 4, 6 and 9 have a closer relationship in the
response of the damped SDOF and MDOF. These histories of response
maintain a good comparison throughout the length of the record.
This study indicates that selection of damping values and methods

6-1

are critical for the prediction of peak dynamic displacements when using the nonlinear MDOF model.

These studies indicate that the following procedure is necessary to determine the damping values imposed on the nonlinear beam model. The peak displacement expected in a seismic hazard zone can be estimated by the following procedure:

- Determine $S_{a(0.3)}$ and $S_{a(1.0)}$ for the site from the maps accompanying the 1991 Edition of the NEHRP Recommended Provisions.

- Estimate the expected period of the structure by using a reduced effective stiffness that is appropriate for the seismic risk and the degraded stiffness of the lateral load resisting system.

- Calculate a base shear in accordance with the Provisions, distribute the loading prescribed on the lateral load resisting elements and calculate a displacement of the system using the stiffness used to estimate period. Multiply this displacement by the displacement amplification factor, C_d.

- Use the nonlinear finite element program (Ewing, 1987, 1990) to determine the energy dissipated on cycles subsequent to the calculated displacement and to one-half of the calculated displacement.

- Follow the methods used in this report to determine the appropriate damping values to be used for the MDOF model in the nonlinear analysis.

- Analyze the structure using a minimum of five scaled ground motions. The ground motions should be scaled to a response spectrum having an $S_{a(0.3)}$ and $S_{a(1.0)}$ predicted for the seismic risk of the site.

- Use the mean of the dynamic displacements calculated to determine the drift ratio of the structural system. Compare this calculated drift ratio with recommended maximum drift ratio.

If the behavioral data needed for modeling the lateral load resisting element by an equivalent SDOF model is available, the process of determining damping used in this study may be followed.

Studies of buildings designed in accordance with proposed limit state design standards (Kariotis, 1992) have shown that the MDOF beam element model is useful for predicting the distribution of dynamic shear over the height of the lateral load resisting system. These studies indicate that the shear associated with primary mode response, the base shear calculated by the equivalent SDOF model, understates the base shear. The SDOF model cannot predict shear due to higher mode response.

In conclusion, use of an equivalent SDOF nonlinear model and of a nonlinear beam element MDOF model is recommended for analysis of multi-story reinforced masonry shear wall buildings.

SECTION 7
REFERENCES

Biggs, J.M., Introduction to Structural Dynamics, McGraw-Hill Book Company, Inc., 1964, pp. 202-205.

Clough, R.W., and J. Penzien, Dynamics of Structures, McGraw-Hill Book Company, Inc., 1975.

Ewing, R.D., K.T. Dill and R.W. Fellner (1982) User's Guide for STARS/III: A Computer Program for the Nonlinear, Dynamic Analysis of Lumped Parameter Systems. El Segundo, CA: Agbabian and Associates.

Ewing, R.D., A.M. El-Mustapha and J.C. Kariotis (1987) FEM/I, A Finite Element Computer Program for the Nonlinear Static Analysis of Reinforced Masonry Building Components, TCCMAR Report 2.2-1.

Ewing, R.D. (1990) Improvements in FEM/I, A Finite Element Computer Program for the Nonlinear Static Analysis of Reinforced Masonry Walls. Report of the Sixth Meeting of the Joint Technical Coordinating Committee on Masonry Research, Section D, Modeling and Design, TCCMAR, Boulder, CO.

Kariotis, J.C., A.M. Rahman, O.M. Waqfi and R.D. Ewing (1992) LPM/I, Version 1.03, A Computer Program for the Nonlinear, Dynamic Analysis of Lumped Parameter Models. TCCMAR Report 2.3-4.

Kariotis, J.C., O.M. Waqfi, R.D. Ewing, (1992) A Computer Program Using Beam Elements for the Nonlinear, Dynamic Analysis of Lumped Parameter Models. TCCMAR Report 2.3-5.

Kariotis, J.C., O.M. Waqfi (1992) Trial Designs Made in Accordance With Tentative Limit States Design Standards for Reinforced Masonry Buildings. TCCMAR Report 9.1-2.

Saiidi, M. and M.A. Sozen (1981) Simple Nonlinear Seismic Analysis of R/C Structures, Journal of the Structural Division, ASCE, Vol. 107, ST5.